

University of Alberta

**Assessing the Osseointegration of Cementless Hip Prostheses
using FE Vibrational Analysis**

by

Anita Ka-Yee Ho



A thesis submitted to the Faculty of Graduate Studies and Research
in partial fulfillment of the requirements for the degree of
Master of Science

Department of Mechanical Engineering

Edmonton, Alberta
Fall, 2005



Library and
Archives Canada

Bibliothèque et
Archives Canada

Published Heritage
Branch

Direction du
Patrimoine de l'édition

395 Wellington Street
Ottawa ON K1A 0N4
Canada

395, rue Wellington
Ottawa ON K1A 0N4
Canada

Your file *Votre référence*
ISBN: 978-0-494-22427-4
Our file *Notre référence*
ISBN: 978-0-494-22427-4

NOTICE:

The author has granted a non-exclusive license allowing Library and Archives Canada to reproduce, publish, archive, preserve, conserve, communicate to the public by telecommunication or on the Internet, loan, distribute and sell theses worldwide, for commercial or non-commercial purposes, in microform, paper, electronic and/or any other formats.

The author retains copyright ownership and moral rights in this thesis. Neither the thesis nor substantial extracts from it may be printed or otherwise reproduced without the author's permission.

AVIS:

L'auteur a accordé une licence non exclusive permettant à la Bibliothèque et Archives Canada de reproduire, publier, archiver, sauvegarder, conserver, transmettre au public par télécommunication ou par l'Internet, prêter, distribuer et vendre des thèses partout dans le monde, à des fins commerciales ou autres, sur support microforme, papier, électronique et/ou autres formats.

L'auteur conserve la propriété du droit d'auteur et des droits moraux qui protègent cette thèse. Ni la thèse ni des extraits substantiels de celle-ci ne doivent être imprimés ou autrement reproduits sans son autorisation.

In compliance with the Canadian Privacy Act some supporting forms may have been removed from this thesis.

Conformément à la loi canadienne sur la protection de la vie privée, quelques formulaires secondaires ont été enlevés de cette thèse.

While these forms may be included in the document page count, their removal does not represent any loss of content from the thesis.

Bien que ces formulaires aient inclus dans la pagination, il n'y aura aucun contenu manquant.


Canada

Abstract

Total hip arthroplasty (THA) procedures are performed in order to alleviate the symptoms of trauma or degeneration of the hip joint and to restore function. Currently available clinical methods to determine periprosthetic bone quality and osseointegration are relatively subjective and are not sufficient for evaluating implant stability, especially in the absence of symptoms such as pain. This investigation evaluates the feasibility of utilizing vibrational analysis to quantitatively assess the quality of periprosthetic bone and osseointegration following a total hip replacement procedure. This *in vivo*, non-invasive diagnostic approach could be used to supplement current clinical assessment techniques and provide health-monitoring information for the life of the implant. The results indicate that the frequency response of an implant could be used to identify certain types of non-osseointegration in the form of deteriorating periprosthetic bone quality.

Abstract

Acknowledgements

First and foremost, I would like to Dr. Walied Moussa for providing this incredible opportunity for me and for sharing his ideas and experience. His encouragement, support, patience and generosity of spirit was always comforting and unwavering. Thank-you for inviting me to join your group.

I would also like to express my deepest appreciation to Dr. Edmond Lou. Thank-you for allowing me to work on this project. I am also thankful for his advice, support and patience and for sharing his expertise and resources for the last couple of years.

I am very grateful for the unconditional love and support from my parents, William and Connie, as well as my brothers, Andrew and Michael. I am also fortunate enough to enjoy the support of many good friends (Elma, Shafi, Tyler, Adrien, Steve, Monetta, Sandeep, Kerly, Michelle, Jesse, Fiona...). I need to also thank Derek and Trylan for all their love and encouragement.

To the faculty and staff of the Mechanical Engineering Department, I am thankful for their assistance throughout the years. I would also like to thank my fellow lab members as well as Dr. Jeffrey Yokota. Furthermore, I am appreciative of Dr. John Cinats for generously sharing his orthopaedic knowledge with me and for providing an opportunity for me to observe a total hip replacement procedure. I would also like to acknowledge Brian Goertz and Darcy Kipp from Stryker Canada.

Financial support from the Natural Sciences and Engineering Research Council, the Glenrose Rehabilitation Hospital and the Department of Mechanical Engineering was also greatly appreciated.

Acknowledgements

*To My Parents,
William and Connie*

Table of Contents

Abstract

Acknowledgements

Table of Contents

List of Tables

List of Figures

Definitions

Chapter 1: Introduction

1.1	Problem Description	1
1.2	Objective and Scope of Thesis	3
1.3	Background Information.....	4
1.3.1	Anatomical Direction Nomenclature	4
1.3.2	Anatomy of the Hip Joint.....	5
1.3.3	Causes and Symptoms of Hip Deterioration	6
1.3.4	Hip Implant Assembly	10
1.3.5	Total Hip Arthroplasty: Rate of Occurrence and Demographic	12
1.3.6	Total Hip Replacement (THR) Procedure	12

Chapter 2: Literature Review

2.1	Mechanical assessment of bone properties	16
2.2	Diagnostic assessment techniques following total hip replacement	17
2.2.1	Current diagnostic assessment techniques	17
2.2.2	Proposed vibrational diagnostic techniques for health-monitoring of loosened hip prosthetics	17
2.2.3	Other proposed diagnostic techniques for health-monitoring of loosened hip prosthetics	20

Table of Contents

Chapter 3: Material Definition and Mechanical Properties

3.1	Bone Physiology	21
3.1.1	Wolff's Law	21
3.1.2	Stress-Shielding Effect.....	22
3.1.3	Structure of Bone	24
3.2	Mechanical Properties of Bone	27
3.2.1	Heterogeneity and Anisotropy of Bone	27
3.2.2	Mechanical Properties of Cortical Bone: Cited Values.....	27
3.2.3	Mechanical Properties of Cortical Bone: Implemented Values.....	30
3.2.4	Mechanical Properties of Cancellous Bone: Cited Values	30
3.2.5	Mechanical Properties of Cancellous Bone: Implemented Values ..	35
3.2.6	Mechanical Properties of Periprosthetic Bone.....	36
3.3	Femoral Stem	38
3.3.1	Type and Model of Femoral Stem.....	38
3.3.2	Mechanical Properties of Femoral Stem	41

Chapter 4: Finite Element Modeling and Geometry

4.1	The Finite Element Method and Discretization of the Continuum.....	43
4.1.1	Finite Element Method.....	43
4.1.2	Discretization the Continuum	44
4.2	Femoral Implant: CAD Model and Finite Element Model.....	46
4.2.1	Creation of Finite Element Model and CAD Model.....	46
4.2.2	Original CAD Implant Model (S16M2) vs. Implemented CAD Implant Model (S16M9)	48
4.2.3	Numerical validation of Implant Model.....	53
4.3	Femoral Bone: CAD Model and Finite Element Model	56
4.3.1	Creation of Finite Element Model and CAD Model of the Femoral Bone.....	56
4.3.2	Generation of Periprosthetic Bone Model.....	65
4.3.3	Approximating the topography of the cancellous bone volume using a constant-thickness section.....	65

Table of Contents

4.4	Type and Size of FEA Elements	70
4.4.1	Type of FEA Elements	70
4.4.2	Size of FEA Elements	71

Chapter 5: Results and Analysis

5.1	Review of Objectives	74
5.1.1	Defining the Manipulated Variables	74
5.2	Non-Dimensionalizing the Frequency-Response of the Implant	75
5.3	Mode Shapes	77
5.4	Effects of Periprosthetic Bone Density	79
5.4.1	Results	79
5.4.2	Range and resolution	85
5.5	Effects of Periprosthetic Bone Thickness	86
5.6	Effects of Localized Non-Osseointegrated Periprosthetic Bone along the porous-coated body of the implant	95
5.6.1	Anterior vs. Posterior Non-Osseointegration	95
5.6.2	Medial vs. Lateral Non-Osseointegration	103
5.6.3	Proximal-to-Distal Non-Osseointegration	109
5.6.4	Osseointegration in Physiologically-Significant Regions (variation of the Gruen Zones)	115
5.7	Effects of varying Cancellous Host Bone Thickness	122

Chapter 6: Conclusions and Future Work

6.1	Summary and Conclusions	127
6.3	Future Work	130

Bibliography	131
---------------------------	------------

List of Tables

Table	Page
3.1 Available data on the Poisson's ratio of Femoral Cortical Bone.	28
3.2 Summary of cited mechanical properties (apparent density and elastic modulus) of Femoral Cortical Bone, by selected investigators.....	29
3.3 Implemented values for Cortical Bone in this study.....	30
3.4 Summary of cited mechanical properties of Femoral Cancellous Bone, by selected investigators using various testing methods and protocols.....	31
3.5 Summary of power law relationships between apparent density and modulus of elasticity of cancellous bone by selected investigators using various testing methods and protocols.....	34
3.6 Implemented values for Healthy Cancellous bone in this study.....	36
3.7 Values of the Host and Periprosthetic cancellous bone properties used in this study.....	37
3.8 Published mechanical properties of TMZF™.....	41
3.9 A comparison of material and geometric properties: Secur-Fit™ stem versus S16M9 model.....	41
3.10 Implemented mechanical properties of TMZF™ in this study.....	42
4.1 S16M2 vs. S16M9: Material properties and modal analysis comparison.....	51
4.2 Implemented mechanical properties of the implant material (TMZF™) in this study.....	52
4.3 Modal analysis comparison of various similar models.....	54
4.4 Comparison of the mode frequencies predicted by theory and ANSYS.....	54
4.5 Modal Analysis of Full Implant Models vs. Partial Stem Models.....	55
4.6 Comparison of the mode frequencies of Full Implant Model vs. Distal Stem Model.....	55
4.7 Volumetric comparison of implant with bone and beam with sleeves.....	62
4.8 Mechanical properties of beam and sleeves.....	63
4.9 Percent error between modal analysis results (Mode #1 to #5) of beam with and without simulated cortical bone sleeve.....	64

Table	Page
4.10	Comparison of modal analysis results of an Implant with Typical Proximal Femur Topography and Implant with Simulated Cancellous Bone Layer..... 66
4.11	Percent deviation between modal analysis results (Mode #1 to #5) of an Implant with Typical Proximal Femur Topography and an Implant with Simulated Host Bone Layer 67
4.12	Percent error between modal analysis results (Mode #1 to #5) of an Implant with Typical Proximal Femoral Topography and an Implant with Simulated Cancellous Bone Layer 69
5.1	Varying periprosthetic bone thickness and its effect on the frequency range (Mode #1)..... 87
5.2	Various permutations of periprosthetic bone thickness (t_1) and periprosthetic bone density (ρ_1) that produce a first mode frequency-response of approximately 950 Hz..... 91
5.3	Geometric Properties of Proximal and Distal sections..... 109

List of Tables

List of Figures

Figure	Page
1.1 Anatomical Directions.....	4
1.2 Anatomical Directions of the Femoral Bone (thighbone).....	5
1.3 Anatomy of the Hip Joint.....	6
1.4 Hip joint damage due to osteoarthritis.....	7
1.5 Common types of Femoral Bone Fractures of the Femoral Neck and Intertrochanteric Region	8
1.6 Collapse of Femoral head bone due to Avascular Necrosis.....	8
1.7 Exploded View and Assembled Views of a typical modular Total Hip Replacement system	10
1.8 Detailed view of the uncemented implant surface and periprosthetic bone interface.	11
1.9 Total Hip Replacement procedure	14
1.10 Completed Total Hip Replacement.....	15
3.1 Femur – Cancellous and Cortical bone components	24
3.2 Structure of Femoral Bone.....	25
3.3 Cortical Bone - dense bone tissue consisting of an arrangement of closely associated Haversian systems of osteons.....	25
3.4 A scanning electron microscopic view of the sheet and strut arrangement of the cancellous bone lattice from the upper femur	26
3.5 CAD model of Femoral Host bone and Periprosthetic Bone surrounding a femoral implant stem.....	36
3.6 Stryker® Howmedica Osteonics' Secur-Fit™ HA stem.....	38
3.7 Manufacturer Breakdown for Total Hip Replacement Components	39
3.8 Manufacturer Breakdown for Femoral Stem Components.....	40
3.9 Manufacturer Breakdown for Acetabular Components	40
4.1 Finite Element Analysis Process	44
4.2 Discretization (meshing) of a Continuum.....	44
4.3 Various 2-dimensional and 3-dimensional Element Types.....	45
4.4 CAD model (Version S16M2) vs. Secur-Fit™ Implant	47
4.5 CAD model (Version S16M2) of Secur-Fit™ Implant: with and without normalizations	48
4.6 Comparison of S16M2 vs. S16M9 CAD models of the implant	49
4.7 S16M9 model - Fully constrained nodes on the hydroxapatite- covered, coarsened surface on the body of the proximal stem	50
4.8 S16M2 vs. S16M9: Comparison of modal analysis results.....	51

Figure	Page
4.9	Percent variation of modal analysis results between Case 2 and 3..... 52
4.10	Numerical Validation Process..... 53
4.11	Models of cantilever beam, distal stem and full implant model with boundary constraints shown 53
4.12	Rendered view of Greer's left-sided femoral bone model after importing IGES format file into SolidWorks®. 58
4.13	Truncation of Distal Femur in SolidWorks® before importing the IGES model into ANSYS®. 59
4.14	Creation of a solid femoral model from a trimmed surfaces model, in the ANSYS® environment..... 59
4.15	Truncation of cancellous bone stock above and below hydroxyapatite-covered surface on implant 60
4.16	Implant and cancellous bone volume with and without cortical bone 61
4.17	Comparison of geometrically accurate implant and bone volumes assembly and geometric equivalent beam with sleeves of simulated bone layers..... 63
4.18	Modal analysis results (Mode #1) of beam with and without simulated cortical bone sleeve 64
4.19	Generation of the Periprosthetic Bone Volume by offsetting constant-thickness volumes from the surface of the implant body..... 65
4.20	An Implant with Typical Proximal Femoral Topography and an Implant with Simulated Cancellous Bone 66
4.21	Modal analysis (Mode #1) of Implant with Typical Proximal Femur Topography and Implant with Simulated Host Bone Layer..... 67
4.22	Implant with Typical Proximal Femoral Topography and Implant with Simulated Cancellous Bone Layer 68
4.23	Modal analysis (Mode #1) of Implant with Typical Proximal Femoral Topography and Implant with Simulated Cancellous Bone Layer 69
4.24	Type of Element Implemented: SOLID95 – A 20-Node Brick Element 70
4.25	A comparison of element sizes and mesh resolution 71
4.26	Element Size Sensitivity Analysis: Test Case Configuration 72
4.27	Element size sensitivity analysis determined by the frequency response (Mode #1) of an implant with two types of bone layers..... 73
4.28	Computational time for various element sizes 73
5.1	A conceptual example of a time-lapsed (serial) frequency-response of an implanted prosthesis 76
5.2	Mode shapes at Mode #1, #3 and #5 – Implant vibrates predominately in the antero-posterior direction 77

List of Figures

Figure	Page
5.3 Mode shapes at Mode #2 and #4 – Implant vibrates predominately in the medio-lateral direction	78
5.4 Effect of varying periprosthetic bone density: Analysis Configuration	80
5.5 Effect of varying periprosthetic bone density (Results not normalized) - Mode #1.....	81
5.6 Effect of varying periprosthetic bone density (Results normalized) - Mode #1	81
5.7 Effect of varying periprosthetic bone density and comparison of modal response (first five modes) - Results have not been normalized.....	82
5.8 Effect of varying periprosthetic bone density and comparison of modal response (first five modes) - Results have been normalized	82
5.9 Effect of varying periprosthetic bone density – Percent difference between frequency responses.....	84
5.10 Effect of varying periprosthetic bone density – Decrease in resonance frequency.....	84
5.11 Effect of varying periprosthetic bone thickness: Analysis Configuration	87
5.12 Effect of varying periprosthetic bone thickness (Results normalized) - Mode #1.....	88
5.13 Effect of varying periprosthetic bone thickness (Results not normalized) - Mode #1.....	88
5.14 Effect of varying periprosthetic bone thickness, t1: (Mode #2).....	89
5.15 Effect of varying periprosthetic bone thickness, t1: (Mode #3).....	89
5.16 Effect of varying periprosthetic bone thickness, t1: (Mode #4).....	90
5.17 Effect of varying periprosthetic bone thickness, t1: (Mode #5).....	90
5.18 Effect of varying periprosthetic bone thickness, t1 – Percent difference between frequency responses.....	92
5.19 Effect of varying periprosthetic bone density (t1- 0.25 mm): Decrease in resonance frequency.....	93
5.20 Effect of varying periprosthetic bone density (t1- 0.50 mm): Decrease in resonance frequency.....	93
5.21 Effect of varying periprosthetic bone density (t1- 1.00 mm): Decrease in resonance frequency.....	94
5.22 Effect of varying periprosthetic bone density (t1- 1.50 mm): Decrease in resonance frequency.....	94
5.23 Anterior vs. Posterior Non-Osseointegration	96
5.24 Anterior vs. Posterior Non-Osseointegration – Percent difference between frequency responses.....	98
5.24 Anterior Non-Osseointegration – Decrease in resonance frequency	98
5.26 Posterior Non-Osseointegration – Decrease in resonance frequency	99

List of Figures

Figure	Page
5.27	Anterior vs. Posterior Non-Osseointegration – Decrease in resonance frequency (Mode #3)..... 99
5.28	Anterior vs. Posterior Non-Osseointegration – (Mode #1) 100
5.29	Anterior vs. Posterior Non-Osseointegration – (Mode #2) 100
5.30	Anterior vs. Posterior Non-Osseointegration – (Mode #3) 101
5.31	Anterior vs. Posterior Non-Osseointegration – (Mode #4) 101
5.32	Anterior vs. Posterior Non-Osseointegration – (Mode #5) 102
5.33	Medial vs. Lateral Non-Osseointegration..... 103
5.34	Medial vs. Lateral Non-Osseointegration – Percent difference between frequency responses..... 105
5.35	Medial Non-Osseointegration – Decrease in resonance frequency 105
5.36	Lateral Non-Osseointegration – Decrease in resonance frequency relative..... 106
5.37	Medial vs. Lateral Non-Osseointegration – (Mode #1)..... 106
5.38	Medial vs. Lateral Non-Osseointegration – (Mode #2)..... 107
5.39	Medial vs. Lateral Non-Osseointegration – (Mode #3)..... 107
5.40	Medial vs. Lateral Non-Osseointegration – (Mode #4)..... 108
5.41	Medial vs. Lateral Non-Osseointegration – (Mode #5)..... 108
5.42	Proximal vs. Distal Non-Osseointegration 109
5.43	Proximal vs. Distal Non-Osseointegration – Percent difference between frequency responses..... 111
5.44	Proximal Non-Osseointegration – Decrease in resonance frequency 111
5.45	Distal Non-Osseointegration – Decrease in resonance frequency 112
5.46	Proximal vs. Distal Non-Osseointegration – (Mode #1) 112
5.47	Proximal vs. Distal Non-Osseointegration – (Mode #2) 113
5.48	Proximal vs. Distal Non-Osseointegration – (Mode #3) 113
5.49	Proximal vs. Distal Non-Osseointegration – (Mode #4) 114
5.50	Proximal vs. Distal Non-Osseointegration – (Mode #5) 114
5.51	Gruen Zones 115
5.52	Four physiologically-significant regions: Greater Trochanter, Calcar, Mid-Lateral Cortex and Mid-Medial Cortex..... 115
5.53	Non-osseointegration of four physiologically-significant regions – Percent difference between frequency responses 117
5.54	Non-osseointegration of four physiologically-significant regions – Decrease in Mode #3 resonance frequency 117
5.55	Non-osseointegration of four physiologically-significant regions – Decrease in Mode #4 resonance frequency 118
5.56	Non-osseointegration of four physiologically-significant regions – Decrease in Mode #5 resonance frequency 118
5.57	Non-osseointegration of four physiologically-significant regions – (Mode #1)..... 119

List of Figures

Figure	Page
5.58 Non-osseointegration of four physiologically-significant regions – (Mode #2)	119
5.59 Non-osseointegration of four physiologically-significant regions – (Mode #3)	120
5.60 Non-osseointegration of four physiologically-significant regions – (Mode #4)	120
5.61 Non-osseointegration of four physiologically-significant regions – (Mode #5)	121
5.62 Effect of varying cancellous host bone thickness, t2: Analysis Configuration	122
5.63 Effect of varying cancellous host bone thickness, t2 – Percent difference between frequency responses.....	123
5.64 Effect of varying cancellous bone thickness, t2 - (Mode #1).....	124
5.65 Effect of varying cancellous bone thickness, t2 - (Mode #2).....	124
5.66 Effect of varying cancellous bone thickness, t2 - (Mode #3).....	125
5.67 Effect of varying cancellous bone thickness, t2 - (Mode #4).....	125
5.68 Effect of varying cancellous bone thickness, t2 - (Mode #5).....	126

List of Figures

Definitions

Antero-posterior: Relating to both front and back.

Apparent density (of cancellous bone): The mass of mineralized trabeculae divided by the volume occupied by both trabeculae and pores (bulk volume).

Aseptic loosening: Loosening of an artificial hip or knee component in the absence of infection.

Atrophy: A wasting or decrease in size of a body organ, tissue, or part owing to disease, injury, or lack of use, and caused by death and reabsorption of cells, diminished cellular proliferation, pressure, ischemia, malnutrition, decreased function, or hormonal changes.

Cephalo-caudal: Proceeding or occurring in the long axis of the body especially in the direction from head to tail.

Densitometry: Measuring the optical density of a substance by shining light on it and measuring its transmission.

Diaphysis: The shaft of a long bone.

Epiphysis: The proximal or distal end of a long bone.

Excised: To remove by or as if by cutting.

Ex vivo: In an artificial environment outside the living organism; (synonym: *in vitro*; antonym: *in vivo*).

Histologic: The microscopic structure of tissue.

Hydroxyapatite: A calcium phosphate based compound of a similar composition to bone.

Hypertrophy: A nontumorous enlargement of an organ or a tissue as a result of an increase in the size rather than the number of constituent cells.

In vivo: Within a living cell or organism; Refers to an experiment conducted in the body.

Definitions

In vitro: Refers to an experiment conducted in the laboratory.

Isostrain: Equal strain condition.

Material density (of cancellous bone): The mass of trabeculae, divided by the volume of the trabeculae alone.

Medio-lateral: Relating to the median plane and a side.

Metaphysis: The zone of growth between the epiphysis and diaphysis during development of a bone. The transitional zone at which the diaphysis and epiphysis of a bone come together. This is the region of long bone on the diaphyseal side of the epiphyseal plate.

Osseointegration: The firm anchoring of a surgical implant (as in dentistry or in bone surgery) by the growth of bone around it without fibrous tissue formation at the interface.

Osteoarthritis: A form of arthritis, occurring mainly in older persons, that is characterized by chronic degeneration of the cartilage of the joints. Also known as degenerative joint disease.

Osteogenesis: The formation and development of bony tissue.

Osteopenia: A condition of bone in which decreased calcification, decreased density, or reduced mass occurs.

Osteoporosis: A disease in which the bones become extremely porous, are subject to fracture and heal slowly and is characterized by decrease in bone mass with decreased density and enlargement of bone spaces producing porosity and brittleness.

Osteonecrosis: Death of bone cells or tissues, especially in a localized area of the body, due to impaired or disrupted blood supply (as that caused by traumatic injury or disease) and marked by severe pain in the affected region and by weakened bone that may flatten and collapse.

Periprosthetic: Of or relating to, or occurring in the tissues surrounding the prosthetic.

Porosity: The ratio of the volume of all the pores in a material to the volume of the whole.

Radiolucency: Allowing the passage of x-rays or other radiation; not radiopaque.

Definitions

Radiopaque : Not allowing the passage of x-rays or other radiation.

Revision surgery: A procedure whereby a failed implant is replaced with a new one.

Rheumatoid arthritis: A chronic disease marked by stiffness and inflammation of the joints, weakness, loss of mobility, and deformity.

Roentgenography : A radiographic technique that uses X-rays to produce a roentgenogram (a photograph made with x-rays).

Definitions

Chapter 1

Introduction

1.1 Problem Description

Total hip arthroplasty (THA), or total hip replacement (THR) procedures, are performed in order to alleviate the symptoms caused by a dysfunctional hip and to restore function and mobility for the patient. Dysfunctional hips are usually attributed to trauma and injury or deterioration of the hip joint due to bone erosion or atrophy in combination with a variety of joint-related diseases. Typically, patients who have severe hip arthritis suffer joint stiffness, have difficulty walking and experience pain in the groin and thigh regions. Many patients report an overwhelming decrease of pain and restoration of hip function and vast improvements on patient mobility following a hip replacement procedure.

Following a THR, the patient's follow-up is crucial. Health professionals monitor the patient's healing progress and identify any problems that may require revision surgery. Currently, post-operative monitoring and diagnosis has been determined on a patient-by-patient basis and is generally dependent on the amount of time that has passed since the surgery. In addition, roentgenograms (x-ray photographs) or other methods of medical imaging such as the use of dual-energy x-ray absorptiometry (DXA or DEXA) and the patients' self-assessments are also taken into account. Clinical appraisals alone are insufficient for evaluating the stability of total hip prostheses, since unstable components do not always produce early symptoms [Engh *et al.*, 1990] even in the presence of substantial bone loss or atrophy [Maloney *et al.*, 1990a,b]. Clinical radiographs are useful for providing gross

information concerning architectural changes of periprosthetic bone remodelling during the post-operative phase, but reliable quantitative information is difficult to assess [Maloney *et al.*, 1996]. Relatively large decreases in bone mineral content must also occur before it is evident on plain radiographs. It has been shown that densitometric differences of 9-21% only yield relatively small changes on radiographs [West *et al.*, 1987]. Huiskes *et al.* [1992] also noted that traditional roentgenographs are unsuitable to accurately determine net changes in bone mass of less than 30%. Differences in radiographic technique (target distance, exposure setting and field variability) can also affect the accuracy of clinical assessments [Maloney *et al.*, 1996].

Clearly, the ability to monitor and quantify the osseointegration progression of the periprosthetic bone is very significant to orthopaedic surgeons as well as patients. However, there is little consensus among surgeons in the assessment of the progression of fracture healing [Bhandari *et al.*, 2002]. Perceptions of the concept of fracture healing are widely varying. Currently, there is no universally accepted standard of measuring and quantifying fracture healing. Therefore, tangible mechanical measurements concerning bone quality assessment would be very advantageous.

Herein lies the need to develop a monitoring technique to quantify the healing progression of periprosthetic bone. Ideally, this method would be a non-invasive technique that characterizes *in vivo* periprosthetic bone properties. This will aid in determining the most effective prescription to facilitate the patient in recovering as quickly as possible and to resume normal activities, with less chance of over-stressing the repairing fracture during the recovery and rehabilitation stages. This health-monitoring technique could also identify patients who potentially require revision surgery before catastrophic bone loss occurs.

1.2 Objective and Scope of Thesis

The purpose of this research is to determine the feasibility of an *in vivo*, periprosthetic bone osseointegration monitoring technique. Advanced osseointegration is indicative of mechanical and structural stability of the bone and implant interface. This study will determine the possibility of monitoring the progression of biologic fixation between periprosthetic bone tissue and a cementless hip implant within the proximal shaft of the femoral stem.

Specifically, this particular study investigates the feasibility of detecting and monitoring the frequency response of an implant, as the stiffness of the periprosthetic bone (bone tissue surrounding the implant) changes. The stiffness of the periprosthetic bone can be influenced by a number of variables. Most notably, these variables are bone density and bone thickness. These variables will be individually identified and its influence on the modal response of the implant will be examined. Therefore, the scope of this thesis will include examining the effects of:

- 1) Periprosthetic bone density
- 2) Periprosthetic bone thickness
- 3) Periprosthetic bone density variations in localized regions along the porous coated body:
 - a. Anterior vs. Posterior Non-Osseointegration
 - b. Medial vs. Lateral Non-Osseointegration
 - c. Proximal vs. Distal Non-Osseointegration
 - d. Non-Osseointegration in Physiologically-Significant Regions (variation of the Gruen Zones)
- 4) Cancellous Host Bone Thickness

1.3 Background Information

This section is intended to apprise the reader of the various terms that will be used in the following chapters. The anatomy of the hip will be introduced as well as some information regarding hip diseases and hip replacement surgery.

1.3.1 Anatomical Direction Nomenclature

The various sections of the anatomy, directional nomenclature that are typically used, in regards to the human body, will be introduced and defined. The anatomical directions used in this study are defined and illustrated in Figures 1.1 and 1.2.

- Anterior: Located on or near the front of the body.
- Posterior: Located on or near the back of the body.
- Lateral: Relating to, or situated at or on the side.
- Medial: Relating to, or extending toward the middle.
- Proximal: On the limbs, a point closer to the main body.
- Distal: On the limbs, a point farther away from the main body.

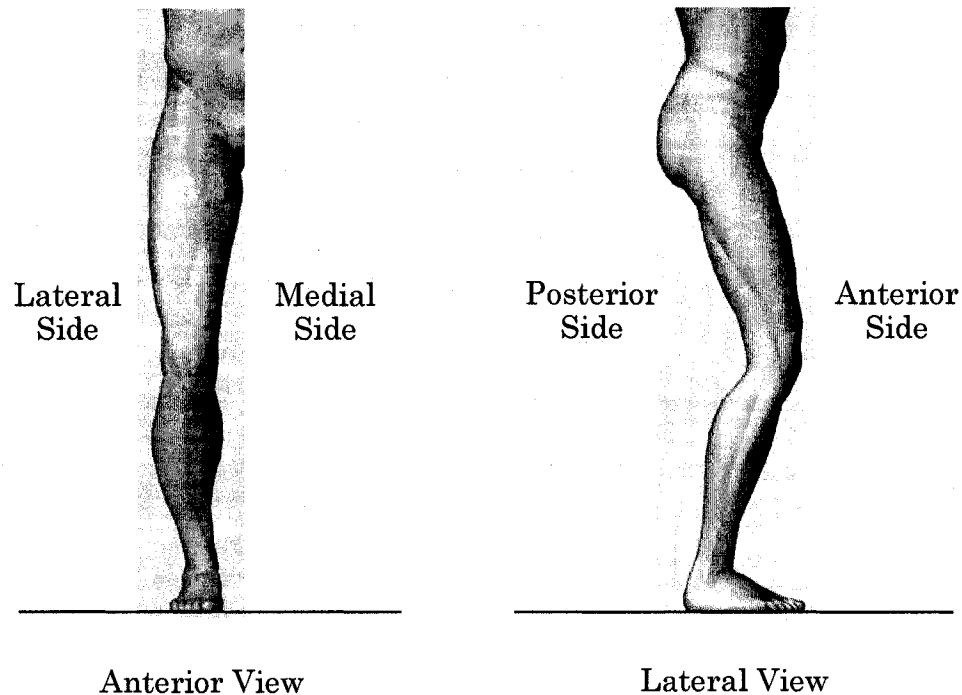


Figure 1.1: Anatomical Directions

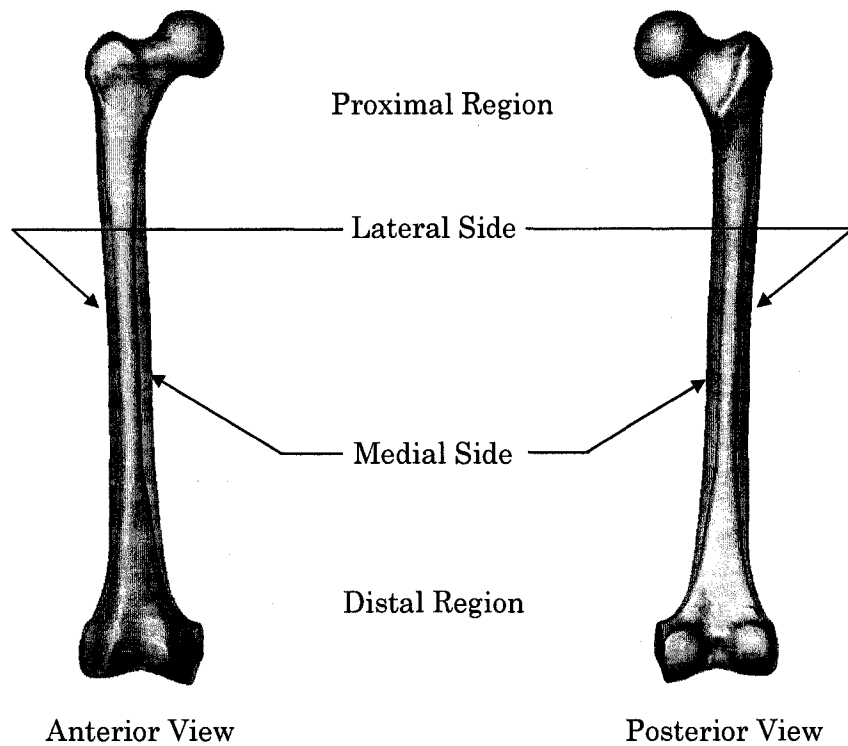


Figure 1.2: Anatomical Directions of the Femoral Bone (thighbone)

1.3.2 Anatomy of the Hip Joint

The hip joint is comprised of a “ball and socket” assembly that permits the huge range of motion required for walking, running, squatting, climbing and sitting. This “ball and socket” assembly consists of two main sections: the pelvis and the femur (thighbone), as shown in Figure 1.3. The top end of the femur (femoral head) is ball-shaped and fits into the round socket (acetabulum) of the pelvis. In between the femoral head and the acetabulum is articular cartilage, which cushions the femoral head and the acetabulum socket of the pelvis. The articular cartilage allows the two bony surfaces to move against each another without wearing down the bones and also acts as a shock absorber. Chronic deterioration of articular cartilage (osteoarthritis) is one of the main reasons for undergoing a hip replacement procedure.

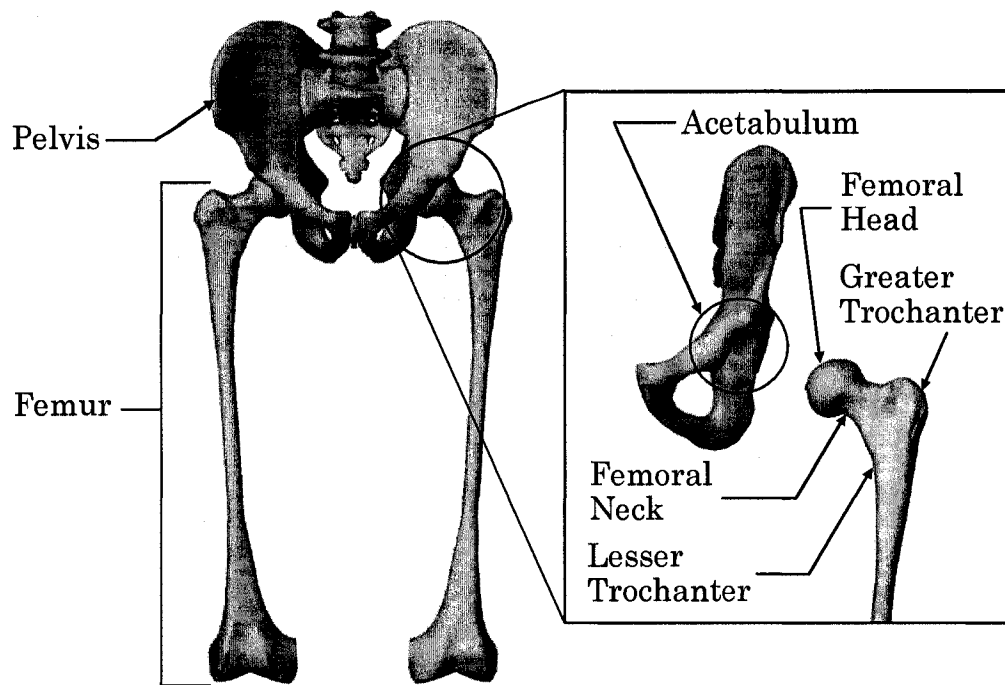
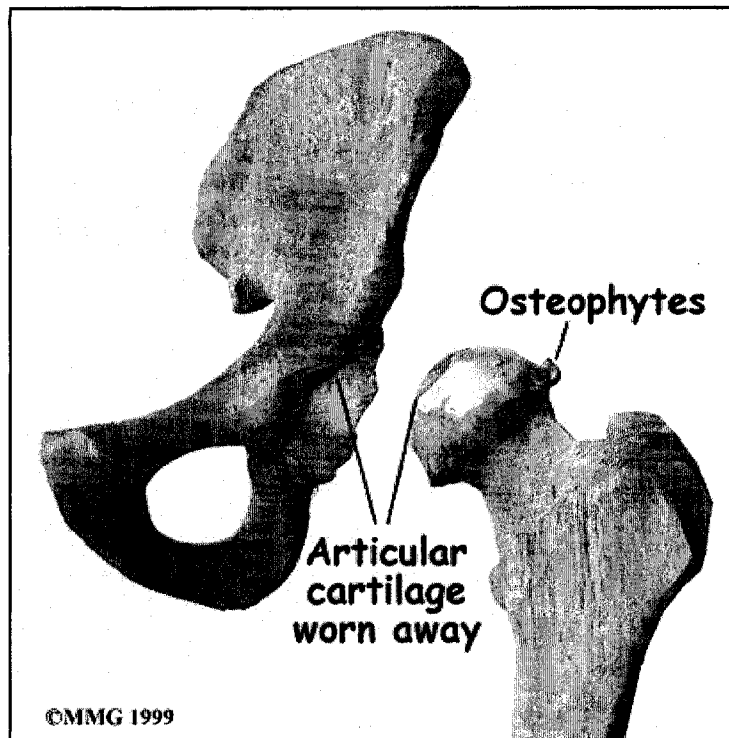


Figure 1.3: Anatomy of the Hip Joint

1.3.3 Causes and Symptoms of Hip Deterioration

The most common cause for total hip replacement surgery is osteoarthritis, or degenerative joint disease. This type of arthritis (inflammation of the joint) develops over time and occurs mainly in older people and is also commonly referred to as typical “wear and tear” arthritis. Over time, deterioration of the hip joint, due to articular cartilage erosion, can cause pain and result in a loss of motion. Eventually the diseased parts of the hip joint can wear away and bone can begin to rub against bone. Chronic bone rubbing may lead to painful outgrowths (bone spurs or osteophytes) on the worn bony surfaces as shown in Figure 1.4.



**Figure 1.4: Hip joint damage due to osteoarthritis
(Image provided courtesy of Medical Multimedia Group, LLC)**

Other common causes of hip deterioration are osteopenia, osteoporosis, injury and bone tumors. Osteopenia, a condition of bone in which decreased calcification, decreased density, or reduced mass occurs, is most likely caused by osteoporosis. Osteoporosis, a disease in which the bones become extremely porous, can lead to fracture of the femoral bone as shown in Figure 1.5. When the bone is fractured, there is also risk of rupturing the blood vessels as well. Since bone is a living tissue that requires blood supply, if the blood supply is damaged, the disengaged bone will begin to die. All of the blood supply to the femoral head (the ball portion of the hip joint) comes through the neck of the femur. Therefore, when the femur is fractured, damage can occur to these blood vessels and the femoral head can no longer maintain its structure. This type of bone loss caused by insufficient blood supply (Figure 1.6) is known as osteonecrosis, or is also known as avascular necrosis (AVN).

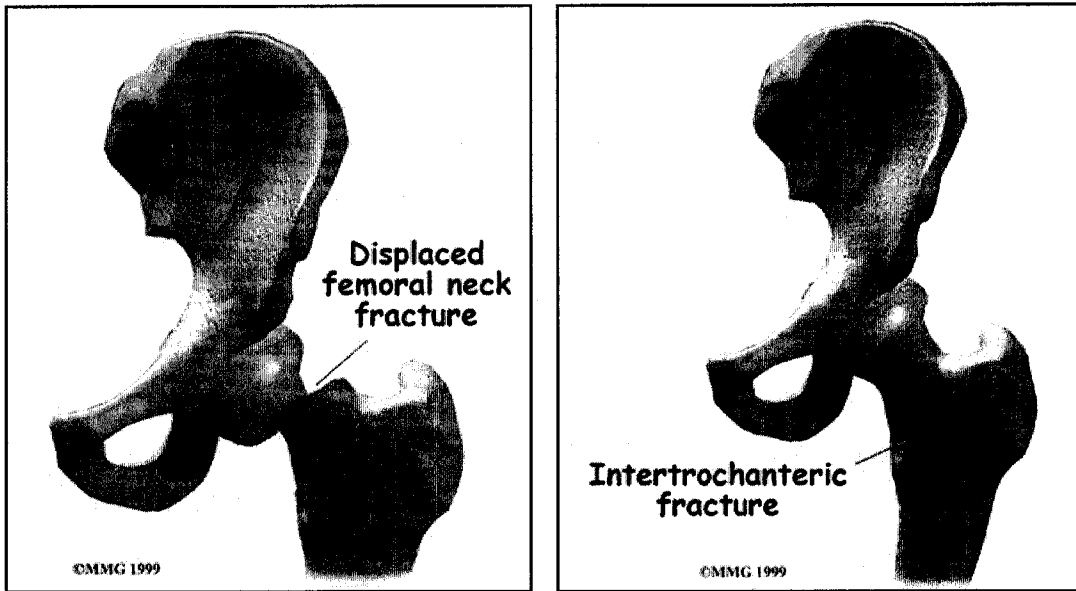


Figure 1.5: Common types of Femoral Bone Fractures of the (a) Femoral Neck and (b) Intertrochanteric Region (between the greater and less trochanter) (Image provided courtesy of Medical Multimedia Group, LLC)

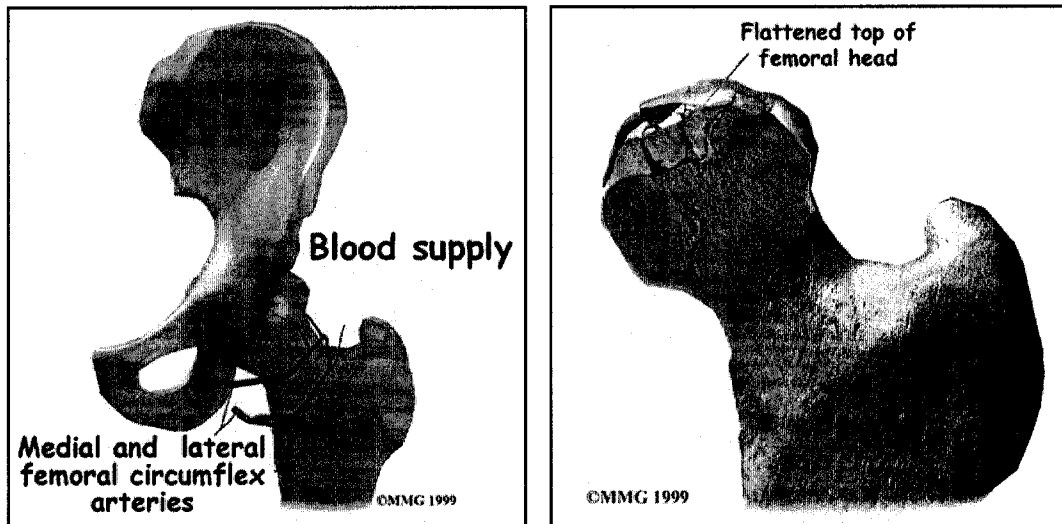


Figure 1.6: Collapse of Femoral head bone due to Avascular Necrosis (Image provided courtesy of Medical Multimedia Group, LLC)

Another possible cause of joint problems is rheumatoid arthritis, which also causes persistent joint inflammation. While osteoarthritis affects individual joints, rheumatoid arthritis usually causes multiple joints to become inflamed in a symmetrical pattern (both sides of the body affected). Rheumatoid arthritis is an autoimmune disease, which occurs when the antibodies of the immune system mistakenly attacks its own body tissue. When this occurs, the lining tissue of the joint (synovium) becomes inflamed, resulting in the production of excessive joint fluid (synovial fluid), which will cause swelling. The immune system improperly identifies the synovial membranes that secrete the lubricating fluid in the joints as foreign. Swelling and inflammation will damage the surrounding synovial membrane and the body will replace damaged tissue with scar tissue, causing the normal spaces within the joints to become narrow and the bones to fuse together. Because it can affect multiple organs of the body, rheumatoid arthritis is referred to as a systemic illness and is sometimes called rheumatoid disease.

The most common place to experience pain is the groin area, although patients may also suffer from thigh, back and knee pain. As a result, most potential hip replacement candidates will also experience reduced mobility, joint stiffness and are in constant discomfort.

1.3.4 Hip Implant Assembly

A total hip prosthesis consists of “ball and socket” assembly of three components – the femoral stem, the femoral head, and the acetabulum cup and sleeve that fits into the pelvis (Figure 1.7). The acetabulum sleeve provides a smooth surface for the femoral head to fit into and allows the femoral stem to rotate and swivel.

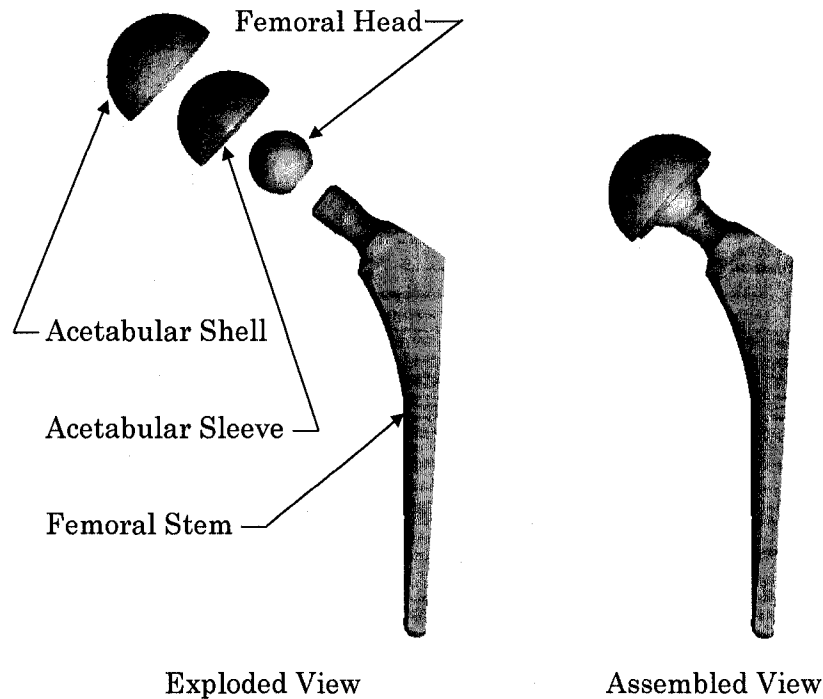


Figure 1.7: Exploded View and Assembled Views of a typical modular Total Hip Replacement system

Depending on the particular design and model, the prosthesis can be fitted with or without bone cement. In a cemented procedure, bone cement would be used to fixate the femoral stem into the medullary canal of the femur. However, in an uncemented procedure, no bone cement is used and the femoral stem is press-fitted into the femoral canal. In order to facilitate stability and fixation of the implant, uncemented prostheses are specially designed to fixate with surrounding bone without the aid of cement. The surface of the proximal femoral stem component is

coarsened with pores to facilitate mechanical macro-interlocking with the bony ingrowth to the anterior-posterior (AP) stem (Figure 1.8). The proximal stem is also coated with a thin hydroxyapatite (HA) layer (minimum 50 microns thick). Hydroxyapatite, $\text{Ca}_{10}(\text{PO}_4)_6(\text{OH})_2$, is a bioactive material which promotes healing bone to grow into the pores to permanently fixate the prosthesis. This process is known as “osseointegration”.

The term “osseointegration” was introduced by Brånemark when it was observed that chambers made of titanium could become permanently incorporated with living bone tissue [Brånemark, P.I., 1983]. This biological phenomenon allows the formation of a permanent and stable fixation of bone tissue with the titanium oxide layer of an implant. When an implant is osseointegrated, there is no progressive relative movement between the implant and the bone with which it has direct contact.

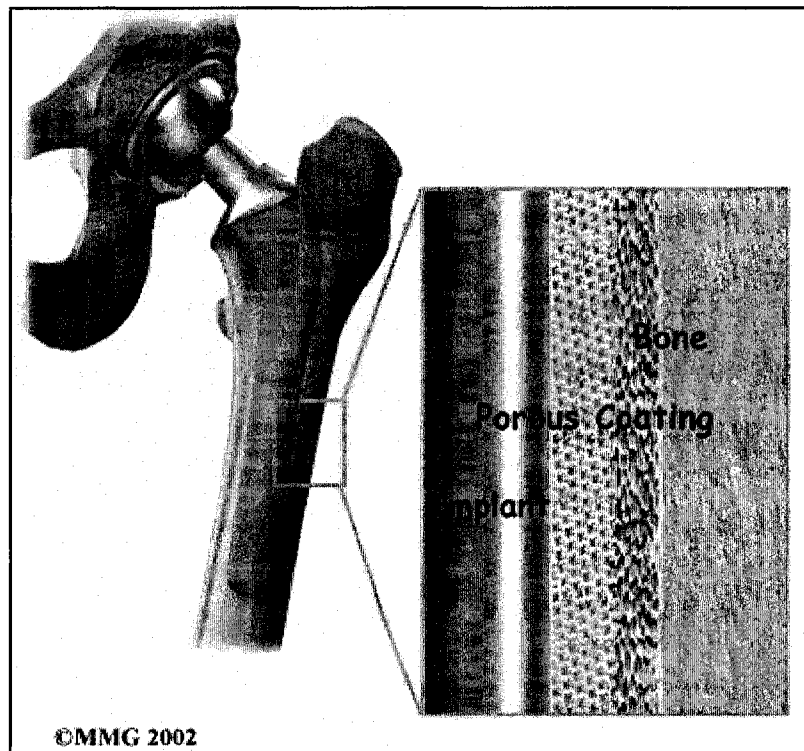


Figure 1.8: Detailed view of the uncemented implant surface and periprosthetic bone interface.
(Image provided courtesy of Medical Multimedia Group, LLC)

1.3.5 Total Hip Arthroplasty: Rate of Occurrence and Demographic

According to the Canadian Joint Replacement Registry, there were approximately 48,400 total hip and total knee replacement procedures in 2002-2003, representing a one-year increase of 10% from approximately 44,000 procedures in 2001-2002 [Canadian Institute for Health Information, 2005]. In the United States alone, according to the American Academy of Orthopaedic Surgeons, there were approximately 491,000 hip and knee arthroplasty procedures performed in 2001 [American Academy of Orthopaedic Surgeons (AAOS), 2004]. AAOS also reported that total hip replacement surgeries accounted for approximately 165,000 of these performed procedures. Internationally, nearly 800,000 total hip arthroplasties are performed annually [White *et al.*, 2000].

In the past, hip replacement surgery was an option primarily for people over 60 years of age. In the United States, approximately 60% of total hip replacement recipients are aged 65 and over [American Academy of Orthopaedic Surgeons, 2004]. More recently, younger and more active people have also been receiving hip replacements due to injuries sustained during highly active activities and participation in more extreme sports.

1.3.6 Total Hip Replacement (THR) Procedure

Total hip replacement is a major operation and is usually performed under a general anaesthetic. The patient is sedated and experiences no pain or surgical pressure during the procedure. The operation itself takes approximately two to three hours and the patient stays in the hospital for approximately a week or less, until it is safe to walk with the aid of sticks or crutches.

Once the patient is sedated and ready for the procedure, the orthopaedic surgeon begins by making an incision on the anterior-lateral side of the thigh, over the hip joint. After the incision is made, the ligaments and muscles are separated and clamped back to allow the surgeon access to the hip joint area. When the hip joint is exposed, the femoral head is disjointed from the acetabulum socket. Using a

power saw, the femoral head is then separated (Figure 1.9a) from the femur bone.

After the femoral head is removed, the acetabulum socket is also prepared using a reamer (Figure 1.9b). The reamer removes the articular cartilage and prepares the acetabulum socket to receive the acetabular shell and sleeve (Figure 1.9c). The acetabular component of the hip prosthesis is now ready for the femoral component.

To prepare the femur to receive the femoral stem, a special set of rasps are used to gradually shape and hollow out the cancellous bone of the femur to the exact shape of the distal stem of the femoral component of the hip prosthesis, as shown in Figure 1.9d. During an uncemented prosthesis procedure, once the proper shape is achieved, the femoral stem is press-fitted into the cavity (Figure 1.9e) using a mallet. If the surgeon has elected to use a cemented type of prosthetic, bone cement would be applied to fixate the stem with the surrounding bone material. Once the femoral stem is in place, the femoral head component (ball) is placed onto the neck of the femoral stem, as shown in Figure 1.9f. The prosthetic femoral head can now be inserted into the prosthetic acetabular sleeve. The total hip replacement system is now fully assembled (Figure 1.10). Before the incision is closed, the surgeon will perform a series of tests to confirm that the total hip replacement system is in place and performing properly. If necessary, the surgeon will make adjustments prior to closure.

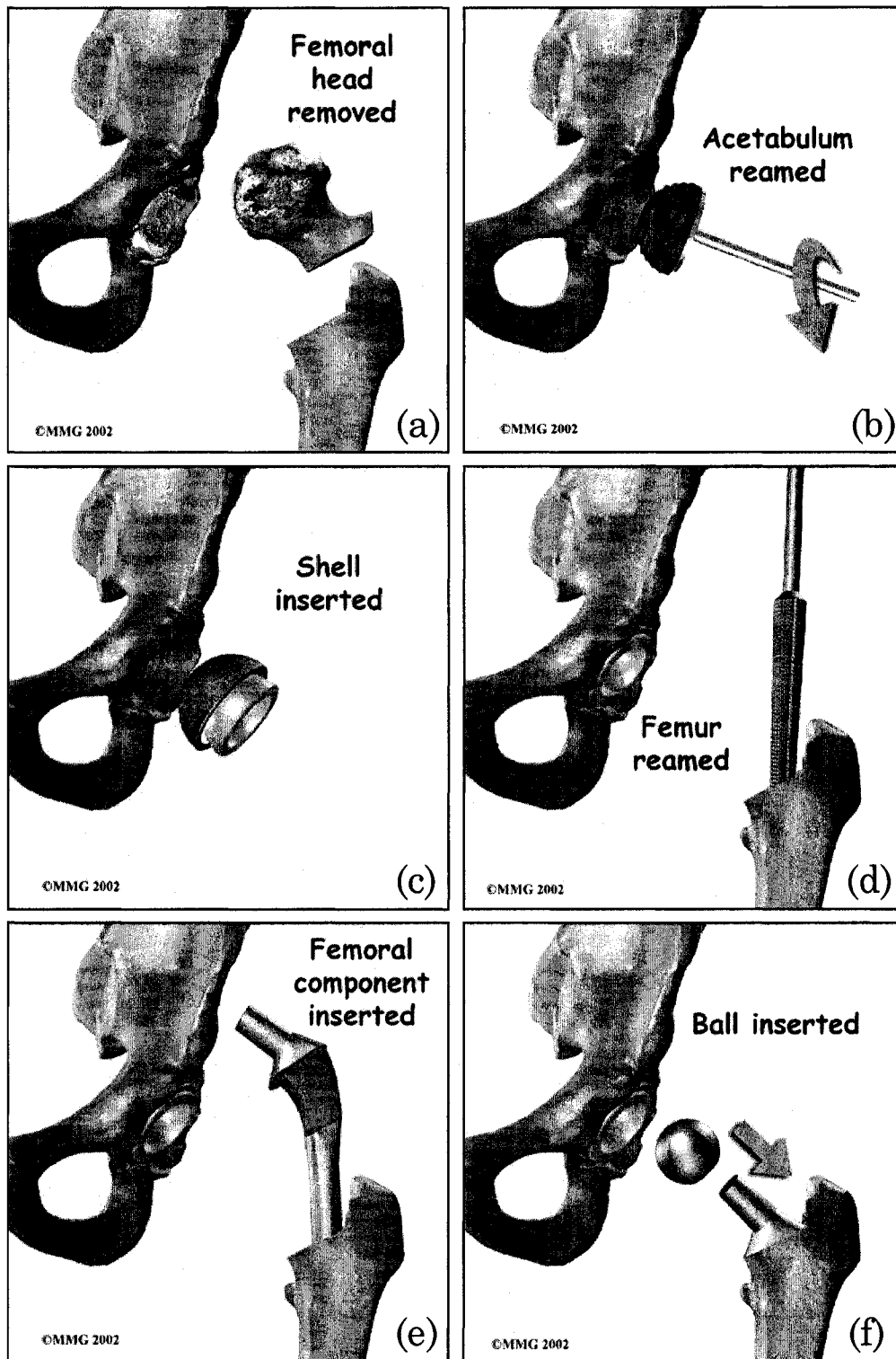


Figure 1.9: Total Hip Replacement procedure
 (Image provided courtesy of Medical Multimedia Group, LLC)

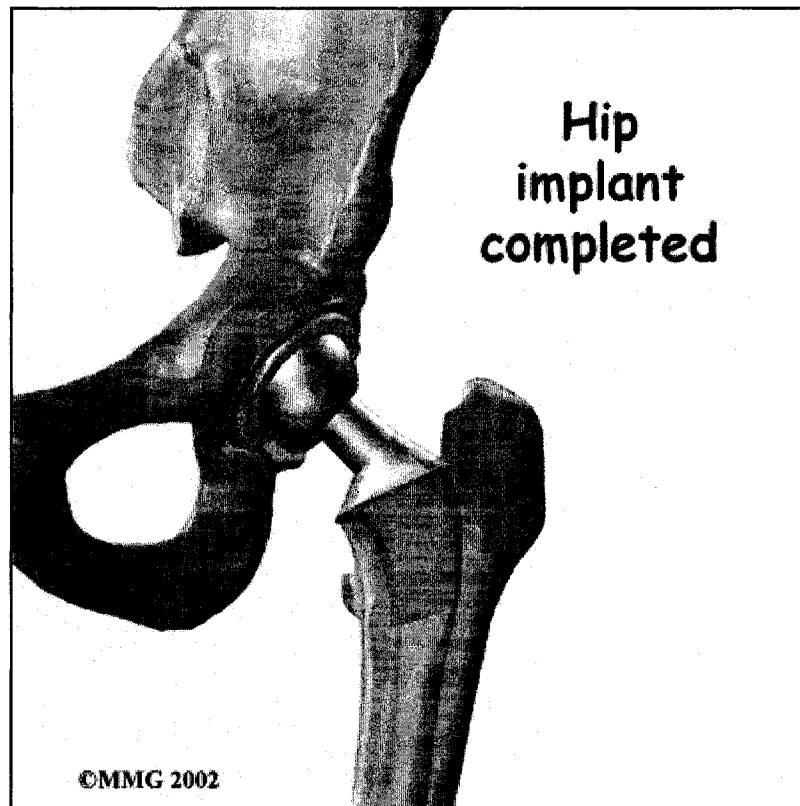


Figure 1.10: Completed Total Hip Replacement
(Image provided courtesy of Medical Multimedia Group, LLC)

Chapter 2

Literature Review

2.1 Mechanical assessment of bone properties

Mechanical testing of bones has been performed for over a century. Various investigators have attempted to characterize the mechanical properties of bones using a variety of methods such as tensile [Rho *et al.*, 1993], compressive [Carter *et al.*, 1977], indentation, flexure, fatigue and vibrational [Doherty *et al.*, 1974; Khalil *et al.*, 1981] testing on a variety of different bone specimens, from small sections to intact long bones.

Although these various methods are mechanically proven, these techniques are only applicable for *in vitro* testing for excised bone material or cadaver bones.

More recently, in the last thirty years, investigators have utilized ultrasonic techniques [Yoon and Katz, 1976; Singh, 1989; Rho, 1996; Strelizki *et al.*, 1997; Ouedraogo *et al.*, 2002; Lasaygues *et al.*, 2005], quantitative computed tomography (QCT) [Lotz *et al.*, 1990; Ciarelli *et al.*, 1991; Rho *et al.*, 1991; Kuiper *et al.*, 1997; Cuppone *et al.*, 2004] as well as dual energy x-ray absorptiometry (DEXA) methods [Pearson *et al.*, 1995; van Lenthe *et al.*, 2001] to quantify bone properties.

2.2 Diagnostic assessment techniques following total hip replacement

2.2.1 Current diagnostic assessment techniques

Previously mentioned quantitative techniques are also used for clinical assessment of fixation quality of hip prostheses. A number of authors have reported using dual energy X-ray absorptiometry for determination of periprosthetic bone quality [Kiratli *et al.*, 1992; Cohen *et al.*, 1995; Kroger *et al.*, 1996; Nakamura, 1996; Wixson *et al.*, 1997; Venesmaa *et al.*, 2001; Okano *et al.*, 2002].

However, the most commonly utilized clinical *in vivo* assessment technique of fixation quality involve conventional imaging-based techniques such as plain x-ray radiographs and its various forms [Phillips and Kattapuram, 1982; O'Neill and Harris, 1984; Van der Lande *et al.*, 1986]. The diagnostic sensitivity and reproducibility of these methods are inadequate in quantitatively assessing or predicting loosening of hip prosthetics [Gerogiou and Cunningham, 2001; Röder *et al.*, 2003] and there is no real consensus on the radiological signs [Li *et al.*, 1995]. In addition, exposure to x-radiation may impose health hazards and would not be suitable for long-term monitoring [Huang *et al.*, 2002].

2.2.2 Proposed vibrational diagnostic techniques for health-monitoring of loosened hip prosthetics

A number of researchers have proposed and investigated the validity of a number of non- or low-invasive diagnostic techniques to aid in ascertaining loosening of hip prosthetics. In 1979, Chung *et al.*, first explored the concept of using vibration testing to diagnose prosthesis loosening. Chung *et al.* developed a diagnostic technique that assessed the integrity of cemented total hip replacement systems *in-vitro* (in an artificial environment outside the living organism) by using sound in the audio range to mechanically excite the femoral hip components. Using this low energy diagnostic technique, it was proposed that if the coupled bone, implant and cement system were mechanically excited by a sinusoidal force over a band of

frequencies, as the cement cured, it would produce a shifting in the values of the resonant frequencies. This theory was tested by using three embalmed, partially excised human femurs that were fitted posthumously with a cemented femoral prosthetic. The frequency response of the composite bone-implant-cement system was determined at various time intervals after prosthesis implementation. As the cement polymerized and matured, there was indeed an upward shift in the frequency response of the composite system. Another study by Van der Perre [1984] also found variations in the natural frequency measurements of dry femurs with fixed and loose prostheses and also reported a decrease in the resonant frequencies of femurs with loose prostheses.

Rosenstein *et al.*, [1989] also explored the validity of vibration analysis to distinguish between firmly cemented implants and loose femoral prostheses, in *in-vitro* and *in-vivo* situations. This study utilized both cadaveric femurs as well as patients in a clinical study. Rosenstein *et al.* criticized that the techniques presented by Chung *et al.* and Van der Perre required non-realistically available baseline information and proposed a method that did not necessitate this type of information. This study also concluded that the vibrational output signal is altered when loosening occurs. The bone-prosthesis unit produced a pure output signal when the femoral stem was firmly implanted and when loosening occurred, the loosening components produced sustained superimposed output signals. Most significantly, this study determined that a soft tissue interface, such as fat, muscle and skin, does not appreciably alter the ability to obtain satisfactory output signals. Rosenstein *et al.* also reported that the energy levels required to perform the test were not uncomfortable for the patients.

In the mid-1990s, additional work by Li *et al.*, [1995, 1996] was completed to determine the diagnostic sensitivity of vibrational analysis in identifying early prosthetic loosening. Using plastic models and cadaver femora, different stages of loosening were simulated. All the femora were fitted with an implanted prosthesis and the distal third of the femur was introduced to a sinusoidal force. The output signal was detected near the greater trochanter using an accelerometer. The results of this study determined that this particular method was reliably detecting late loosening, but performed poorly in differentiating between early mechanical

loosening and a secure implant. In addition, specimens with cement fracture or fibrous tissue at the interface exhibited a similar vibrational response as the secure implant. The study (Li *et al.*, [1996]) also observed that the results of a securely implanted system were qualitatively consistent with linear vibrating beam theory.

More recently, others have also explored the validity of utilizing vibration-based damage detection techniques to assess the integrity of *in vivo* hip prostheses [Georgiou and Cunningham, 2001; Lieven *et al.*, 2001]. Lieven *et al.* [2001] collected experimental frequency-responses from various patients and presented neural network processed data that could be used to classify loose and fixed prostheses. Georgiou and Cunningham [2001] also gathered experimental data from a number of THR patients and evaluated of the accuracy of the collected vibrometry data and the radiographs. The results of this particular study indicated that vibration testing was shown to be 20% more sensitive and able to diagnose 13% more patients when compared with radiographs from the same patients.

Gang *et al.*, [2003] also addressed the feasibility of a vibrational diagnostic tool in detecting arthroplasty loosening. Using computer models of a cemented, uncollared, straight stem, they concluded that when the size of failure was greater than one-third of the femoral stem length, vibrational analysis provided a reliable diagnosis. In addition, it was observed that motion at higher harmonics was the most sensitive to interface failure.

In 2004, Jacques *et al.* presented a vibrational technique to assess the quality of fixation of cementless hip prostheses. A full modal analysis was performed using hammer excitation of a horizontally suspended femur with a cemented implant. In addition, finite element analysis was utilized to determine the mode shapes of two commercially available cemented stems as well as a custom-made cementless stem. Experimentally, three conditions were addressed: (1) well cemented, (2) only cemented in the distal region and (3) "clinically mobile" (displacement of approximately 1mm sensed by hand). These experiments indicated that only severe loosening would be detectable when the first bending mode of the femur was excited. Their preliminary finite element analysis (of the various prostheses alone) suggests that distal defect of the bone/implant interface should be more readily detectable than a proximal deflections. In addition, an increase in the

resonance frequency shift was observed during higher mode numbers. Jaecques *et al.* also commented that accurate non-invasive vibration measurement would require an instrumented prosthesis with telemetry capabilities. Interestingly, Puers *et al.* [2000] presented a prototype telemetry system and tested the apparatus in non-specific cadaver experiments. Data collection was achievable and the authors suggested clinical trials of the device would be necessary to determine the value of such a device. However, published follow-up studies of such a device are unavailable to date. Nevertheless, interest in the application of vibrational techniques to assess post-operative total hip replacement is ongoing.

2.2.3 Other proposed diagnostic techniques for health-monitoring of loosened hip prosthetics

Arpaia *et al.* [2005] introduced an EIS-based approach (Electrical Impedance Spectroscopy) to diagnose prosthetic osseointegration. The study detailed a method for resolution improvement and noise reduction. The experimental results indicated that this particular approach is capable of detecting the presence of an interface layer as well as potentially characterizing its thickness and biological nature.

Another approach was explored by Browne *et al.* [2005] and they presented an acoustic emission (AE) technique to monitor structural degradation and predict failure mechanisms for cemented total hip replacement constructs. The experimental results suggest that the use of acoustic emission can successfully locate and monitor damage in bone cement. In addition, this particular method can simultaneously monitor debonding and cement cracking.

Chapter 3

Material Definition and Mechanical Properties

3.1 Bone Physiology

3.1.1 Wolff's Law

In the late 19th century, Julius Wolff attributed the concept of “functional adaptation” to describe the adaptive ability of bone to structurally optimize itself (its internal architecture) in response to the magnitude of mechanical stimuli (or applied load) that the bone experiences. In summary, Wolff proposed that “mechanical stress was responsible for determining the architecture of bone....” [Forwood and Turner, 1995]. In other words, "remodelling of bone ... occurs in response to physical stresses - or to the lack of them - in that bone is deposited in sites subjected to stress and is resorbed from sites where there is little stress" [Salter, 1999]. This concept is known as “Wolff's Law” and is generally accepted as the foundation of bone remodelling. As published in 1892, Wolff's Law states:

“Every change in the form and the function of a bone or of their function alone is followed by certain definite changes in their internal architecture, and equally definite secondary alterations in their external confirmation, in accordance with mathematical laws.”

3.1.2 Stress Shielding Effect

The capacity of bones to properly remodel itself around an implanted prosthesis is vital and it has been proven that mechanical stress is necessary in order to stimulate osteogenesis and bone remodelling. Within 24 - 48 hours following a hip replacement surgery, patients are encouraged to walk a couple of steps at a time with the aid of a walker. Around the third postoperative day, the patient is allowed full weight-bearing walking with the aid of crutches [Gustilo, 1988] and start transferring loads to the implant to stimulate bone formation on the bone and implant interface. However, it is also now known that the certain implant designs are more successful than others for transferring stress onto the periprosthetic bone. This is due to a phenomenon known as “stress shielding”. According to Hooke’s Law (Equation 3.1), in every composite (multi-component) system of varying material properties, the component that is stiffer (higher elastic modulus, E_{high}) will sustain the greater part of the load (or localized stress, σ), thereby “stress shielding” the less stiffer components (lower elastic modulus, E_{low}).

$$\sigma = E\varepsilon \quad (3.1)$$

Where:

- σ = stress
- E = modulus of elasticity (Young’s Modulus)
- ε = strain

For an isostrain condition (perfect interfacial adhesion) [see Voigt, 1889], the strain at the bone and implant interface is assumed equal and therefore:

$$\varepsilon_{effective} = \varepsilon_{bone} = \varepsilon_{implant} \quad (3.2)$$

Furthermore:

$$\varepsilon_{effective} = \frac{\sigma_{bone}}{E_{bone}} = \frac{\sigma_{implant}}{E_{implant}} \quad (3.3)$$

Since the femoral stem is comprised of a material with a much higher elastic modulus (such as titanium) than the periprosthetic bone, the bone is subjected to a proportionally lower localized load. Therefore, in accordance with Wolff's Law, less applied stress on the bone will facilitate resorption of the bone, osteopenia or bone lysis, which can lead to aseptic loosening of the implant or femoral fracture [Fredin *et al.*, 1987].

In order to reduce stress shielding, various implant manufacturers are developing components that attempt to diminish the stress shielding effect by minimizing the stiffness differential between the femoral stem component and the cancellous bone. Currently, most commercially available hip prostheses are made of cobalt-chrome and stainless steel (titanium) alloys due to its biocompatibility, high corrosion resistance and high wear debris resistance. However, metallic stems are approximately 20 to 40 times stiffer than femoral bone. More recently, some manufacturers are exploring the possibility of utilizing advanced composites for implant applications.

Advanced composite materials appear to be promising since manufacturers can determine variables such as material selection, spatially-controlled ingredient composition and fibre orientation, which can customize the strength and stiffness properties of the composite materials [Allcock and Ali, 1997; Cheal *et al.*, 1992; Evans and Gregson, 1992]. Analytical and experimental studies have shown that stress shielding is lower for a composite prosthesis in comparison with metallic alloy prostheses [Cheal *et al.*, 1992; Huiskes *et al.*, 1992; Otani *et al.*, 1993a,b; Glassman *et al.*, 2001; Senapati and Pall, 2002]. Clinical studies with animals have also demonstrated that the use of composite stems can increase proximal bony ingrowth [Turner *et al.*, 1997], enhance stability [Magee *et al.*, 1988], increase proximal medullary bone density [Turner *et al.*, 1997] and enhance proximal load transfer [Sumner *et al.*, 1997]. However, despite the number of advantages of composite implants, there are potential drawbacks and concerns that must also be addressed. Lower stiffness stems, although more mechanically compatible, will also inherently produce higher particulate wear debris generation due to lower wear resistance [Li *et al.*, 2003]. Also, existing sterilization techniques that are associated with metallic implants, involve high temperatures and cleaning solvents which may lead to

damage to the composite implant or subsequent leaching of toxic material into the bio-environment [Evans and Gregson, 1998] or inversely, the composite implant may be susceptible to swelling and degradation from joint fluids [Park, 1984].

3.1.3 Structure of Bone

Bones in the arms and legs, such as the femur, are considered to be long bones, while bones in the wrists and ankles are known as short bones. In general, bones are comprised mainly of two main types: cortical and cancellous bone (Figure 3.1). The shaft of the long bone is known as the diaphysis and the transitional region between the diaphysis and epiphysis regions is known as the metaphyseal region.

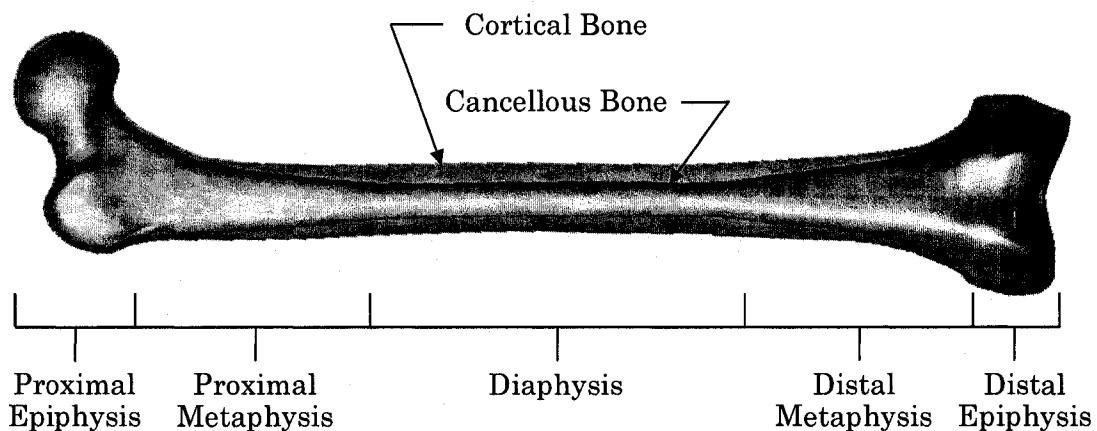


Figure 3.1: Femur – Cancellous and Cortical bone components.

Cortical bone (also known as compact bone) is dense and forms a protective layer around the cancellous bone material. The cortical bone is comprised of a series of adjacent concentric formations called osteons, which form a Haversian system (Figure 3.2). Within the osteons, Haversian canals contain capillaries, arterioles, venules and nerves. Each osteon is composed of concentric layers of lamellar tissue that alternate in fibre orientation, which contributes to the strength properties of the cortical bone. Between the concentric lamellar tissues, the bone cells (osteocytes) are located in cavities called lacunae. Small channels (canaliculi) radiate from the lacunae to the osteonic canal to provide a system of interconnecting pathways throughout the lamellae [Nordin and Frankel, 2001] as shown in Figure 3.3.

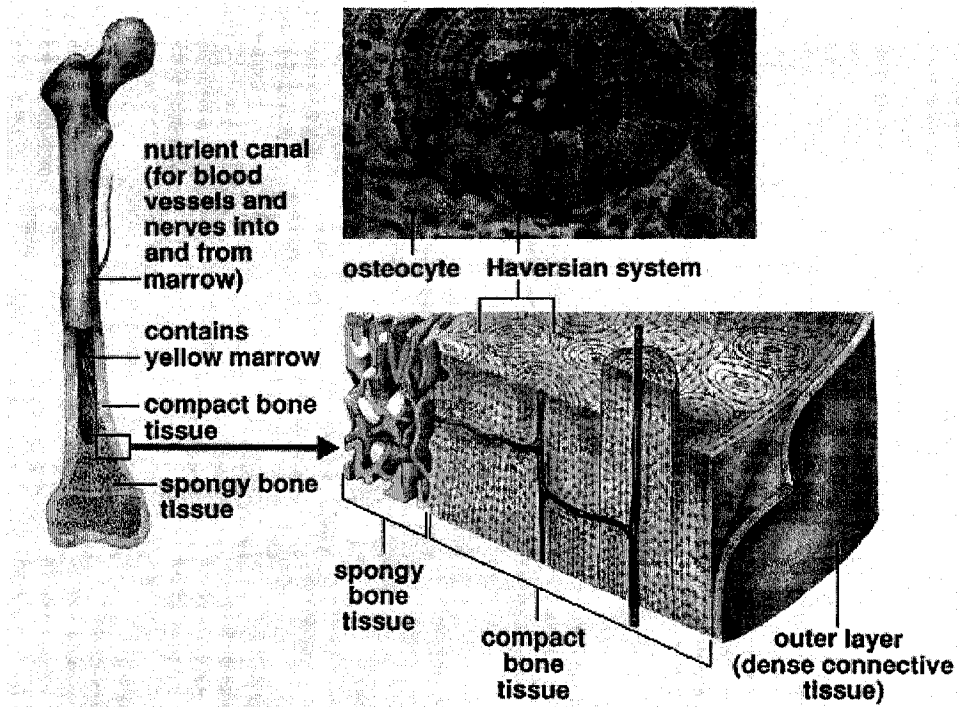


Figure 3.2: Structure of Femoral Bone.
 [Adapted from Starr and Taggart, 2001, page 652]

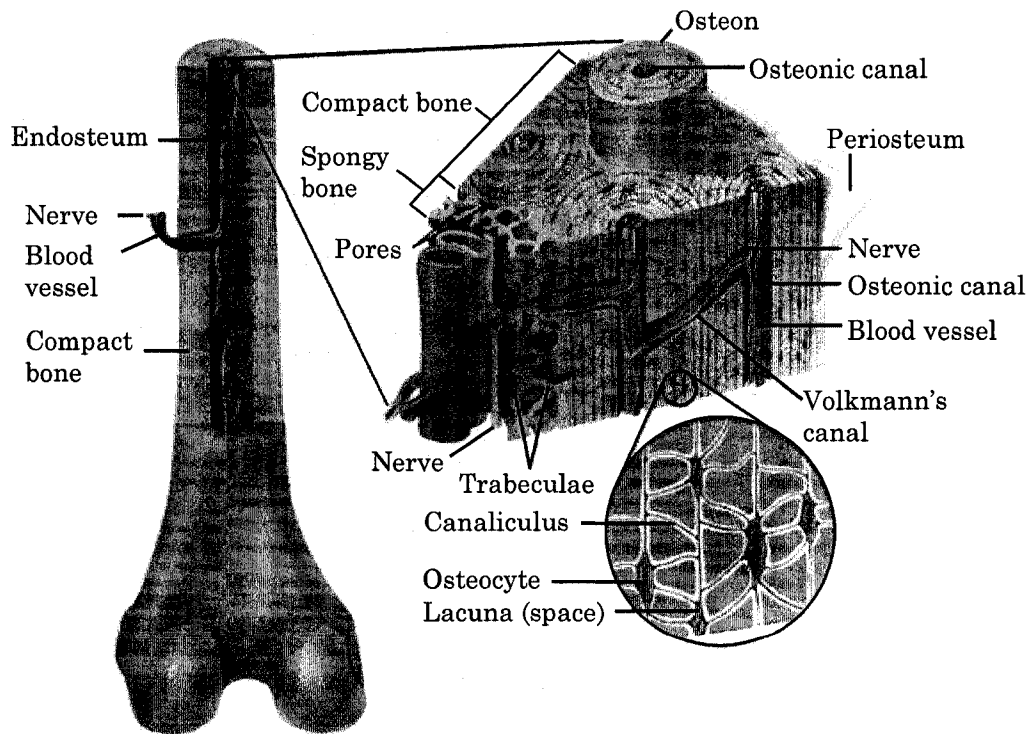


Figure 3.3: Cortical Bone - dense bone tissue consisting of an arrangement of closely associated Haversian systems of osteons.
 [Adapted from Shier *et al.*, 1996, page 190].

Cancellous bone is a network of spongy-appearing, trabecular bone tissue resembling a lattice of bars, struts, plates and marrow filled cavities with large spaces between them (Figure 3.4) and is found within the inner canal of the bone. The term “cancellous bone” refers to the porous bulk material matrix of the bone while the term “trabecular bone” is used when describing the tissue of the bars, struts and plates itself [Rho *et al.*, 1993]. Mechanical measurements show that the elastic and strength properties of the individual trabeculae are much larger than the bulk volume of cancellous bone [Ashman *et al.*, 1988], which also includes the influence of the pores. For cancellous bone, the ratio of the combined volume of the pores to the total bone volume (porosity) may range from 30 to 90%, while compact bone has a porosity of approximately 5 to 30 % [Carter *et al.*, 1977].

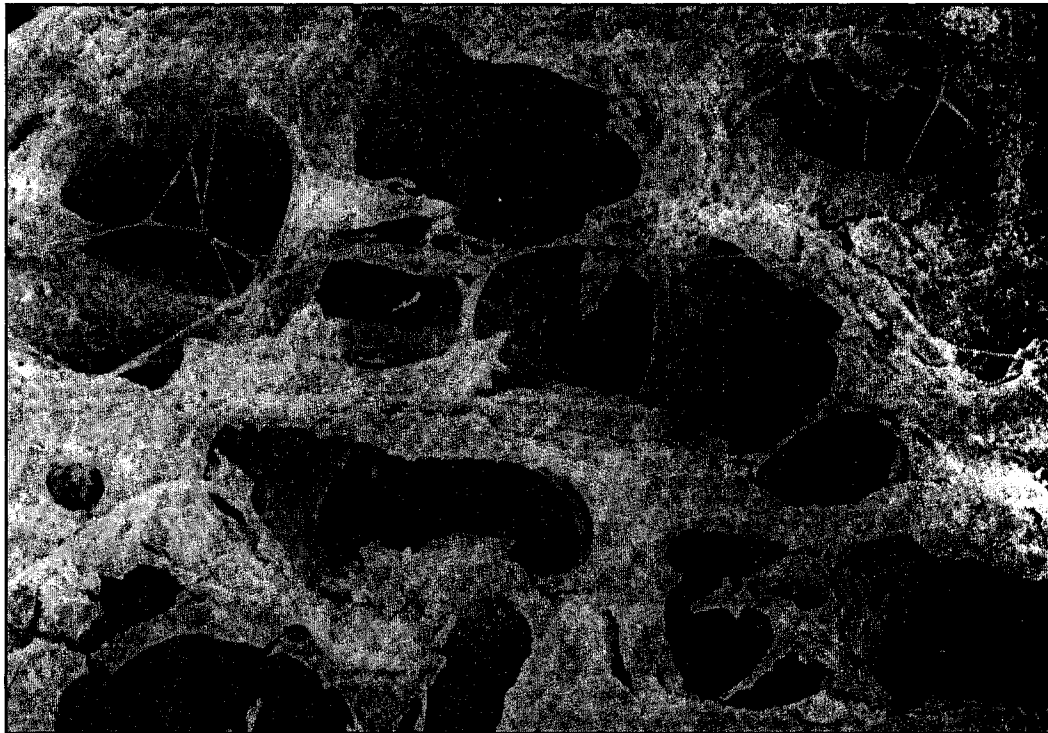


Figure 3.4: A scanning electron microscopic view of the sheet and strut arrangement of the cancellous bone lattice from the upper femur. [Martens *et al.*, 1983]

3.2 Mechanical Properties of Bone

3.2.1 Heterogeneity and Anisotropy of Bone

Bone is a composite material that exhibits both anisotropy (material elasticity varies with loading direction) as well as substantial heterogeneity (material elasticity varies with location) [Pope and Outwater, 1974; Ashman *et al.*, 1988]. Trabecular bone, in particular, is highly anisotropic in both modulus and strength [Hodgkinson and Currey, 1990; Ciarelli *et al.*, 1991; Galante *et al.*, 1970]. Since the anisotropic behaviour of trabecular bone develops in response to its functional responsibilities [Wolff, 1986], the principal mechanical axis (longitudinal) is generally associated with the largest modulus.

Although bone is highly anisotropic and heterogeneous, two major experimental studies of trabecular bone properties in the proximal femur by Brown and Ferguson [1980] and Martens *et al.*, [1983] have shown that density differences account for 10- to 100-fold deviations in material properties, whereas anisotropy accounts for only 2- to 4-fold differences. Therefore, it is reasonable to assume that a first-order estimate of the material properties of trabecular bone can be made with data on density alone. [Lotz *et al.*, 1990]. Furthermore, since the elastic modulus of the implant's titanium material is substantially larger (20- to 80-fold difference) in comparison with the cancellous bone material, it is also reasonable to apply isotropic properties for the cancellous bone to parametrically establish the influence of density (and hence elastic modulus) on the modal response of the implant.

3.2.2 Mechanical Properties of Cortical Bone: Cited Values

Since cortical bone material is anisotropic [Katz and Meunier, 1987], there are slight variations in reported material properties (Table 3.1 and 3.2). These differences may be attributed to variations in porosity, mineralization and osteonal direction [Currey, 1988; Schaffler and Burr, 1988; Reilly and Burstein, 1974]. The anisotropy of cortical bone has been characterized by various investigators [Reilly and Burstein,

1975; Yoon and Katz, 1976] and it is now commonly accepted that cortical bone material is approximately transversely isotropic (higher strength and stiffness in the longitudinal direction than in the transverse direction) [Carter and Spengler, 1978]. Experiments by Morgan [2003] and Reilly *et al.* [1974] showed no significant difference ($p = 0.9$) in modulus of elasticity values that were determined by tension or compression tests. Burstein *et al.* [1976] also noted that there was not any appreciable difference ($p > 0.05$) in cortical bone properties between males and females. In addition, the same study revealed that the elastic modulus of the femoral diaphyseal cortex tissue only decreased by approximately 2.2% per decade.

The available data on Poisson's ratio (ν) for cortical bone is very limited and only a small number of investigators have published values. It is generally accepted and reasonable to utilize a Poisson's ratio of 0.3.

Table 3.1: Available data on the Poisson's ratio of Femoral Cortical Bone.

Authors	Specimen Site (No. of Specimens)	Poisson's Ratio
Ashman <i>et al.</i> (1984)	Metaphysis and Diaphysis of Femur (60)	0.235 - 0.422
Reilly <i>et al.</i> (1975)	Middle third cortex of femora (201)	0.460 - 0.580

Table 3.2: Summary of cited mechanical properties (apparent density and elastic modulus) of Femoral Cortical Bone, by selected investigators using various testing methods and protocols.

Where available, values are quoted as mean \pm standard deviation.

Authors	Specimen Site (No. of specimens)	Position of bone specimen	Young's Modulus (MPa)	Apparent Density (g/cm ³)	Method
Ashman <i>et al.</i> (1984)	Metaphysis and Diaphysis of Femur (60)	Superior-Inferior	20000	N/A	Ultrasonic
		Radial	12000		
		Circumferential	13400		
Bayraktar <i>et al.</i> (2004)	Femoral diaphyseal region (74)	Principal orientation of local trabeculae	19900 \pm 1800	0.43 - 0.75	Mechanical Testing and FEA
Burstein <i>et al.</i> (1976)	Femoral diaphyseal cortex (11)	Superior-Inferior (20-29 yrs. old)	18000 \pm 280	N/A	Mechanical Testing
	Femoral diaphyseal cortex (9)	Superior-Inferior (30-39 yrs. old)	18600 \pm 140		
	Femoral diaphyseal cortex (12)	Superior-Inferior (40-49 yrs. old)	18700 \pm 1480		
	Femoral diaphyseal cortex (18)	Superior-Inferior (50-59 yrs. old)	18200 \pm 610		
	Femoral diaphyseal cortex (27)	Superior-Inferior (60-69 yrs. old)	15900 \pm 680		
	Femoral diaphyseal cortex (14)	Superior-Inferior (70-79 yrs. old)	18000 \pm 1860		
	Femoral diaphyseal cortex (4)	Superior-Inferior (80-89 yrs. old)	15400		
Lotz <i>et al.</i> (1991)	Metaphyseal shell of proximal femora (123)	Longitudinal	12500 \pm 2140	1.72 \pm 0.1	Mechanical Testing
		Transverse	5990 \pm 1520	1.73 \pm 0.07	
Evans (1976)	Femoral Cortex (35) Avg. age = 41.5 yrs.	Longitudinal	14600	1.91	Mechanical Testing
	Femoral Cortex (35) Avg. age = 71 yrs.	Longitudinal	13600	1.85	
Reilly <i>et al.</i> (1975)	Middle third cortex of femora (170)	Superior- Inferior	17000	N/A	Mechanical Testing
	Middle third cortex of femora (31)	Transverse	11500	N/A	
Reilly <i>et al.</i> (1974)	Human femoral diaphysis (196)	Superior- Inferior	17100 \pm 3150	N/A	Mechanical Testing
Rho <i>et al.</i> (1993)	Tibial diaphyseal cortex (20)	Superior- Inferior	18600 \pm 3500	1.817 \pm 0.138	Mechanical Testing and FEA
Zysset <i>et al.</i> (1999)	Femoral diaphyseal cortex (1401)	Superior- Inferior	20100 \pm 5400	N/A	Nanoinden- tation

3.2.3 Mechanical Properties of Cortical Bone: Implemented Values

Given the available data regarding the material properties of femoral cortical bone, the mechanical properties that were implemented in this study are listed in Table 3.3. The value used for the modulus of elasticity (12000 MPa) is based on an extensive investigation by Ashman *et al.* [1984] and is in close to agreement to Reilly's results [1975]. It would also seem reasonable to apply an apparent density of 1.8 g/cm³ and a Poisson's ratio of 0.3.

Table 3.3: Implemented values for Cortical Bone in this study.

Material	Young's Modulus (E)	Apparent Density (ρ)	Poisson's ratio (ν)
Femoral Cortical Bone	12000 MPa (Radial)	1.8 g/cm ³	0.3

3.2.4 Mechanical Properties of Cancellous Bone: Cited Values

In order to conduct a parametric study of the bone properties and include a wide range of potential patients (due to biological variations in age, gender, weight, state of health), an investigation of the mechanical behaviour of cancellous bone in the proximal femur was required. As well, a range of the material properties values would need to be established.

There have been numerous published studies [Wirtz *et al.*, 2000; Turner *et al.*, 1999; Ashman and Rho, 1999; Rice *et al.*, 1988; Martens *et al.*, 1983; Reilly *et al.*, 1974] attempting to establish cancellous and trabecular bone properties. However, the collected data is widely varying and very inconsistent (Table 3.4) due to its substantial heterogeneity and anisotropy [Keaveny *et al.*, 2001; Goldstein, 1987].

Table 3.4: Summary of cited mechanical properties of Femoral Cancellous Bone, by selected investigators using various testing methods and protocols. Where available, values are quoted as mean \pm standard deviation.

Authors	Specimen Site (n)*	Position† of bone specimen	Apparent Density (ρ) (g/cm ³)	Young's Modulus (E) (MPa)	Method
Ashman and Rho (1988)	Human Femora (3)	Principal orientation of local trabeculae	0.28 - 0.38	959 - 2170	Ultrasound
Augat <i>et al.</i> (1998)	Human proximal Femora (29)	SI	N/A	137 \pm 25	Computed Tomography (CT Scan)
		ML		68 \pm 10	
		AP		54 \pm 11	
Banse (1996)	Human femoral heads (20)	Parallel to femoral head axis	N/A	Right: 1142 \pm 570 Left: 1132 \pm 546	Mechanical Testing
Brown and Ferguson (1980)	Proximal femur (800)	SI	N/A	3386	Mechanical Testing
		ML		2595	
		AP		1967	
Carter <i>et al.</i> (1980)	Proximal and Distal Femora (2)	Principal orientation of local trabeculae	0.20 - 0.80	50 - 2000	Mechanical Testing
Ducheyne <i>et al.</i> (1977)	Distal Intracondylar femur (183)	SI	0.60 - 0.12	59 - 5943	Mechanical Testing
Galante <i>et al.</i> (1970)	Human Vertebral bone (71)	SI	0.16 - 0.27	N/A	Mechanical Testing
		ML	0.17 - 0.30		
		AP	0.15 - 0.36		
Marten <i>et al.</i> (1983)	Proximal Femora (Intertrochanteric area) (20)	SI	N/A	317 \pm 293	Mechanical Testing
		ML		263 \pm 170	
		AP		12.5 \pm 6.4	

* n = number of specimens tested.

† Orientation of bone specimen during testing:

AP = Anterior-Posterior Direction

ML = Medial-Lateral Direction

SI = Superior-Inferior Direction

While the previously mentioned studies focused on measuring mechanical properties, various authors [Morgan *et al.*, 2003; Augat *et al.*, 1998; Goldstein, 1987] have also postulated that the architecture and location of the trabecular structures contribute to the strength properties of the cancellous bone. Pope and Outwater [1974] also considered the variation in the mechanical properties as a function of position and orientation of the bone. As well, Whitehouse and Dyson [1974] presented micrographs from various regions in the proximal femur and a comparison of the micrographs showed that in regions of low stress, it appeared lower in density. In addition, open-celled, rod-like structures were present. In areas of high stress, the region was higher in density and was comprised of closed cells and plate-like structures. However, Morgan *et al.* [2003], Harrigan *et al.* [1981] and Ducheyne *et al.* [1977] also reported that trabecular specimens with the same density could exhibit different strength properties due to anatomic location, directional orientation and the structure of the individual trabecula. The variability of these numerous parameters could possibly account for the inconsistency of reported material properties and the anisotropy of cancellous bone. Goldstein [1987] also noted that testing protocols and conditions such as loading direction, temperature, moisture content, specimen preparation technique and storage conditions of the cancellous bone specimens would also make it difficult to compare data from various investigators.

Despite the huge inconsistencies in material properties, several investigators have also attempted to ascertain a mechanical relationship between apparent density and the elastic modulus of cancellous bone. The “apparent density” of cancellous bone is defined as “the mass of mineralized trabeculae divided by the (bulk) volume occupied by both trabeculae and pores” [Ashman and Rho, 1988], whereas the term “material density” corresponds to the “mass of trabeculae, divided by the volume of the trabeculae alone” [Ashman and Rho, 1988]. The “elastic modulus” (or Young’s modulus, E) describes the measure of the stiffness (resistance to deformation) of a given material and, within the limits of elasticity, it is defined as the ratio of the applied linear stress (σ) to the resulting strain (ϵ), as shown in Equation 3.4 and 3.5.

$$E = \frac{\sigma_{\text{applied}}}{\epsilon_{\text{resulting}}} \quad (3.4)$$

Where:

$$\epsilon_{\text{resulting}} = \frac{\Delta L}{L} = \frac{L' - L}{L} \quad (3.5)$$

And: L = original length prior to applied load
 L' = deformed length after applied load

Published data suggests that, within an appropriate density range, the compressive elastic modulus can be expressed as a function of density using an empirically derived linear relationship [Ciarelli *et al.*, 1991; Martens *et al.*, 1983; Ducheyne *et al.* 1977] or a power-law model, as shown in Equation 3.6 and 3.7 [Morgan *et al.*, 2003; Ciarelli *et al.*, 1991; Lotz *et al.*, 1990; Carter and Hayes, 1977], with the density raised to the power between one and three as shown in Table 3.5.

$$E = A\rho^B \quad (3.6)$$

Or: $\log E = \log A + B \log \rho \quad (3.7)$

Where: E = modulus of elasticity
 ρ = apparent density
 A, B = experimentally derived constants

Table 3.5: Summary of power law relationships between apparent density and modulus of elasticity of cancellous bone by selected investigators using various testing methods and protocols.

Note: r^2 = variation in the dependent variable (E) accounted for by the independent variable (ρ). A r^2 value close to one denotes a strong correlation between E and ρ .

Authors	Specimen Site (n)*	Position† of bone specimen	Empirical Model E = f(ρ)	r^2	Apparent Density (ρ)	Young's Modulus (E) (MPa)	Method
Carter and Hayes (1977)	Tibial Plateaus (100)	Principal orientation of local trabeculae	$2875\rho^3$ (at strain rate of 0.01 sec ⁻¹)	N/A	0.15 - 0.75 (g/cm ³)	10 - 1213	Mechanical Testing
Ciarell <i>et al.</i> (1991)	Proximal metaphyseal femur (54)	SI	1797ρ	0.50	0.15 - 0.80 (g/cm ³)	186 - 993	Mechanical Testing and CT Scan
		ML	791ρ	0.31		182 - 633	
		AP	1241ρ	0.48		270 - 1438	
Ciarell <i>et al.</i> (1991)	Proximal metaphyseal femur (54)	SI	$A\rho^{2.17}$	0.55	0.15 - 0.80 (g/cm ³)	N/A	Mechanical Testing and CT Scan
		ML	$A\rho^{1.38}$	0.40		N/A	
		AP	$A\rho^{1.94}$	0.48		N/A	
Lotz <i>et al.</i> (1990)	Proximal femora (49)	Principal orientation of local trabeculae	$1304\rho^{1.4}$	0.91	0.13 - 1.20 (g/cm ³)	78 - 1530	Mechanical Testing and CT Scan
Morgan <i>et al.</i> (2003)	Greater trochanter (23)	SI	$15010\rho^{2.18}$	0.82	0.14 - 0.28 (g/cm ³)	203 - 924	Mechanical Testing and CT Scan
	Femoral neck (27)	SI	$6850\rho^{1.49}$	0.85	0.26 - 0.75 (g/cm ³)	921 - 4462	
Rho <i>et al.</i> (1995)	Proximal femora (≥ 32)	SI	$-331+4.56\rho$	0.90	100 - 1000 kg/m ³	≤ 4200	CT Scan
		ML	$-506+3.64\rho$	0.89		≤ 3100	
		AP	$-657+3.91\rho$	0.90		≤ 3200	
Rho <i>et al.</i> (1995)	Proximal femora (≥ 32)	SI	$0.58\rho^{1.3}$	0.91	100 - 1000 kg/m ³	230 - 4607	CT Scan
		ML	$0.01\rho^{1.86}$	0.89		53 - 3802	
		AP	$0.004\rho^{2.01}$	0.94		42 - 4286	

* n = number of specimens tested.

† Orientation of bone specimen during testing:

AP = Anterior-Posterior Direction, ML = Medial-Lateral Direction, SI = Superior-Inferior Direction

3.2.5 Mechanical Properties of Cancellous Bone: Implemented Values

For this particular study, the material properties assigned for the cancellous bone will be based on the results published by Lotz *et al.* [1990]. The material properties documented by Lotz *et al.* were used for a number of reasons. The development of Lotz *et al.*'s power law addressed the heterogeneity of cancellous bone due to factors such as location of trabecular bone sample and age of sample population. This particular research was one of few studies that specifically investigated the relationship between apparent density and the modulus elasticity of cancellous bone in the proximal femur region. In addition, the distribution of population studied by Lotz *et al.* was also older (average age = 65) and more age-appropriate, given the physical status of a typical hip replacement recipient. In addition, the apparent density (ρ) range that was evaluated by Lotz was also reasonable (0.13 - 1.20 g/cm³). The lower end of the density range would characterize a patient with bone lysis present, while the higher end of the density range would be indicative of a patient with a healthy and fully osseointegrated implant.

Lotz *et al.* reported a power law relationship between the modulus of elasticity and apparent density as:

$$E = 1310\rho^{1.4} \quad (3.8)$$

Where: E = modulus of elasticity (MPa)
 ρ = apparent density (g/cm³)

And: $0.13 \text{ g/cm}^3 \leq \rho \leq 1.20 \text{ g/cm}^3$

Therefore, for healthy cancellous bone, the implemented value of elastic modulus is 1691 MPa and the apparent density is 1.20 g/cm³. The Poisson's ratio (ν) of cancellous bone has a range of 0.01 - 0.35 with an average of 0.12, as cited by Wirtz *et al.* [2000]. As a result, the Poisson's ratio of healthy cancellous bone is 0.12 for this study, as shown in Table 3.6.

Table 3.6: Implemented values for Healthy Cancellous bone in this study. Healthy cancellous bone will also be referred to as “Host” bone to differentiate from cancellous periprosthetic bone.

Material	Apparent Density (ρ) (g/cm ³)	Young's Modulus (E) (MPa)	Poisson's ratio (ν)
Healthy Femoral Cancellous (Host) Bone	1.2	1691	0.12

3.2.6 Mechanical Properties of Periprosthetic Bone

Periprosthetic bone is defined as the volume of cancellous bone that surrounds the implant and exhibits changes in material properties, as the implant becomes osseointegrated. The “host” bone is defined as the original healthy cancellous bone that surrounds the healing, periprosthetic bone volume and is assumed to be beyond the range of influence of the periprosthetic bone and implant interface (Figure 3.5).

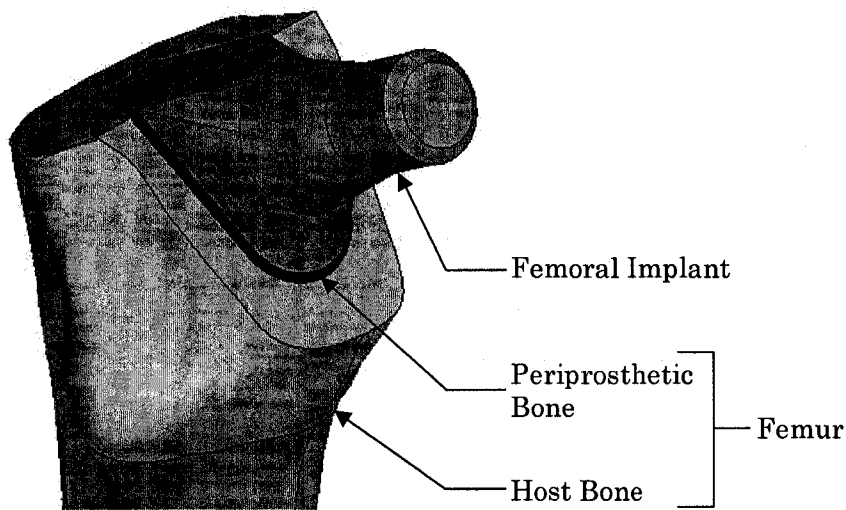


Figure 3.5: CAD model of Femoral Host bone and Periprosthetic Bone surrounding a femoral implant stem.

The apparent density of the periprosthetic bone varied between 0.13 - 1.20 g/cm³ while the host bone (or “healthy” bone) was constant at 1.20 g/cm³. The bone properties used in this study are summarized in Table 3.7 and the corresponding

elastic modulus was calculated using Lotz's power law (Equation 3.8). As mentioned previously, the apparent density range (0.13 - 1.20 g/cm³) that Lotz *et al.* evaluated encompasses a wide range of health conditions. The lower end of the density range would characterize a patient with severe bone lysis present, while the higher end of the density range would be indicative of a patient with healthy periprosthetic bone and a fully osseointegrated implant.

Table 3.7: Values of the Host and Periprosthetic cancellous bone properties used in this study. The values of the elastic modulus and apparent density were determined using the power law relationship ($1310\rho^{1.40}$) developed by Lotz *et al.* [1990] and the Poisson's ratio is cited from Wirtz *et al.* [2000].

Type of Cancellous Bone	Apparent Density (ρ) (g/cm ³)	Young's Modulus (E) (MPa)	Poisson's ratio (ν)
Periprosthetic Bone	0.13 - 1.20	75.3 - 1690.9	0.12
Host Bone	1.20	1690.9	0.12

3.3 Femoral Stem

3.3.1 Type and Model of Femoral Stem

The femoral stem utilized in this particular study is a Secur-Fit™ HA stem by Stryker® Howmedica Osteonics (Kalamzoo, Michigan). This particular model is made of titanium alloy (TMZF™) and is a cementless, interference-fit femoral stem (as shown in Figure 3.6).

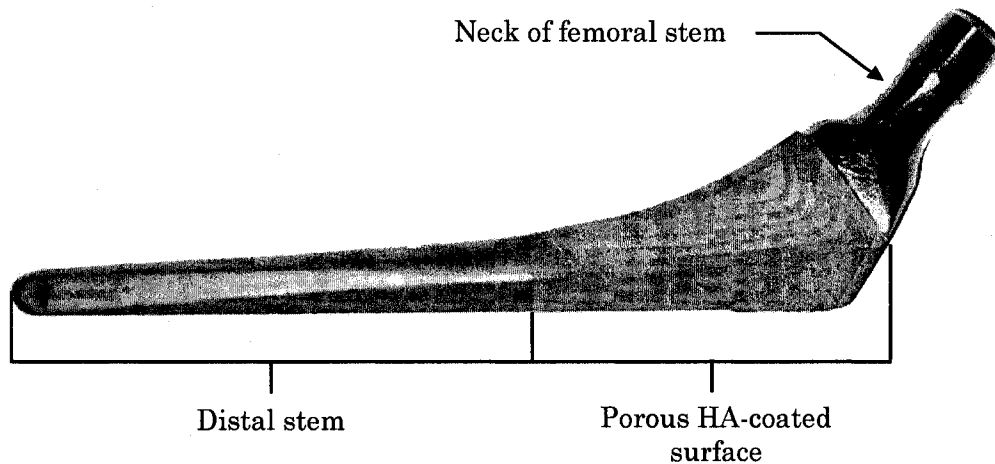


Figure 3.6: Stryker® Howmedica Osteonics' Secur-Fit™ HA stem.

The Secur-Fit™ HA femoral stem was chosen for a number of reasons. Firstly, this study required the inclusion of a cementless-type femoral stem in order to eliminate the necessity of modeling and incorporating the *in vivo* response of bone cement and its affect on the modal analysis of the implant. In addition, according a national survey (with a participation rate of 67%) by the Canadian Institute for Health Information (CIHI) and the Canadian Joint Replacement Registry (CJRR; a national registry that collects information on total hip and total knee replacements performed in Canada), 61% of the hip replacements were cementless [Canadian Institute for Health Information, 2005]. Secondly, the Secur-Fit™ HA stems have a good clinical track record [Cinats, 2005] and are clinically versatile since it is available in different sizes and neck angles and are easy to insert [Cinats, 2005].

In addition, according to a preliminary survey of 992 hip replacement recipients compiled by the Canadian Institute for Health Information (CIHI) and the Canadian Joint Replacement Registry, between May 2001 and March 2002, Stryker® Howmedica Osteonics provided more than half (54%) of the total hip components. A list of manufacturers is shown in Figure 3.7. The next most common supplier provided only 23% of the components (of the patients surveyed) during the same time period. Component-specific (femoral stem and acetabular component) manufacturer distributions are shown in Figures 3.8 and 3.9, respectively. It should be noted that the sample size was small and represented approximately 5% of the total number of hip replacements performed in Canada during the aforementioned time period.

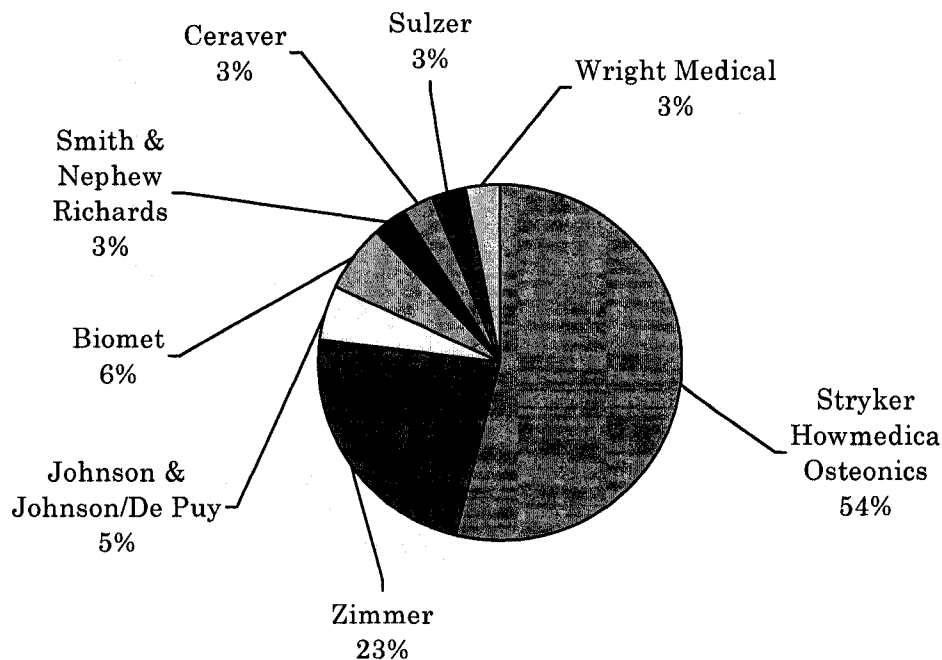


Figure 3.7: Manufacturer Breakdown for Total Hip Replacement Components based on a survey of 992 hip replacement recipients between May 1, 2001 – March 31, 2002. Survey was conducted in Canada by the Canadian Institute for Health Information. [Adapted from CIHI, 2002]

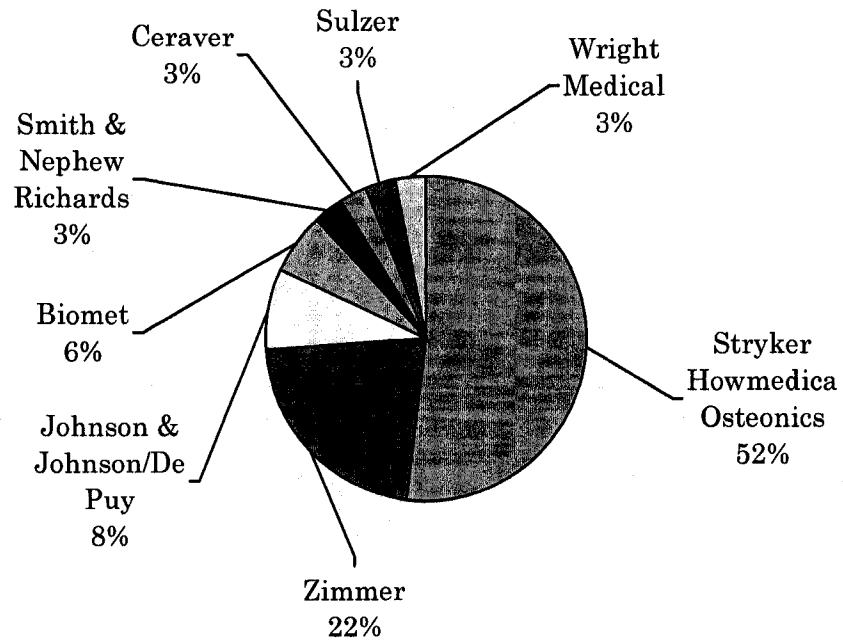


Figure 3.8: Manufacturer Breakdown for Femoral Stem Components based on a survey of 992 hip replacement recipients between May 1, 2001 – March 31, 2002. Survey was conducted in Canada by the Canadian Institute for Health Information. [Adapted from CIHI, 2002]

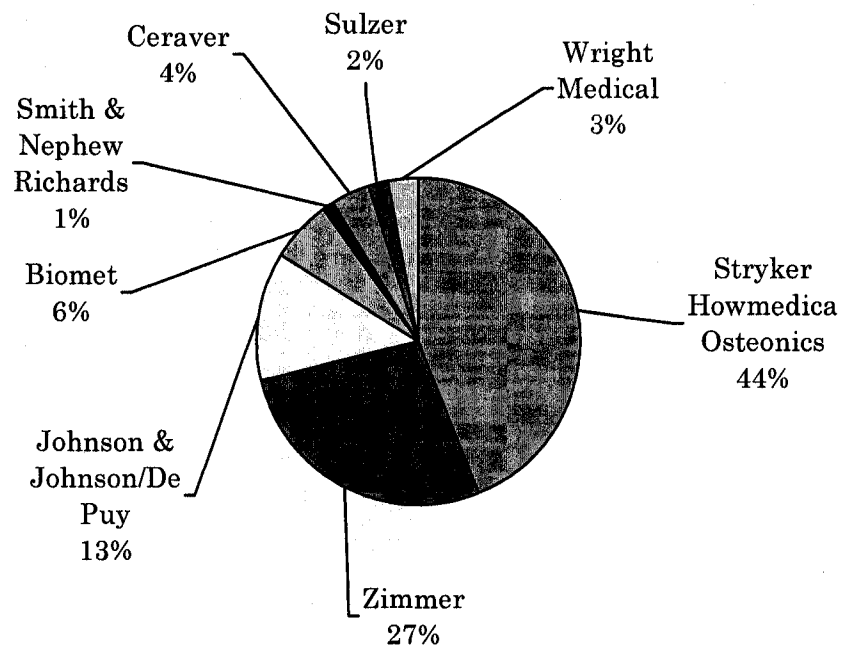


Figure 3.9: Manufacturer Breakdown for Acetabular Components based on a survey of 992 hip replacement recipients between May 1, 2001 – March 31, 2002. Survey was conducted in Canada by the Canadian Institute for Health Information. [Adapted from CIHI, 2002]

3.3.2 Mechanical Properties of Femoral Stem

Stryker® Howmedica Osteonics' Secur-Fit™ femoral stem is comprised of a beta titanium alloy developed by Howmedica R&D. This particular alloy is identified as Ti-12Mo-6Zr-2Fe and is known commercially as TMZF™. The properties of TMZF™ are summarized in Table 3.8.

Table 3.8: Published mechanical properties of TMZF™.

Alloy Type	Yield Strength (MPa)	Ultimate Strength (MPa)	Elongation in Area (%)	Material Density (kg/m ³)	Elastic Modulus (MPa)
TMZF™	1000 - 1060	1060 - 1100	18 - 22	4982	74000 – 85000

The 3-D, computer-aided design (CAD) version of the Secur-Fit™ HA stem is designated in this study as model S16M9 (Stryker, Version 16, Metric Model, Version 9). Due to geometric differences in the CAD model, the volume of the CAD S16M9 stem was slightly larger than the actual Secur-Fit™ stem (more details in Chapter 4.2.2). Therefore, the applied material density of the TMZF™ was modified so that the mass of the CAD model femoral stem (S16M9) had the same mass as the actual Secur-Fit™ stem (as shown in Table 3.9). The actual values of the TMZF™ properties that were used in this study are shown in Table 3.10. The implemented values for the elastic modulus and the elongation in area percentage were averaged.

Table 3.9: A comparison of material and geometric properties: Secur-Fit™ stem versus S16M9 model.

Implant Model	Material Density (kg/m ³)	Elastic Modulus (MPa)	Poisson's Ratio	Volume (m ³)	Mass (kg)
Secur-Fit™	4982.0	80000	0.2	2.91E-05	0.145
S16M9 (CAD model)	4137.9	80000	0.2	3.50E-05	0.145

Table 3.10: Implemented mechanical properties of TMZF™ in this study.

TMZF™	Elongation in Area (%)	Material Density (kg/m³)	Elastic Modulus (MPa)
Published values	18 - 22	4982.0	74000 - 85000
Implemented values	20	4137.9	80000

Chapter 4

Geometry and Finite Element Modeling

4.1 The Finite Element Method and Discretization of the Continuum

4.1.1 Finite Element Method

In the field of mechanics and engineering, there are many complex problems and not all problems can be solved using analytical methods. In such cases, numerical techniques are employed to simulate the problem and provide a potential solution. In many instances, numerical techniques are used to evaluate a large number of variables within a particular problem. This type of parametric analysis would not be easily achievable using analytical techniques. When utilized properly, numerical techniques such as the Finite Element Method (FEM) can reduce computational time, save money and provide an accurate solution in situations where analytical methods would be too prohibitive. The finite element method is a comparatively simple, robust and efficient method of obtaining an approximate numerical solution for a given mathematical model of a problem.

Before the solution process can occur, the physical problem must first be idealized or computationally simulated (Figure 4.1). This includes relevant physical dimensions, mechanical properties and boundary conditions such as loading conditions and constraints. In addition, the continuum must be discretized with the appropriate element types and element sizes to ensure accurate numerical simulation.

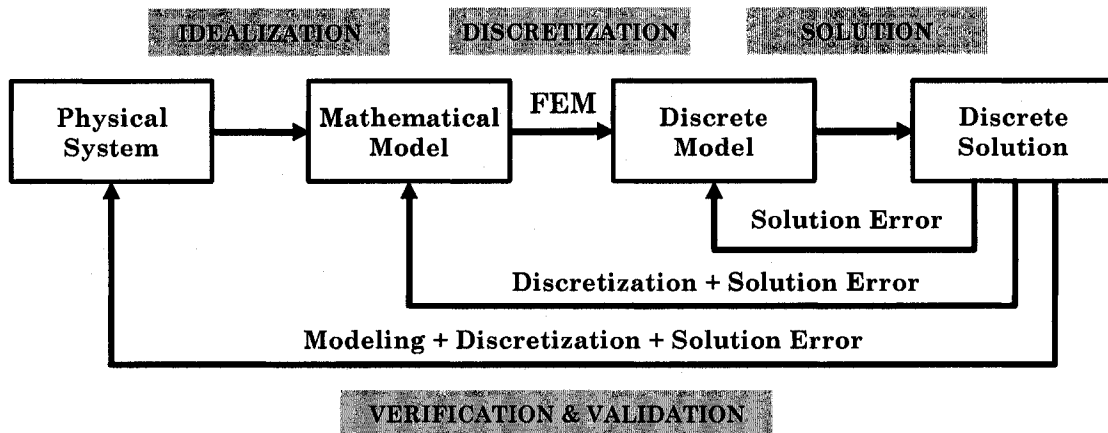


Figure 4.1: Finite Element Analysis Process [Adapted from Felippa, 2004]

4.1.2 Discretization of the Continuum

Conceptually, a body or structure (the continuum) may be divided, or discretized, into a number of smaller elements (Figure 4.2) of finite dimensions and a finite number degrees of freedom. A “node” defines the vertices of each element and these nodes are shared with adjacent elements to ensure continuity throughout the continuum. Some elements contain mid-line nodes, which are available for higher accuracy modeling of high curvature objects (Figure 4.3).

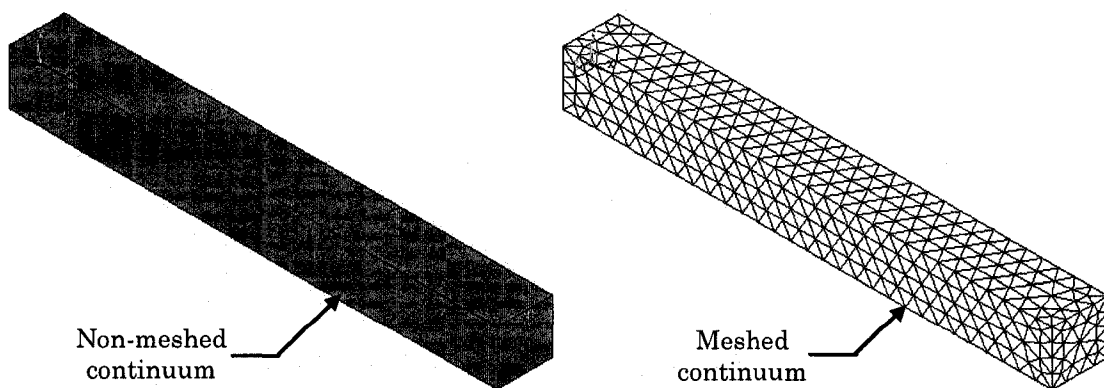


Figure 4.2: Discretization (meshing) of a Continuum

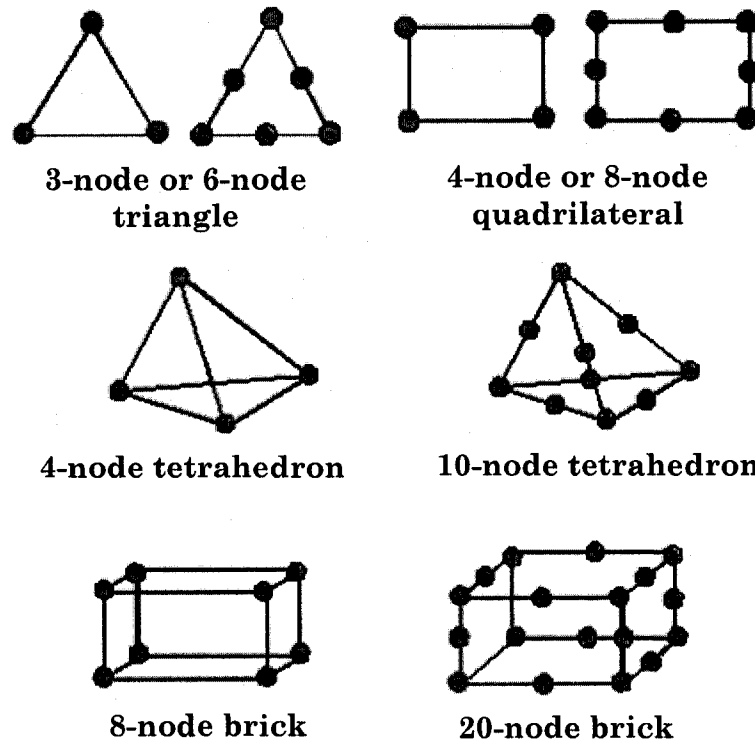


Figure 4.3: Various 2-dimensional and 3-dimensional Element Types

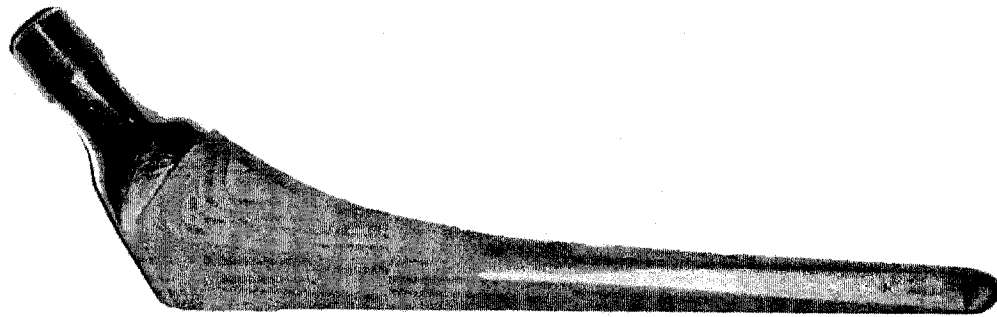
The discretization of the whole continuum (Figure 4.2) enables the formulation of the solution of its constituent elements, since it is usually easier to compute the local solution for each element. When this occurs, the necessary boundary and loading conditions are imposed and the equations of equilibrium are enforced at the nodes and then solved to obtain the global solution for the overall continuum. The essence of the finite element method is to take a complex problem (whose solution may be too difficult to obtain) and to decompose the actual problem into smaller-scaled localized problems upon which a simple approximation of its solution may be constructed. The local approximate solutions are then superpositioned to obtain a global approximate solution. Therefore, proper discretization (or meshing) is very important to the accuracy of the numerical analysis since errors can be compounded once the global solution is assembled.

4.2 Femoral Implant: CAD Model and Finite Element Model

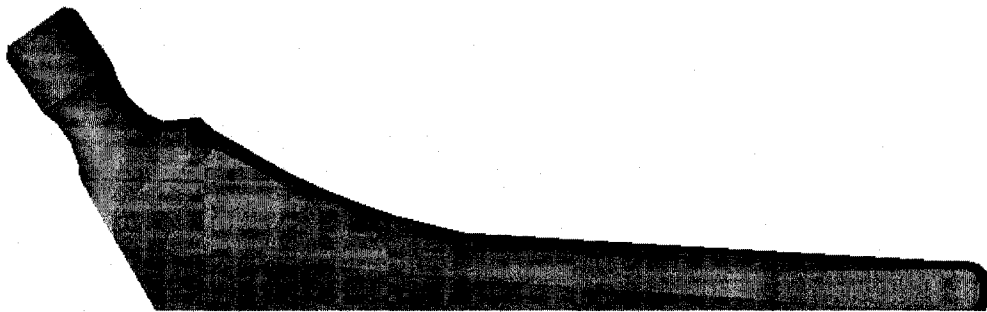
4.2.1 Creation of the CAD and Finite Element Model

The Computer-Aided Design (CAD) model of the Secur-Fit™ implant (Figure 4.4a) was created by the Author using a 3D solid-modeling package (SolidWorks®, Release 2001, SolidWorks Corporation, Concord, Massachusetts). The dimensions of the implant were determined by using reference points on the actual Secur-Fit™ implant and the various dimensions were manually measured using a Vernier caliper. Once the CAD model was created, an IGES file was produced and then imported directly into a Finite Element Analysis (FEA) program (ANSYS®, Release 8.1, Ansys Inc., Canonsburg, Pennsylvania). The IGES (Initial Graphics Exchange Specification) format provides a neutral-exchange file configuration for two-dimensional or three-dimensional CAD models or drawings and is often utilized when interfacing between dissimilar modeling packages and applications.

Although the initial creation of the implant model in the CAD program was relatively simple, the attainment of a SolidWorks®/ANSYS® compatible IGES model proved to be very laborious. In many instances, although the IGES models could be created and imported to ANSYS® per se, depending on the geometry, modeling method, exporting and importing options implemented, it influenced the manipulability of the model in the FEA environment. Once the CAD model is imported into the FEA program as a surface model, a solid volume model is required to be created so that material properties can be assigned to the solid volume. However, early generations of the CAD model did not allow the creation of a solid volume model and further manipulation of the implant model was hindered in the ANSYS® environment due to missing surfaces, Boolean operation tolerances or inconsistencies along adjacent surface boundaries of the IGES model, which prohibited volume creation. However, after many iterations, a compatible CAD model was achieved (Version S16M2 - Stryker, Version 16, Metric Model, Version 2), as shown in Figure 4.4b.



(a)



(b)

Figure 4.4: CAD model (Version S16M2) vs. Secur-Fit™ Implant
(a) Photo of Secur-Fit™ Implant (AP View)
(b) CAD model (Version S16M2) of the Secur-Fit™ Implant (AP View)

All Secur-Fit™ implants have “normalizations” on the anterior and posterior surfaces of the implant (Figure 4.5a). These normalizations are transitional “steps” or striations and were designed to transform hoop stress to compressive loads, provide potential for more efficient load transfer, help resist medial and distal migration and subsidence and also to provide maximized projected area to resist rotation [Stryker, 2004]. However, in order to facilitate the offsetting of the surfaces on the body of the implant to create the periprosthetic bone volume (see Section 4.3.2, Figure 4.19 for more details), the normalizations were removed (Figure 4.5b).

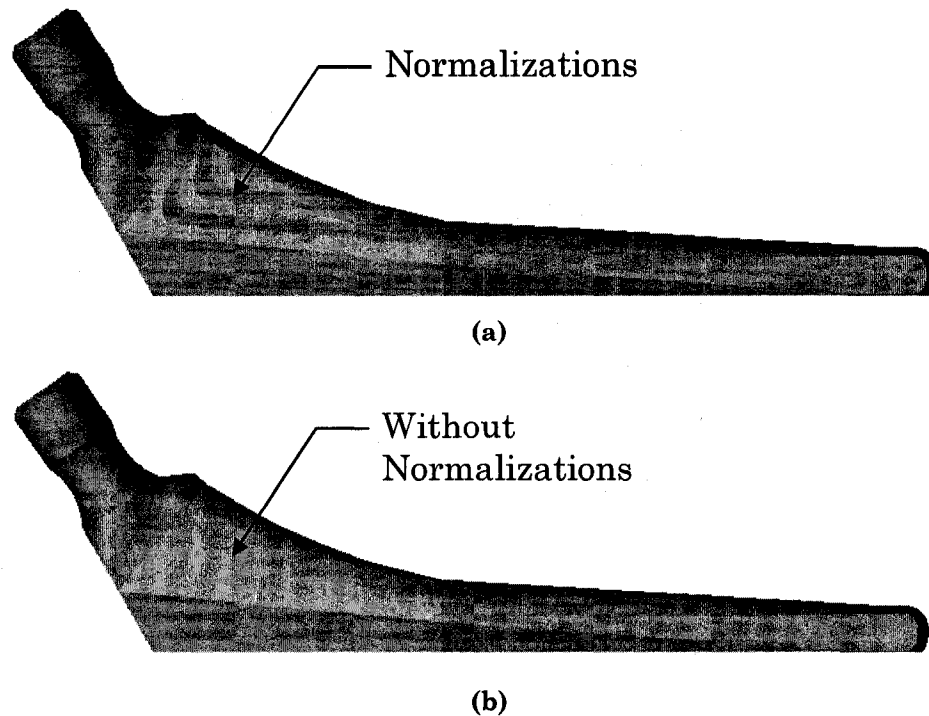


Figure 4.5: CAD model (Version S16M2) of Secur-Fit™ Implant (AP View)
(a) Implant with normalizations (b) Implant without normalizations.

4.2.2 Original CAD Implant Model (S16M2) versus Implemented CAD Implant Model (S16M9)

In order to further manipulate the FEA model of the implant during finite element analysis and decrease the processing time, slight geometric modifications were made to the S16M2 model to accommodate these requirements. Due to the capabilities of the CAD program and the modeling approach utilized by the Author, the original model (S16M2) was defined by a split line on the medial surface (Figure 4.6a) to facilitate the modeling of the curved profile of the body of the implant (Figure 4.6b).

However, it was necessary to remove the split line on the S16M2 model in order to create the periprosthetic bone volume by perpendicularly offsetting the medial surface of the implant. Therefore, the S16M2 model was altered in order to have one continuous surface (Figure 4.6c). However, as a result of this modification on the CAD model, the profile is no longer curved (Figure 4.6b vs. Figure 4.6d). This new model was designated as S16M9.

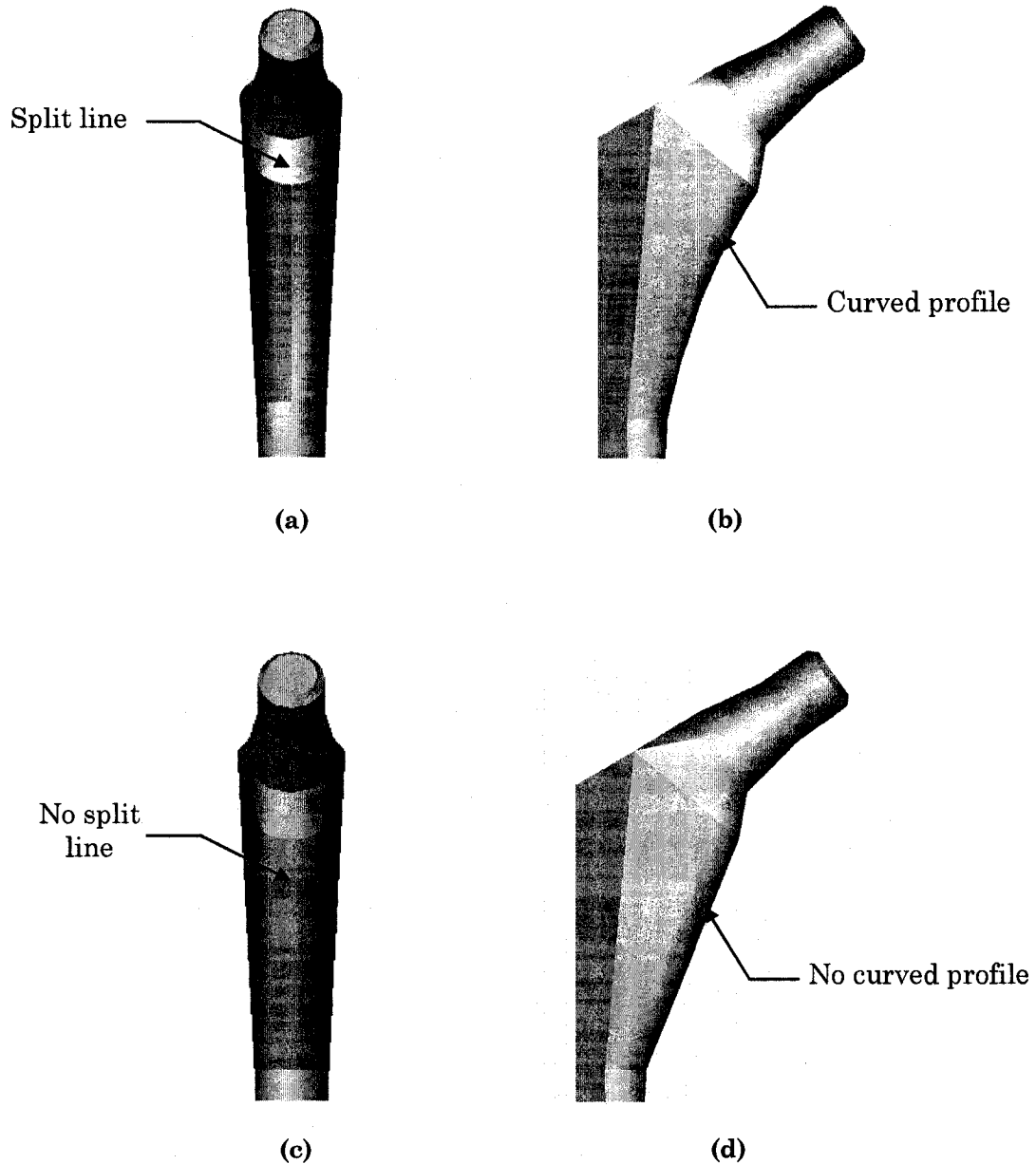


Figure 4.6: Comparison of S16M2 vs. S16M9 CAD models of the implant
(a) S16M2 (Medial View): Note split line along the medial surface of the implant
(b) S16M2 (Anterior-Posterior View): Note curved profile
(c) S16M9 (Medial View): Note NO split line along the medial surface of the implant
(d) S16M9 (Anterior-Posterior View): Note removed curved profile.

Following the previously mentioned geometric modifications of the implant model, an investigation was conducted to evaluate the frequency-response of the new S16M9 model and the old S16M2 model, to determine the consequences of altering the anterior-posterior profile of the implant. Both models were fully constrained on the surface of the hydroxyapatite-covered body of the proximal stem (Figure 4.7) since this is where the surface is coarsened with pores to facilitate osseointegration. As a result of the geometric modifications, the volume of the modified model (S16M9) increased slightly by 5.2%. Since the volume of the new S16M9 model ($3.50\text{E-}5 \text{ m}^3$) is slightly larger than the original S16M2 model ($3.32\text{E-}5 \text{ m}^3$), the density (implemented in the modal analysis) of the TMZF™ was adjusted accordingly to 4137.9 kg/m^3 in order to maintain the original mass of the Secur-Fit™ implant.

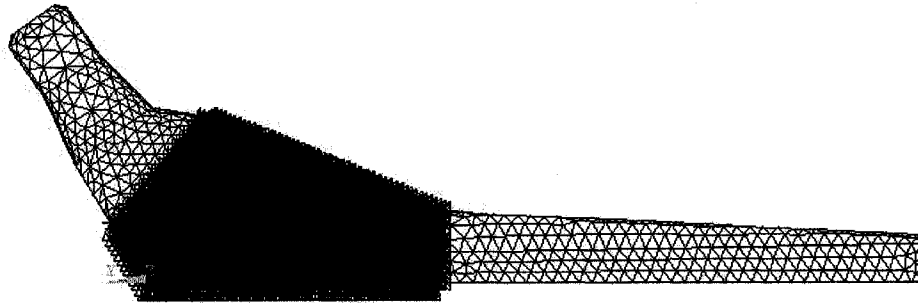


Figure 4.7: S16M9 model - Fully constrained nodes on the hydroxyapatite-covered, coarsened surface on the body of the proximal stem.

The modal analysis (frequency-response) results of the two models (Table 4.1 and Figure 4.8) varied approximately 2.4 – 4.2% (Figure 4.9) while the range and scale of the frequencies remained consistent and largely unaffected. In Case 1, the published density of TMZF™ (4982 kg/m^3) was used during the modal analysis of the S16M2 model. Since the volume of the S16M2 model was slightly larger than the actual implant, the mass of the S16M2 model was 0.164 kg, which is larger than the actual mass of the Secur-Fit™ model (0.145 kg). Therefore, the material densities in Case 2 and 3 were adjusted to correspond to the actual mass of the Secur-Fit™ model.

Table 4.1: S16M2 vs. S16M9: Material properties and modal analysis comparison (Elastic Modulus = 80 GPa).

Case No.	Implant	Properties		Mode No. and Frequency-Reponses (Hz)				
		Material Density (kg/m ³)	Mass (kg)	1	2	3	4	5
1	S16M2 Model	4982.0*	0.164	1107.3	1131.3	4744.1	4948.4	8970.6
2	S16M2 Model	4365.0	0.145	1183.0	1208.6	5068.3	5286.6	9583.7
3	S16M9 Model	4137.9	0.145	1155.1	1178.2	5280.8	5503.7	9869.2

*Density of TMZF™ (beta titanium alloy of femoral stem)

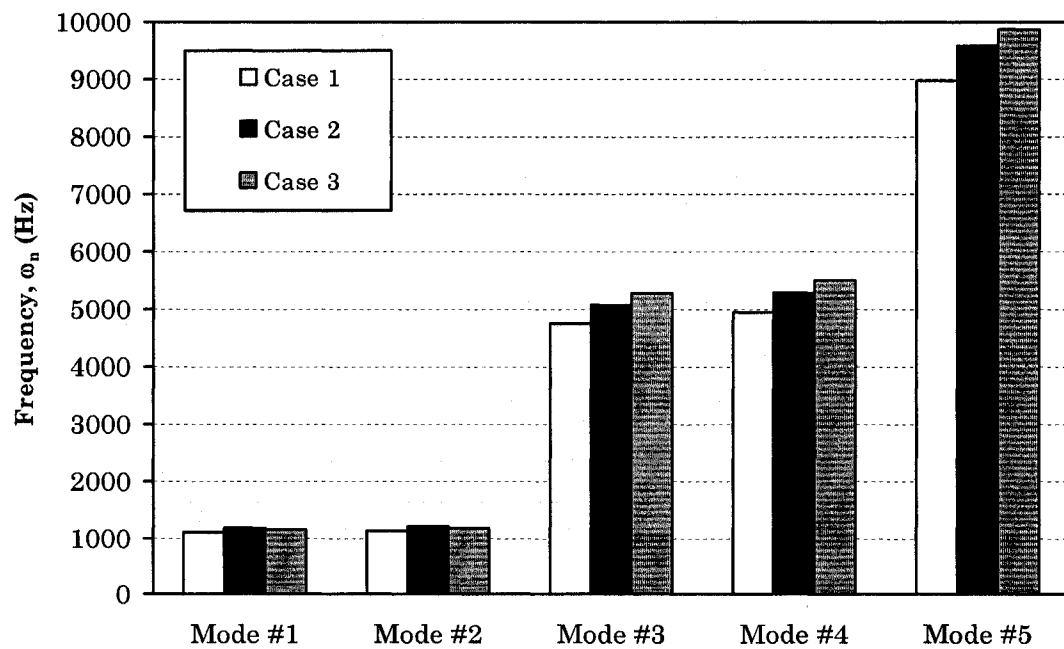


Figure 4.8: S16M2 vs. S16M9: Comparison of modal analysis results.

Since the absolute percent variation between modal results between Case 2 and Case 3 were relatively small (Figure 4.9), it was considered acceptable to continue to adopt and utilize the new S16M9 model. As a result, the properties of the implant material shown in Table 4.2 will be implemented for the modal analysis of the finite element (FE) model.

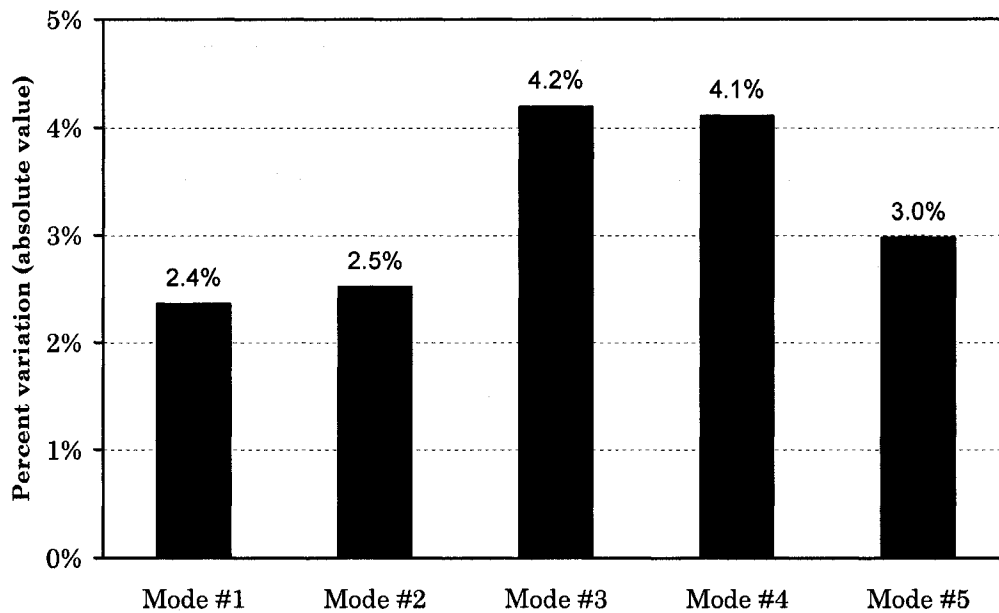


Figure 4.9: Percent variation of modal analysis results between Case 2 and 3 (as shown in Table 4.1), relative to Case 2 results.

Table 4.2: Implemented mechanical properties of the implant material (TMZF™) in this study.

TMZF™	Elongation in Area (%)	Material Density (kg/m ³)	Elastic Modulus (MPa)
Published values	18 - 22	4982.0	74000 - 85000
Implemented values	20	4137.9	80000

4.2.3 Numerical validation of Implant Model

To validate the computational implant model that was used in the study, a parametric modal analysis was conducted and the frequency results were compared. The numerical validation process is shown in Figure 4.10.

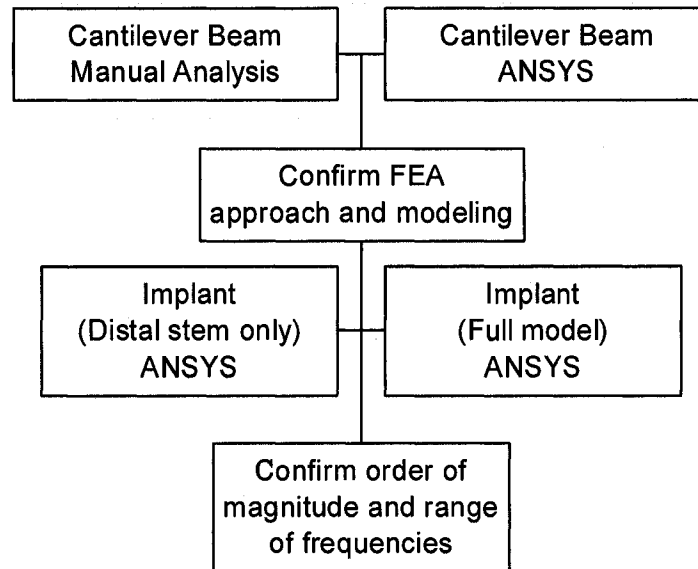


Figure 4.10: Numerical Validation Process

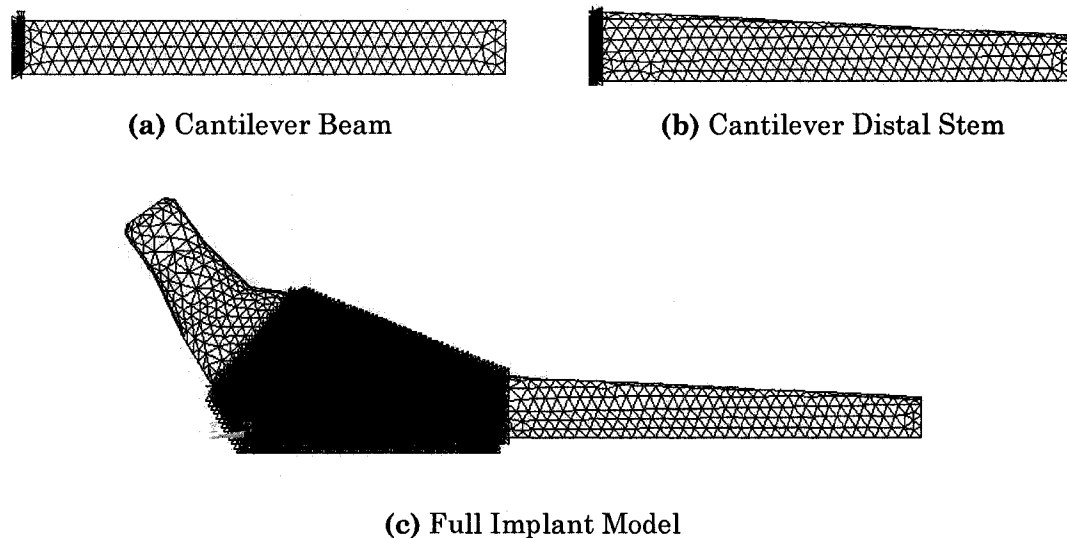


Figure 4.11: Models of cantilever beam, distal stem and full implant model with boundary constraints shown

A geometrically similar cantilever beam (Figure 4.11a) was used as a controlled study and manual analysis using simple beam theory (Table 4.3, Case 1) was used to validate the FEA model (Table 4.3, Case 2) of the cantilever beam. The results from Case 1 and Case 2 indicate that simple beam theory cannot be applied to this particular model (with an aspect ratio of approximately 9.5) since the percent errors for Modes #4 and #5 were 54.8% and 50.6% respectively, as shown in Table 4.4.

Table 4.3: Modal analysis comparison of various similar models (Figure 4.11)

Case	Model (Method)	Mode (Hz)					Properties	
		1	2	3	4	5	Material Density (kg/m ³)	Mass (Kg)
1	Cantilever Beam (Manual Analysis)	837.3	5247.5	14705.8	28796.2	47617.2	4137.9	0.038
2	Cantilever Beam (ANSYS)	831.1	4967.8	11951.0	13011.0	23504.0	4137.9	0.041
3	S16M2 Stem (ANSYS)	1125.6	1150.6	4823.6	5033.3	10253.0	4982.0*	0.043
4	S16M9 Stem (ANSYS)	1177.1	1204.4	5377.4	5617.0	10373.0	4137.9	0.039

* Density of TMZF™

Table 4.4: Comparison of the mode frequencies predicted by theory and ANSYS

Case	Model (Method)	Mode (Hz)				
		1	2	3	4	5
1	Cantilever Beam (Manual Analysis)	837.3	5247.5	14705.8	28796.2	47617.2
2	Cantilever Beam (ANSYS)	831.1	4967.8	11951.0	13011.0	23504.0
	Percent Error (%)	0.62	5.33	18.7	54.8	50.6

For comparison purposes, the distal stems of the S16M2 and S16M9 model were then isolated, fixed at one end (Figure 4.11b) and the frequency-response was determined. These results were then compared to the modal analysis of both models of the full implant, as shown in Figure 4.11c. The resultant frequency responses of the implant models (fully constrained on the proximal porous-covered stem as shown in Figure 4.7) were very similar to the modal analysis of only the distal portion of the implant stem, as shown in Table 4.5. The maximum percent error between the S16M9 models was 5.1% as shown in Table 4.6. These results confirm the numerical analysis process and validate the S16M9 implant model since the results of the modal analysis were similar in range of values and magnitude.

Table 4.5: Modal Analysis of Full Implant Models vs. Partial Stem Models

Case	Implant	Mode (Hz)					Properties	
		1	2	3	4	5	Apparent Density (kg/m ³)	Mass (Kg)
1a	S16M2: Full Model	1107.3	1131.3	4744.1	4948.4	8970.6	4982*	0.164
1b	S16M2: Distal Stem	1125.6	1150.6	4823.6	5033.3	10253.0	4982*	0.043
2a	S16M9: Full Model	1155.1	1178.2	5280.8	5503.7	9869.2	4137.9	0.145
2b	S16M9: Distal Stem	1177.1	1204.4	5377.4	5617.0	10373.0	4137.9	0.039

*Density of TMZF™

Table 4.6: Comparison of the mode frequencies of Full Implant Model vs. Distal Stem Model

Implant	Mode				
	1	2	3	4	5
Percent error (Case 1a and 1b) - S16M2	1.7%	1.7%	1.7%	1.7%	14.3%
Percent error (Case 2a and 2b) - S16M9	1.9%	2.2%	1.8%	2.1%	5.1%

4.3 Femoral Bone: CAD Model and Finite Element Model

4.3.1 Creation of the CAD Model of the Femoral Bone

The use of composite bones as substitutes for cadaveric specimens in experimental research has many obvious advantages. Composite femur are designed to geometrically and mechanically reproduce the response of the human femur with the same physical properties as real bone and can be cut, drilled, tapped, or gouged with standard orthopaedic instruments [Sawbones Pacific Research Laboratories, 2004]. They are primarily used for *ex vivo* testing, comparing or designing of implants and other devices and in surgical skills courses. The use of composite femurs have been extensively validated [Szivek *et al.*, 1990; Cristofolini *et al.*, 1996; Heiner and Brown, 2001] and are consider to be mechanically acceptable and provide a uniform test bed for certain types of comparative testing. These commercially produced femurs are composed of rigid polyurethane to simulate the cancellous bone component and an e-glass fiber-filled epoxy mixture used to replicate the cortical bone. To the Author's knowledge, there is only one company that produces commercially available composite femurs (Sawbones, Pacific Research Laboratories Inc., Vashon, Washington).

In 1995, Dr. Marco Viceconti announced the "Standardized Femur Program" proposed by the Laboratory for Biomaterials Technology, Istituti Ortopedici Rizzoli in Bologna, Italy. This initiative produced a three-dimensional computer rendering of the composite femur as a standardized reference for FE models of the human femur [Viceonti *et al.*, 1996]. This model was developed using computed tomography images (CT scans) of Sawbones' "Second-Generation" composite model. In 1999, Sawbones introduced a "Third-Generation" composite femur with increased anatomic detail and included an intermedullary canal in the mid-shaft area. The geometry of the composite femur was based on the anatomy of the left-side femur of an 89 kg, 183 cm tall male.

With the introduction of the Third-Generation composite femur, Greer [1999]

created a new CAD model using laser-scanned data. The model defined both the cortical bone volume as well as the cancellous bone volume. Greer's CAD model was originally available for downloading from the International Society of Biomechanics (ISB) Finite Element Repository (<http://isb.ri.ccf.org/isb/>). However, this website no longer hosted and the Author received a copy of the IGES file, in its original form, from a colleague who had previously accessed the website before it was no longer available. (It has recently come to this Author's attention that Greer's model is also available at: http://biomech.me.unr.edu/download/whole_femur_IGES.zip.) It should also be noted that a recent search of the Internet found a newer third-generation CAD model (Release Date 17-Jun-2003) available at: http://www.tecno.ior.it/VRLAB/researchers/repository/BEL_repository.html#3rdGenFemur. The owner of this model described the newer model as significantly different from Greer's model, mainly in the head and neck region and the model was obtained via assembly of CT-scan slices.

Greer's model was available in an IGES format and it was initially attempted to import the model directly into the finite element analysis [FEA] program. However, due to the complex surfaces around the condyles on the distal femur, the IGES model proved to be difficult to manipulate into a solid volume model and hindered future Boolean manipulation of the model during the pre-processing phase. As a result, the original IGES model was first imported into a CAD program (SolidWorks®) and a solid volume model was created (Figure 4.12) from the surface geometries by stitching the boundaries of adjacent trimmed surfaces.



(a) Posterior View

(b) Anterior View

Figure 4.12: Rendered view of Greer's left-sided femoral bone model after importing IGES format file into SolidWorks®.

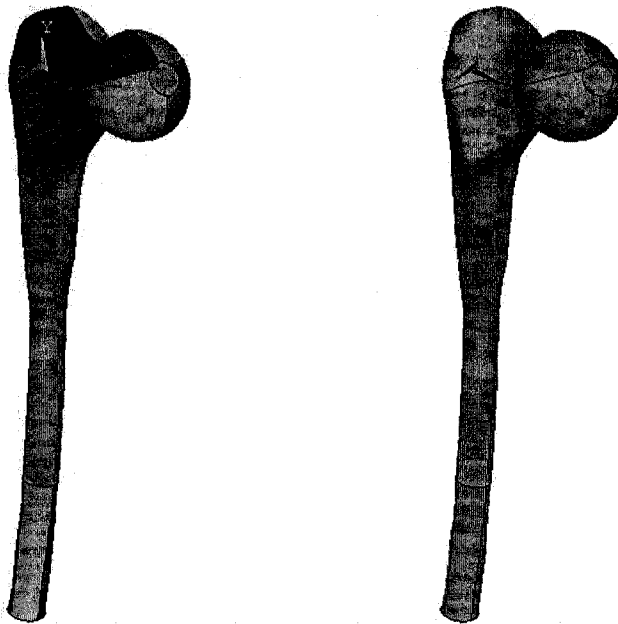
Once a solid model of the femur was established, in order to reduce the number of irrelevant complex surfaces that needed to be exported out of SolidWorks® and then imported into the FEA program, the condyles on the distal portion of the femur were truncated in SolidWorks® (Figure 4.13). The truncated femoral model was then exported as an IGES format and imported into the FEA program as a non-defeatured model of trimmed surfaces (Figure 4.14a), which allowed the creation of the volumetric model (Figure 4.14b). The creation of a volumetric model is necessary so that mechanical properties can be assigned and Boolean operations can be performed with the implant model in the FEA environment. Since the truncated model is smaller than the original model, it also greatly reduced the computational time for each analysis since the number of potential nodes was also reduced.



(a) Full femur model

(b) Truncated femur model

Figure 4.13: Truncation of Distal Femur in SolidWorks® before importing the IGES model into ANSYS®.



(a) Trimmed Surfaces Model

(b) Solid Volume Model

Figure 4.14: Creation of a solid femoral model from a trimmed surfaces model, in the ANSYS® environment.

Since osseointegration only occurs on the coarsened, hydroxapatite-covered surface of the implant, the cancellous bone around the distal stem of the implant cannot mechanically interlock with the smooth surface of the distal stem. When a cementless prosthesis is interference-fitted into the femur, limited immediate stability is produced against crushed and necrotic trabeculae [Furlong and Osborn, 1991]. Although some loads can be transferred through boundary contact, the distal stem is essentially not constrained and potentially allowed to macroscopically shift within the canal against the much softer cancellous tissue, especially when the necrotic bone is resorbed. This is particularly true for proximally porous-surfaced femoral implants, which are designed to achieve only proximal fixation. Since the distal stem is free to shift within the cancellous canal, the bone located immediately above and below the hydroxapatite-covered surfaces was also truncated (Figure 4.15).

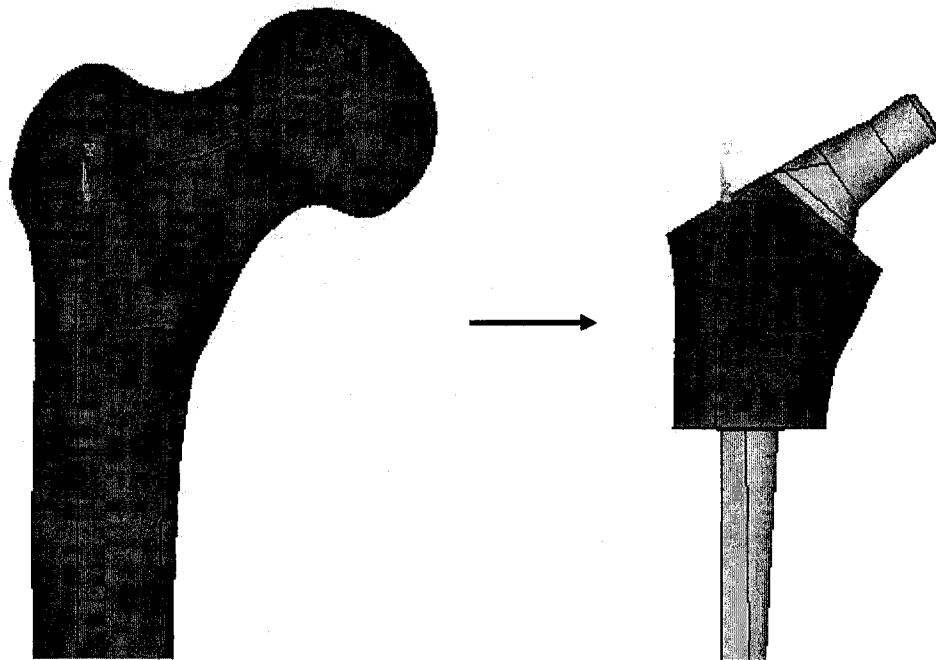
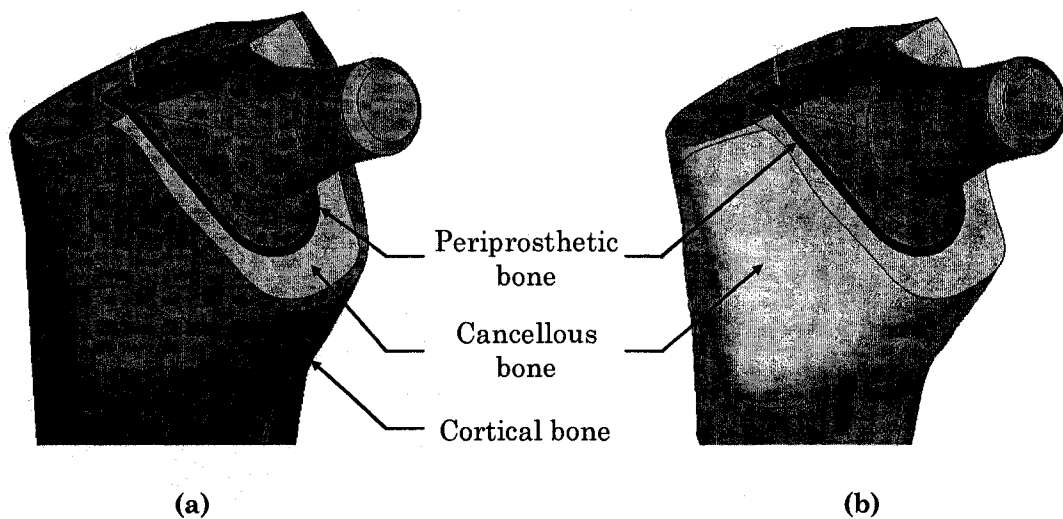


Figure 4.15: Truncation of cancellous bone stock above and below hydroxyapatite-covered surface on implant

In order to further reduce the computational time, it was proposed that cortical bone volume could be excluded during the analysis since the cortical bone is

approximately 7 times stiffer than the cancellous bone and the cortical bone layer is much thinner in comparison to the thickness of the cancellous bone volume. Also, it was hypothesized that the influence of the cortical bone volume would be minimized due to the distance from the implant itself. Based on the reasons mentioned above, it was speculated that constraining the surface of the outermost boundary of the cancellous bone volume, without the cortical bone present, might produce similar results as constraining the outermost surface of the cortical bone volume. To verify this, a comparison of the modal response of the implant with cortical bone (Figure 4.16a) and without cortical bone (Figure 4.16b) was conducted.



**Figure 4.16: Implant and cancellous bone volume
(a) with cortical bone and (b) without cortical bone**

However, although the Author was able to create the cortical bone volume in the FEA program, it was not possible to add the cortical bone layer volume to the implant/periprosthetic/cancellous bone continuum. Therefore, to verify the earlier hypothesis, a beam with similar size and mass properties of the implant (Table 4.7) was created and “sleeves” or hollowed-beams of proportional volumes were added onto the beam to simulate the various bone layers (Figure 4.17). In both cases, the nodes on the surfaces of the outermost bone volume were constrained in all directions. The implemented mechanical properties are shown in Table 4.8.

Table 4.7: Volumetric comparison of implant with bone and beam with sleeves

Implant with bone	Volume (m³)	Ratio of Volumes	Volume (m³)	Beam with sleeves
Implant	3.50E-05	1.24	4.34E-05	Beam
Periprosthetic Bone (1mm thick)	3.71E-06	1.16	4.32E-06	Periprosthetic Sleeve (1mm thick)
Cancellous Bone	3.27E-05	0.96	3.15E-05	Cancellous Sleeve
Cortical Bone	1.40E-05	1.07	1.50E-05	Cortical Sleeve

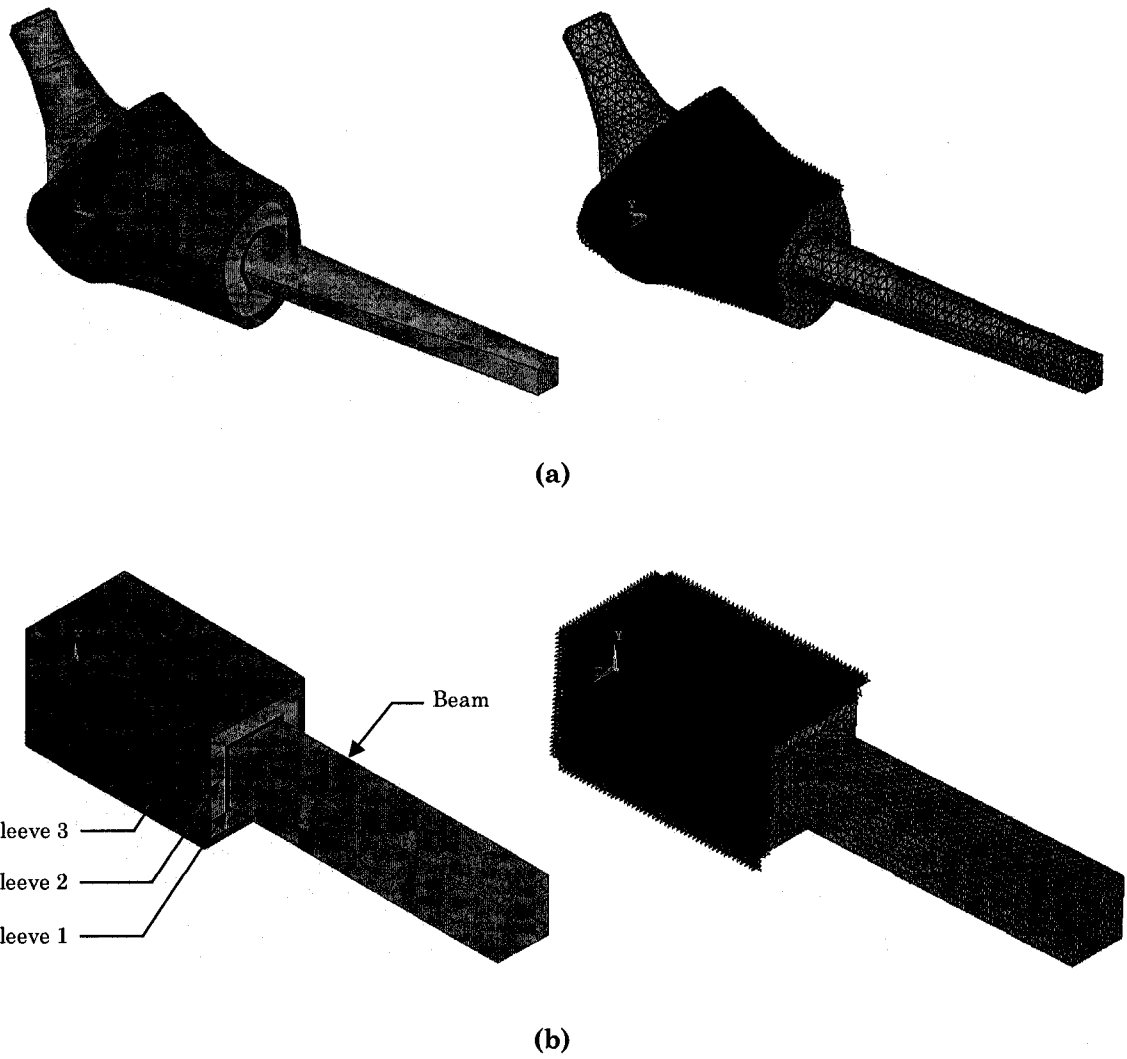


Figure 4.17: Comparison of (a) geometrically accurate implant and bone volumes assembly and (b) geometric equivalent beam with sleeves of simulated bone layers

Table 4.8: Mechanical properties of beam and sleeves

Volume (Simulated Constituent)	Material Density (kg/m³)	Elastic Modulus (MPa)
Beam (Implant)	4137.9	80000.0
Sleeve 1 (Periprosthetic Bone)	130.0	75.3
Sleeve 2 (Cancellous Bone)	1200.0	1690.9
Sleeve 3 (Cortical Bone)	1800.0	12000.0

A modal analysis of the beam and sleeves assembly (with and without the cortical bone volume) was conducted to determine the significance of the cortical bone layer. As shown in Figure 4.18 and Table 4.9, the cortical bone layer had very little influence on the modal response of the beam (implant surrogate). The maximum percent deviation between the modal results of the beam with and without the cortical bone sleeve was 1.87% during Mode #5 at $\rho_1 = 1.20 \text{ g/cm}^3$. Based on these results, it was concluded that the elimination of the cortical bone volume would not greatly influence the modal response of the implant. Therefore, the cortical bone was excluded during the FE analysis.

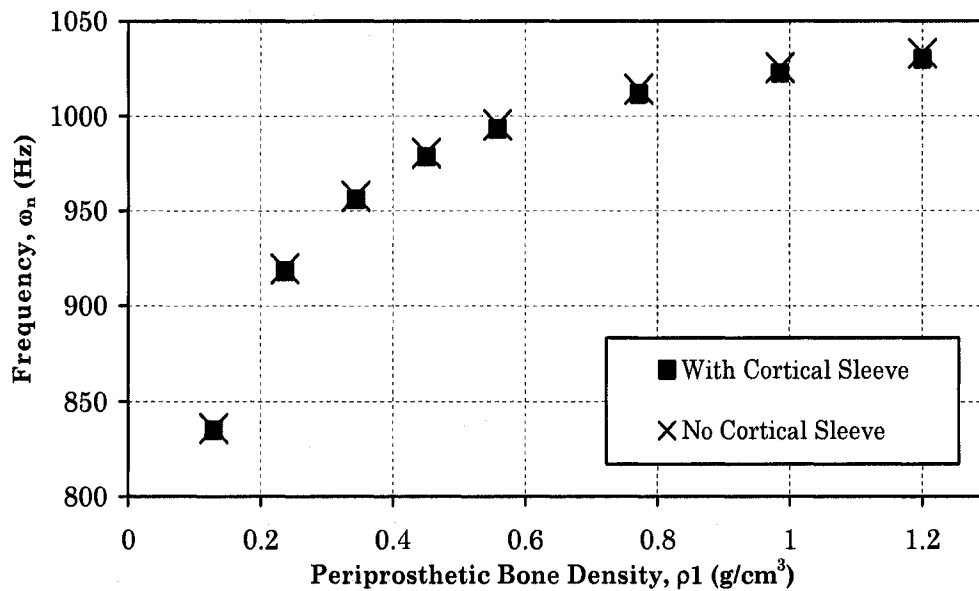


Figure 4.18: Modal analysis results (Mode #1) of beam with and without simulated cortical bone sleeve.

Table 4.9: Percent error between modal analysis results (Mode #1 to #5) of beam with and without simulated cortical bone sleeve.

ρ_1 (g/cm ³)	0.130	0.237	0.344	0.451	0.558	0.772	0.986	1.200
Mode #1	0.11%	0.15%	0.18%	0.21%	0.23%	0.26%	0.27%	0.29%
Mode #2	0.13%	0.20%	0.24%	0.27%	0.30%	0.32%	0.35%	0.36%
Mode #3	0.10%	0.13%	0.23%	1.17%	1.27%	1.38%	1.44%	1.49%
Mode #4	0.35%	0.55%	0.53%	0.55%	0.42%	0.61%	0.64%	0.66%
Mode #5	0.14%	0.46%	0.89%	1.17%	1.36%	1.61%	1.76%	1.87%

4.3.2 Generation of Periprosthetic Bone Volume

The periprosthetic bone volume was created in the FEA environment using constant-thickness sections that were created by perpendicularly offsetting the surface of the implant as shown in Figure 4.19. The thickness of the periprosthetic bone varied from 0.25 mm to 1.50 mm. A thickness of 2.0 mm or more would definitely be visible on a typical radiograph and thus, for this reason, it established the upper boundary of the range of periprosthetic bone thickness to evaluate.

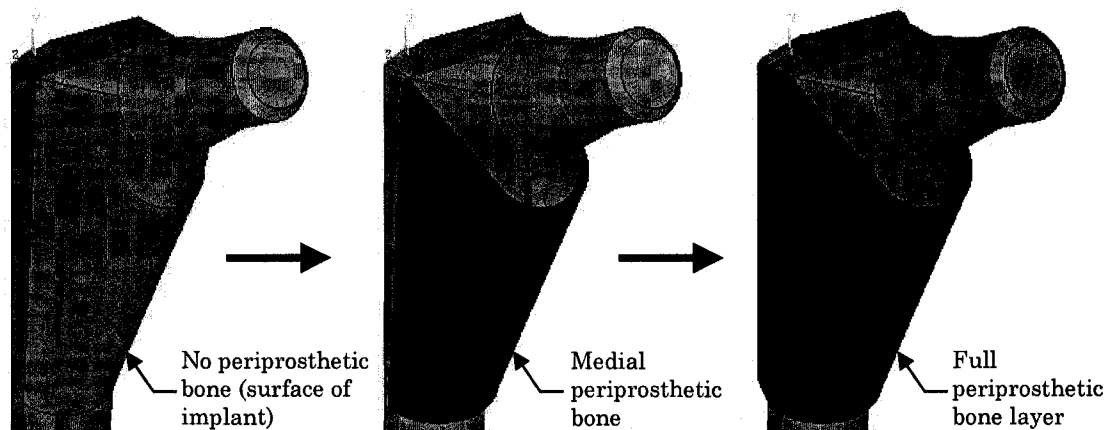


Figure 4.19: Generation of the Periprosthetic Bone Volume by offsetting constant-thickness volumes from the surface of the implant body

4.3.3 Approximating the topography of the cancellous bone volume using a constant-thickness section

To determine the validity of utilizing constant-thickness volumes to simulate varying bone thicknesses, without compromising the accuracy of the model, a study was conducted to verify that a constant-thickness volume could be used to numerically represent the topography of a typical proximal femoral bone section. The study consisted of an implant fitted into a typical proximal femur section and comparing its modal results with the frequency-response of an implant and constant-thickness section (Figure 4.20). The thickness of the simulated bone layer was determined by reproducing an equivalent volume of the proximal femur section

($3.618 \times 10^{-5} \text{ m}^3$). The volume of a 7.65 mm thick bone layer was $3.623 \times 10^{-5} \text{ m}^3$. The results (Table 4.10) confirmed that the simulated constant-thickness bone layer can be utilized and it produced similar results as the proximal femoral bone section. The ability to use constant-thickness layers is significant and aids in determining the effect of varying the thickness of the cancellous host bone (see Chapter 5.7).

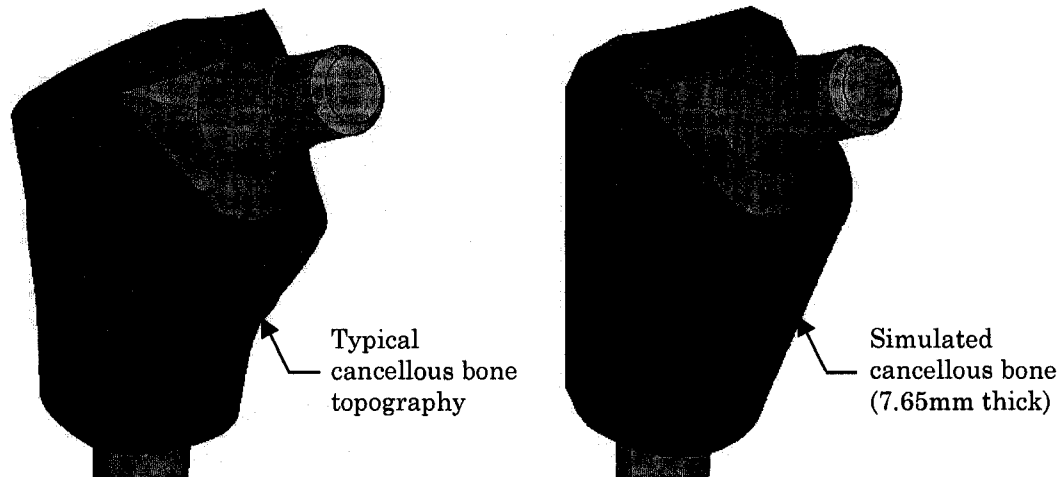


Figure 4.20: An Implant with Typical Proximal Femoral Topography and an Implant with Simulated Cancellous Bone (Constant Radial Thickness = 7.65 mm)

Table 4.10: Comparison of modal analysis results of an Implant with Typical Proximal Femur Topography and Implant with Simulated Cancellous Bone Layer (Thickness = 7.65 mm), as shown in Figure 4.20

Model	Mode No. (Hz)					Bone Properties	
	1	2	3	4	5	Apparent Density (kg/m ³)	Mass (Kg)
Implant with Proximal Femur Topography	989.0	1016.7	4352.6	4554.8	5344.4	1200.0	0.043
Implant with Constant-Thickness Bone Layer	985.4	1016.9	4320.6	4550.3	5307.4	1200.0	0.043

To verify that the constant-thickness simulated bone could be used within the desired apparent density range (0.13 - 1.20 g/cm³), the modal analysis of an implant with a proximal femoral section and an implant with its equivalent constant-thickness bone layer was compared (Figure 4.21). The first mode responses of both cases are very similar and the percent error varied between 0.09% to 1.32% (at $\rho_1 = 0.130$ g/cm³ and $\rho_1 = 0.237$ g/cm³, respectively). The percent errors of all five modes are shown in Table 4.11. The largest percent error was 3.94% during Mode #5 at $\rho_1 = 0.344$ g/cm³. These results validate the implementation of a constant-thickness bone layer.

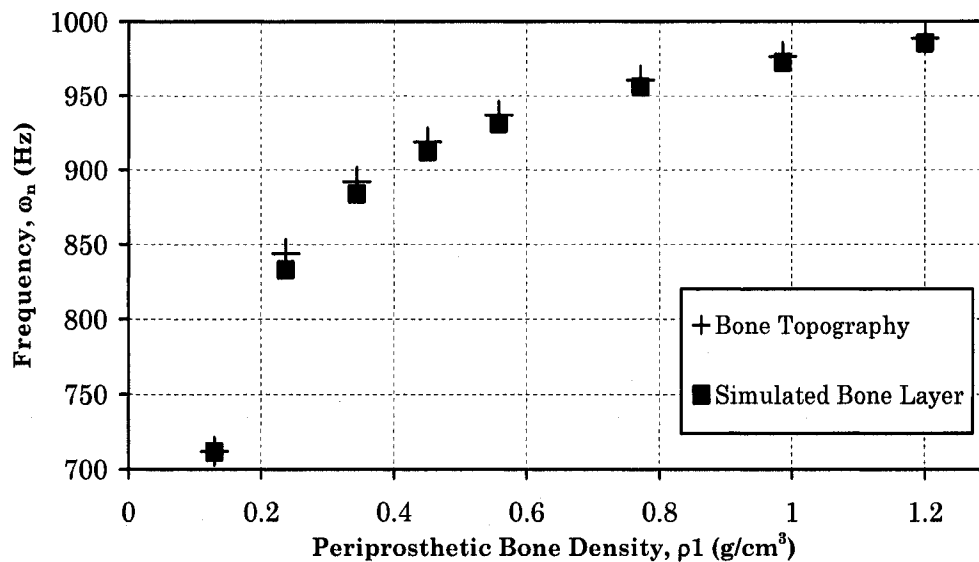


Figure 4.21: Modal analysis (Mode #1) of Implant with Typical Proximal Femur Topography and Implant with Simulated Host Bone Layer (Thickness = 7.65 mm)

Table 4.11: Percent deviation between modal analysis results (Mode #1 to #5) of an Implant with Typical Proximal Femur Topography and an Implant with Simulated Host Bone Layer (Thickness = 7.65 mm)

ρ_1 (g/cm ³)	0.130	0.237	0.344	0.451	0.558	0.772	0.986	1.200
Mode #1	0.09%	1.32%	0.94%	0.74%	0.63%	0.49%	0.42%	0.36%
Mode #2	2.17%	0.11%	0.09%	0.07%	0.05%	0.02%	0.00%	0.02%
Mode #3	2.66%	0.03%	0.12%	0.06%	0.68%	1.24%	0.90%	0.74%
Mode #4	1.94%	0.56%	1.05%	0.79%	0.26%	0.19%	0.09%	0.10%
Mode #5	1.56%	3.86%	3.94%	1.44%	1.10%	1.04%	0.89%	0.69%

After determining that the utilization of a constant-thickness cancellous bone layer was numerically possible and very similar to the modal response of an implant with a typical proximal femoral bone topography, a 1-mm thick periprosthetic bone layer was added in between the implant and host bone volumes (Figure 4.22). The first mode modal response of both test cases is shown in Figure 4.23 and the percent error varied from 0.07% to 0.51%. The maximum percent error was 1.49% during Mode #4 at $\rho_1 = 0.130 \text{ g/cm}^3$, as shown in Table 4.12. These results further validate the implementation of a constant-thickness bone layer. Even with the addition of the periprosthetic bone layer, a comparison of the results from the modal analysis (Figure 4.23 and Table 4.12) further confirmed that the constant-thickness bone layer could be utilized to simulate the regular cancellous bone volume when evaluating the effects of varying the thickness of the cancellous host bone.

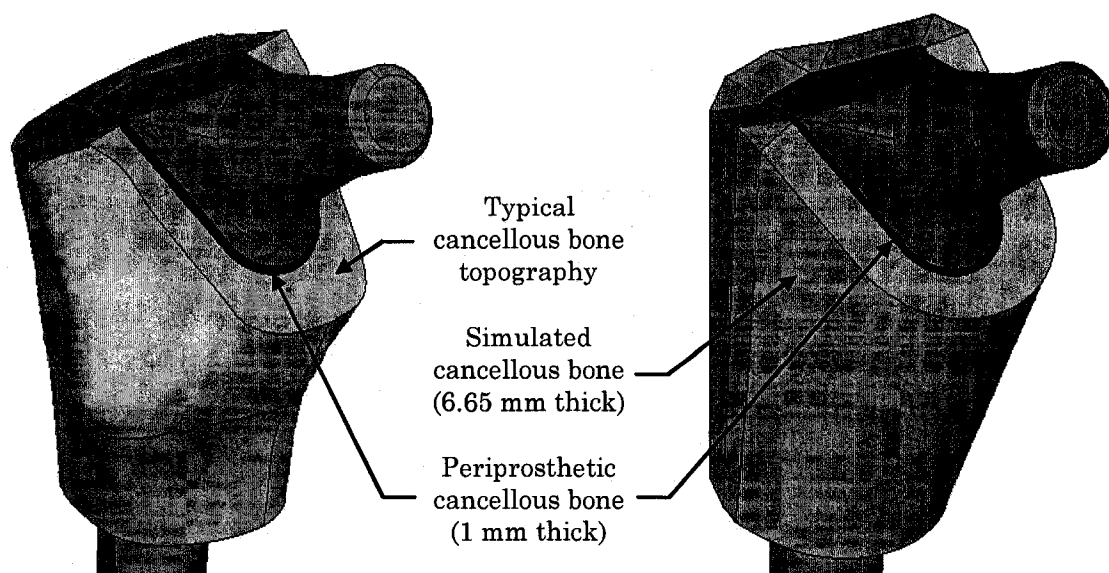


Figure 4.22: Implant with Typical Proximal Femoral Topography and Implant with Simulated Cancellous Bone Layer (Thickness = 6.65 mm). In both instances, the periprosthetic bone layer (in black) is 1 mm thick.

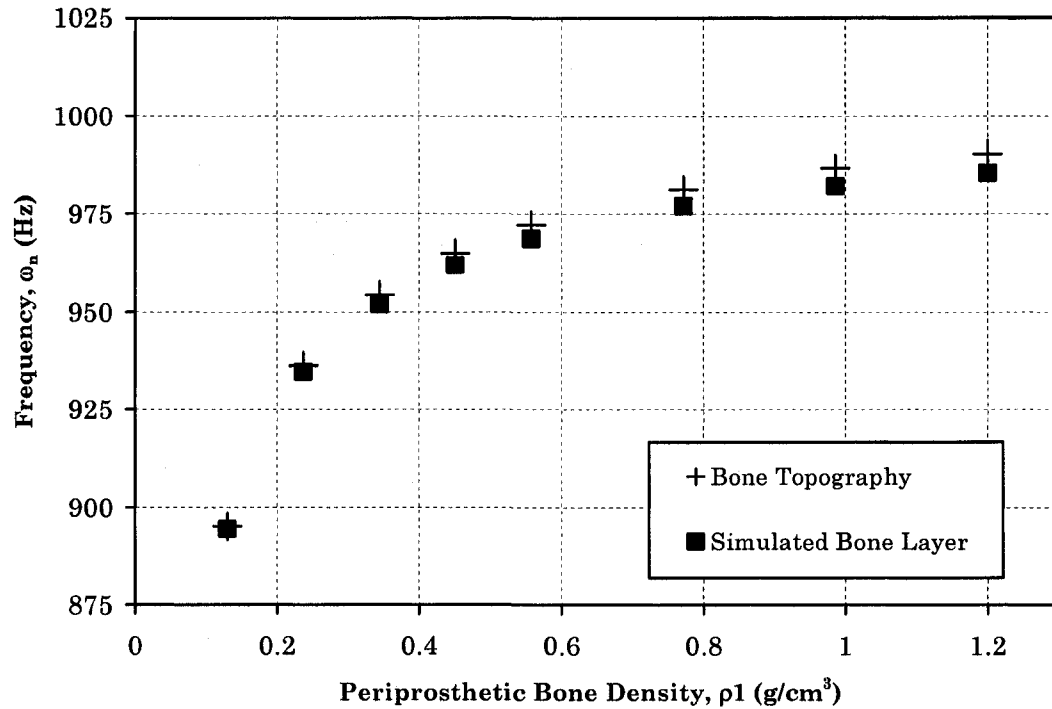


Figure 4.23: Modal analysis (Mode #1) of Implant with Typical Proximal Femoral Topography and Implant with Simulated Cancellous Bone Layer (Thickness = 6.65 mm). In both instances, the periprosthetic bone layer is 1 mm thick (Figure 4.20).

Table 4.12: Percent error between modal analysis results (Mode #1 to #5) of an Implant with Typical Proximal Femoral Topography and an Implant with Simulated Cancellous Bone Layer (Thickness = 6.65 mm). In both instances, the periprosthetic bone layer is 1 mm thick (Figure 4.20).

ρ_1 (g/cm ³)	0.130	0.237	0.344	0.451	0.558	0.772	0.986	1.200
Mode #1	0.07%	0.18%	0.25%	0.31%	0.36%	0.43%	0.47%	0.51%
Mode #2	0.13%	0.03%	0.01%	0.03%	0.05%	0.06%	0.07%	0.08%
Mode #3	0.03%	0.44%	0.57%	0.63%	0.68%	0.77%	0.83%	0.87%
Mode #4	1.49%	1.02%	0.40%	0.10%	0.03%	0.14%	0.18%	0.20%
Mode #5	0.20%	0.26%	0.50%	0.72%	0.87%	1.07%	1.19%	1.26%

4.4 Type and Size of FEA Elements

4.4.1 Type of FEA Elements

To accommodate the geometry of the implant and the high curvature of the original topography of the femoral bone surface, a structural, higher-order 20-node brick element (SOLID95 as shown in Figure 4.24) was chosen for the 3-dimensional model meshing. The 20-node element can accommodate irregular shapes without much loss of accuracy. Other 4-node, 8-node and 10-node elements were also attempted but the model failed to mesh in certain areas. The SOLID95 brick element is versatile and is able to degenerate into tetrahedral-, pyramid- and prism- shaped elements.

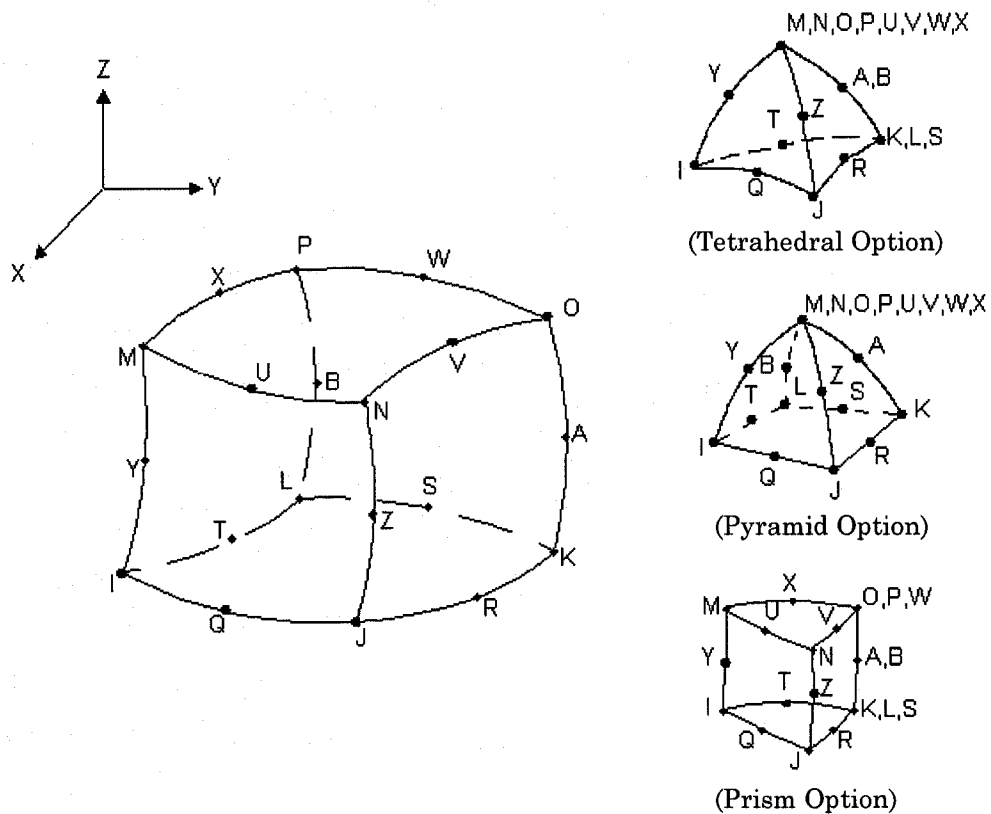


Figure 4.24: Type of Element Implemented: SOLID95 – A 20-Node Brick Element

4.4.2 Size of FEA Elements

A sensitivity analysis was used to determine the appropriate size of elements (Figure 4.25) that should be implemented without compromising the accuracy of the solution. A model analysis of a selected geometric configuration (Figure 4.26) was used to determine the sensitivity of the modal results due to the size of the elements (element edge length). The size of elements will determine the mesh resolution, which influences the number of elements, nodes and computational time. Although there are always trade-offs between accuracy and computation time, optimizing the element size will minimize the effects of these compromises.

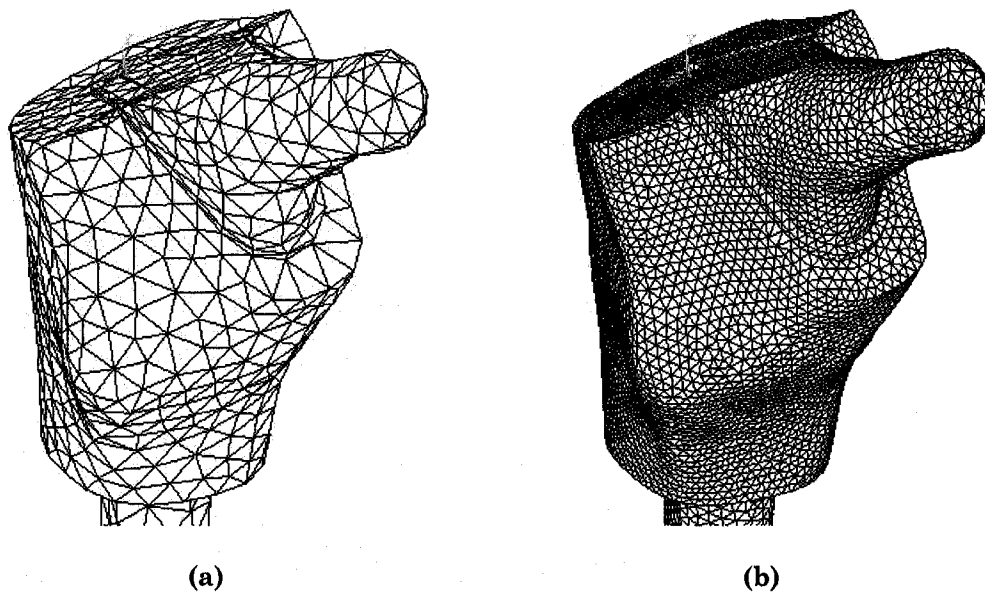


Figure 4.25: A comparison of element sizes and mesh resolution
(a) A course mesh with 5.0 mm size elements
(b) A finer mesh with 1.5 mm size elements

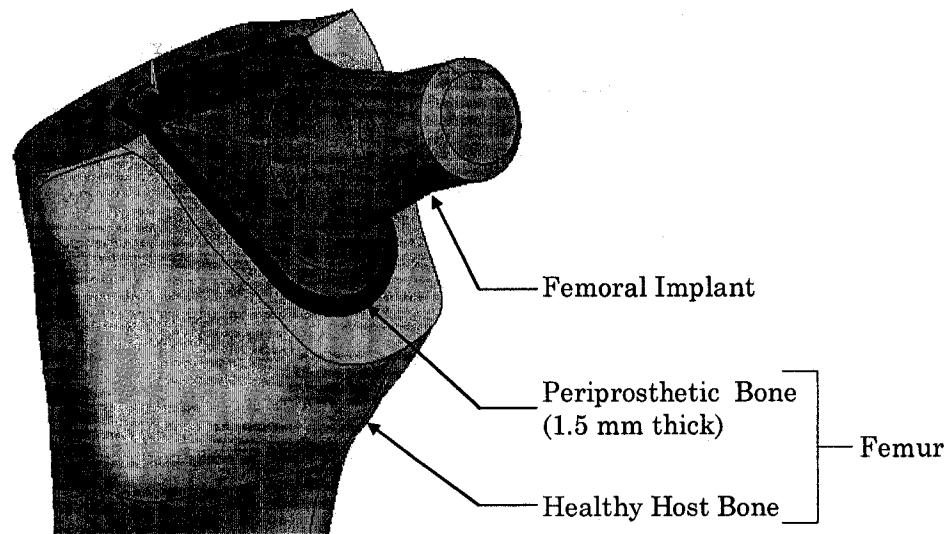


Figure 4.26: Element Size Sensitivity Analysis: Test Case Configuration.
 (Periprosthetic Bone: Density = 0.13 g/cm^3 , Elastic Modulus = 75.3 MPa ,
 Cancellous Host Bone: Density = 1.20 g/cm^3 , Elastic Modulus = 1690.9 MPa)

Based on the results of the sensitivity analysis (Figure 4.27), it was determined that a constant element size of 2.5 mm would be implemented for all the simulations (approximately 45,000 elements and 65,000 nodes). Although it appears that a larger element size could have been used in order to reduce computational time (Figure 4.28), for certain geometries (with high curvature and small features) and periprosthetic bone layer thicknesses, the implementation of a larger element size was not possible. For example, it was not possible to implement an element with an edge length of 3.5 mm for a periprosthetic bone thickness of 0.25 mm. Although local mesh resolution could have been implemented, based on the results shown in Figure 4.27, it would not have dramatically influenced the results of the modal analysis. Therefore, local mesh resolution was considered to be unnecessary.

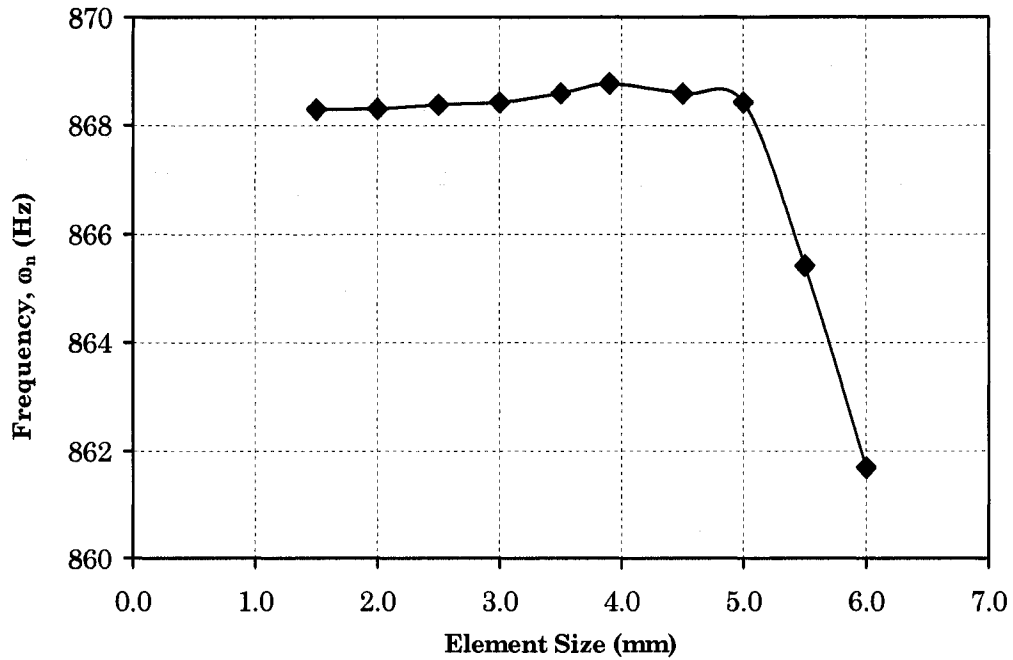


Figure 4.27 Element size sensitivity analysis determined by the frequency response (Mode #1) of an implant with two types of bone layers (see Figure 4.26) (Periprosthetic Bone: Density = 0.13 g/cm³, Elastic Modulus = 75.3 MPa, Cancellous Host Bone: Density = 1.20 g/cm³, Elastic Modulus = 1690.9 MPa)

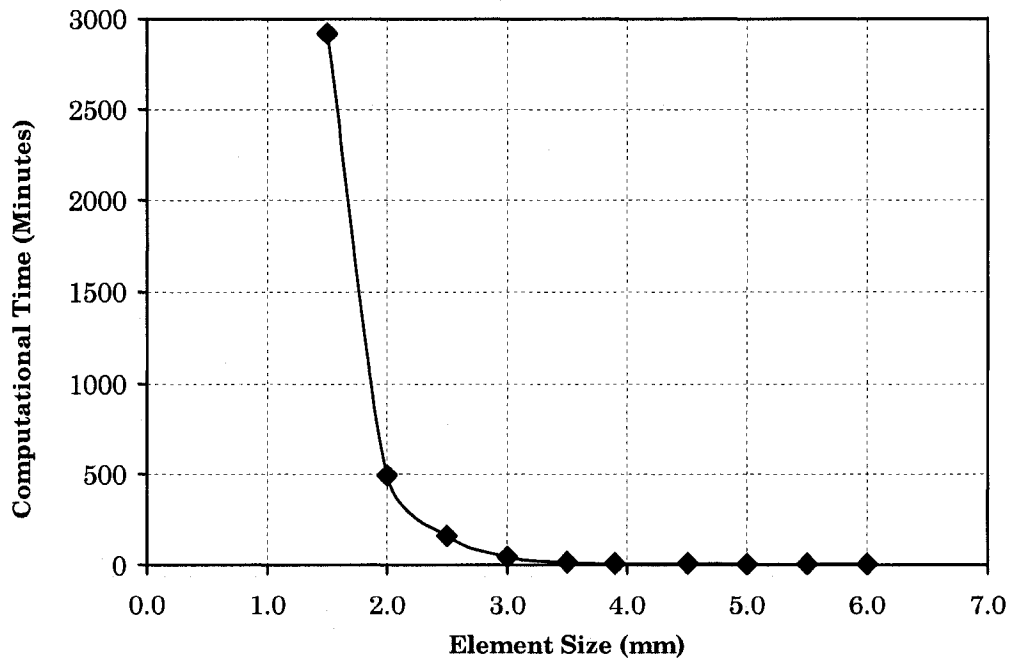


Figure 4.28: Computational time for various element sizes for test configuration shown in Figure 4.26. Analysis performed on an Intel® Xeon™ PC (3.06GHz CPU and 2.00 GB RAM).

Chapter 5

Discussion of Results

5.1 Review of Problem Description

Monitoring of implanted prostheses is critical in identifying patients whose healing is slow-to-progress or if the onset of fracture is highly probable. This is especially important for patients who are asymptomatic and no radiographic signs of mobilization or femoral loosening are visible. Therefore, the development of a new quantitative monitoring technique could advance current diagnostic and health-monitoring practices for identifying at-risk patients.

5.1.1 Defining the Manipulated Variables

As stated in Chapter 1, the objective of this study was to determine the feasibility of detecting and monitoring the progression of osseointegration of the bone surrounding an implant. Specifically, it was proposed that this type of health monitoring could be accomplished by evaluating the frequency response (ω) of an *in vivo* prosthesis as a result of variations in the stiffness of periprosthetic bone stock (bone tissue surrounding the implant). This study will explicitly focus on the non-osseointegration of periprosthetic bone adjacent to the porous-coated areas along the implant surface of the femoral stem.

The stiffness of the periprosthetic bone is influenced by a number of factors, but most notably, bone density and bone thickness. These variables have been individually identified and its affects on the modal response of the implant will be examined. Therefore, the scope of the analysis protocol includes examining the

effects of:

- 1) Periprosthetic bone density
- 2) Periprosthetic bone thickness
- 3) Periprosthetic bone density variations in localized regions along the porous coated body:
 - a. Anterior vs. Posterior Non-Osseointegration
 - b. Medial vs. Lateral Non-Osseointegration
 - c. Proximal vs. Distal Non-Osseointegration
 - d. Non-Osseointegration in Physiologically-Significant Regions (variation of the Gruen Zones)
- 4) Cancellous Host Bone Thickness

5.2 Non-Dimensionalizing the Frequency-Response of the Implant

It should be emphasized that the purpose of this study is not to correlate the absolute value of an implant's frequency-response to a specific state of physiological osseointegration. Rather, the objective is to establish that, over a period of time, changes in the material properties of the periprosthetic bone (due to osseointegration or atrophy) are reflected by a detectable change in the modal response of the implant. Conceptually, in a clinical situation, the frequency-monitoring-system ("sensor") would be calibrated or initialized to provide a baseline measurement, following a hip replacement procedure. The change in frequency, relative to its baseline value, would be monitored over time during regularly scheduled post-operative evaluations (Figure 5.1).

A single measurement of one frequency-response value will not be able to uniquely quantify the status of osseointegration of the bone and the actual values of the frequencies will most likely vary slightly from patient-to-patient. For this reason, some of the following results will be normalized relative to the frequency-response value at the lowest density ($\rho_1 = 0.13 \text{ g/cm}^3$) in each particular test case,

using Equation (5.1).

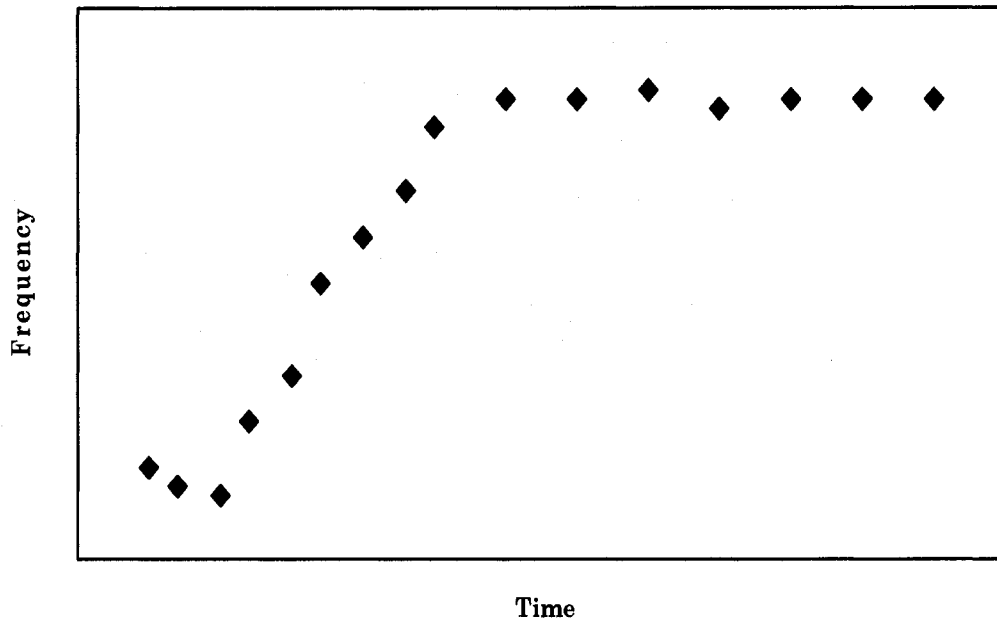


Figure 5.1: A conceptual example of a time-lapsed (serial) frequency-response of an implanted prosthesis.

$$\omega_r = \frac{\omega_\rho - \omega_{0.13}}{\omega_{0.13}} \quad (5.1)$$

Where:

- ω_r = normalized frequency-response
- ω_ρ = frequency-response at ρ of interest
- $\omega_{0.13}$ = frequency-response at $\rho = 0.13 \text{ g/cm}^3$

5.3 Mode Shapes

This study will focus on the first five modes of the frequency-response of the implanted prosthesis. Each mode number corresponds to a different and specific mode shape. During the first, a third and fifth mode, the implant vibrates predominately in the antero-posterior direction (Figure 5.2), while the implant vibrates mostly in the medio-lateral direction during the second and fourth mode (Figure 5.3). As each mode number increases, the frequency-response of the implant also increases. In addition, the results reveal that certain mode numbers are more responsive (than others) for indicating variations in material and geometric properties, which will be examined in the following chapter.

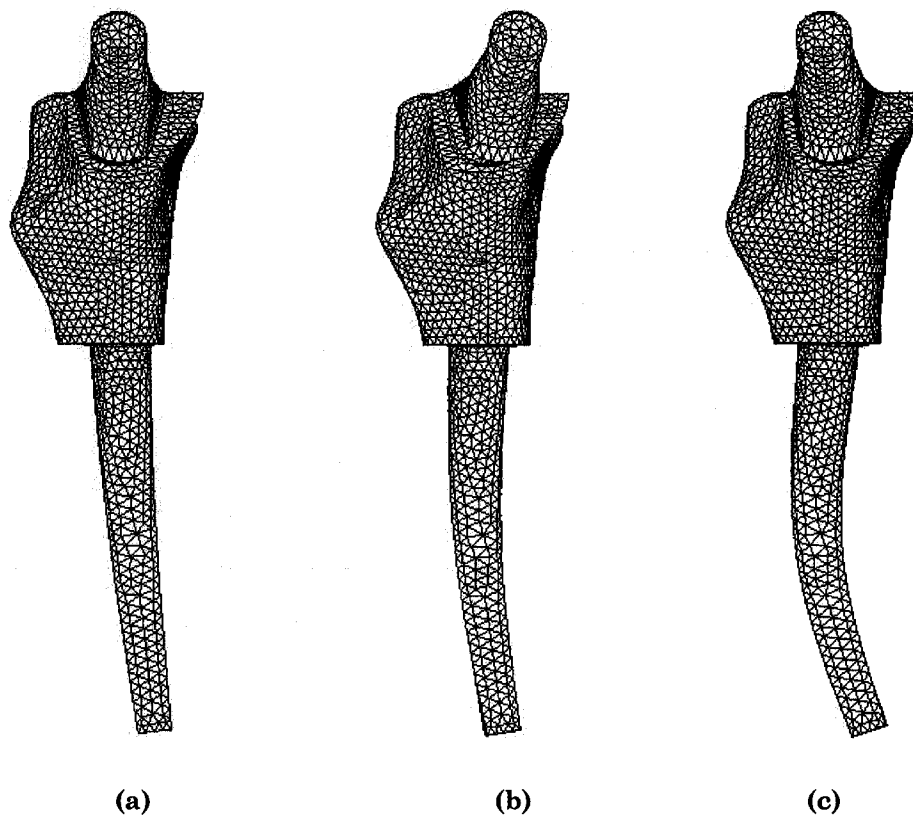


**Figure 5.2: Mode shapes at Mode #1, #3 and #5 –
Implant vibrates predominately in the antero-posterior direction
(a) Mode #1 (b) Mode #3 (c) Mode #5**

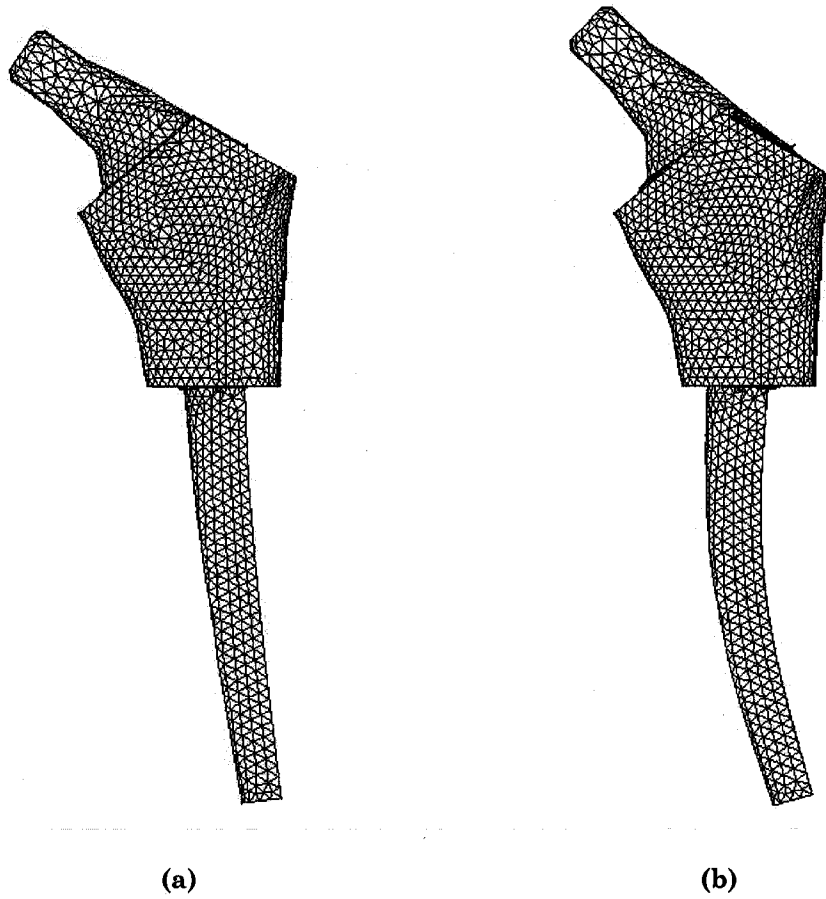


**Figure 5.3: Mode shapes at Mode #2 and #4 –
Implant vibrates predominately in the medio-lateral direction
(a) Mode #2 (b) Mode #4**

5.4 Effects of Periprosthetic Bone Density

5.4.1 Results

Trevisan *et al.*, [1997] stressed the increasing importance of evaluating periprosthetic bone density since prosthetic fixation and stability may be affected by bone density [Dorr *et al.*, 1990; Lee *et al.*, 1991]. Poss [1992] also identified that age-related decreases in bone density could also be a potential factor of failure. Early identification of patients with lower-than-normal density changes during the early-stage, bone-remodelling phase may be prescribed bisphosphonates to reduce loss of periprosthetic bone stock in conditions associated with accelerated bone turnover [Bhandari *et al.*, 2005]. As such, atypical decreases in density of periprosthetic bone stock could be indicative of delayed osseointegration or bone atrophy. This has been observed during roentgenographic or radiographic assessments where the presence of radiolucencies and reactive lines around the implant are symptomatic of bone loss. Inversely, if the implant is osseointegrated, the density of the periprosthetic bone should progressively increase until it peaks and maintains a steady-state. Presumably, this occurs when a permanent physiological union has occurred or when the osseointegration process has reached its plateau. As the density (ρ) of the periprosthetic bone increases, the elastic modulus (E) also increases. The density and elastic modulus relationship was determined by using the power-law relationship (Equation 5.2) reported by Lotz *et al.*, [1990], as mentioned in Section 3.2.5.

$$E = 1310\rho^{1.4} \quad (5.2)$$

Where: E = modulus of elasticity (MPa)
 ρ = apparent density (g/cm^3)

And: $0.13 \text{ g/cm}^3 \leq \rho \leq 1.20 \text{ g/cm}^3$

Based on a periprosthetic bone thickness (t_1) of 1 mm (as illustrated in Figure 5.4), Figures 5.5 and 5.6 show the first mode response (with and without normalized results) of the implant due to density variation of the periprosthetic bone. The results shown in Figures 5.5 and 5.6 both indicate that the frequency-response (ω_n as shown in Equation 5.3) of the implant increased as the density of the periprosthetic bone (ρ_1) increased. This is predicted by Equation (5.2) since the elastic modulus (or stiffness) of the periprosthetic bone increased by a power of 1.4 with the density. As the stiffness increases, Equation 5.3 indicates that the frequency-response will also increase. This trend is also reflected in the first five modes as shown in Figures 5.7 and 5.8.

$$\omega_n = \frac{1}{2\pi} \sqrt{\frac{k}{m}} \quad (5.3)$$

Where:

ω_n	=	natural frequency
k	=	stiffness of the system
m	=	mass of the system

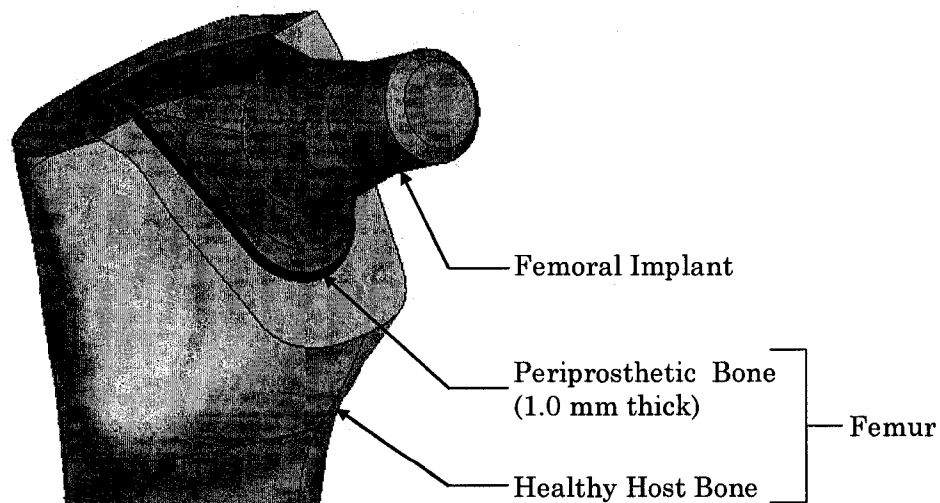


Figure 5.4: Effect of varying periprosthetic bone density: Analysis Configuration.
**(Periprosthetic Bone: $t_1 = 1.0$ mm, $0.13 \text{ g/cm}^3 \leq \rho_1 \leq 1.20 \text{ g/cm}^3$, $E = 1310\rho^{1.4}$,
 Cancellous Host Bone: Density = 1.20 g/cm^3 , Elastic Modulus = 1690.9 MPa)**

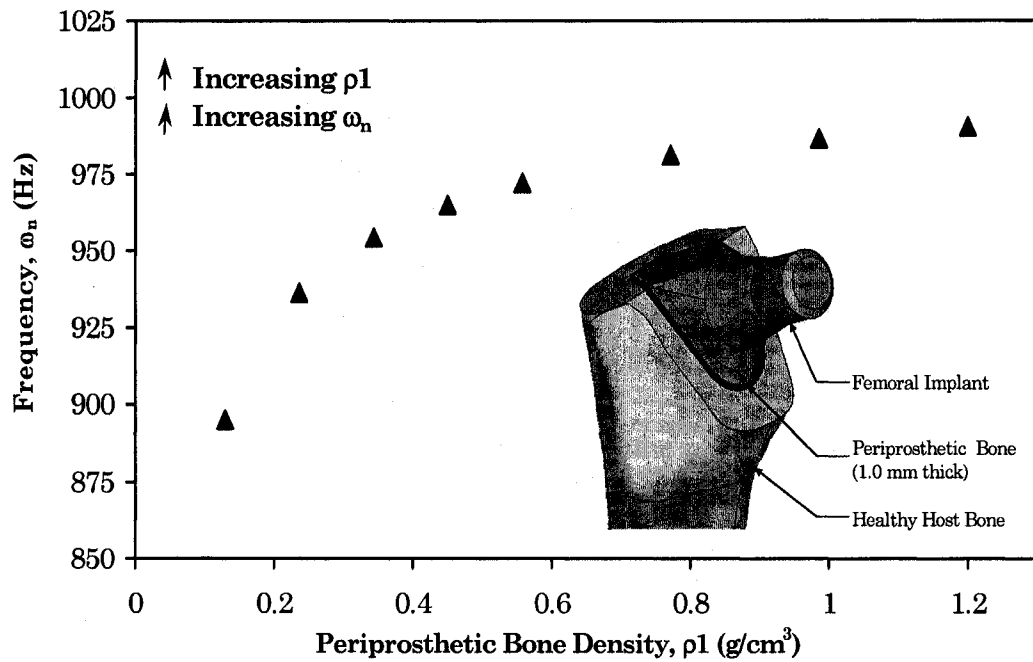


Figure 5.5: Effect of varying periprosthetic bone density (Results NOT normalized). Modal response (Mode #1) of implant with two types of bone layers (see Figure 5.4) (Periprosthetic Bone: $t_1 = 1.0$ mm, $0.13 \text{ g/cm}^3 \leq \rho_1 \leq 1.20 \text{ g/cm}^3$, $E = 1310\rho_1^{1.4}$, Cancellous Host Bone: Density = 1.20 g/cm^3 , Elastic Modulus = 1690.9 MPa)

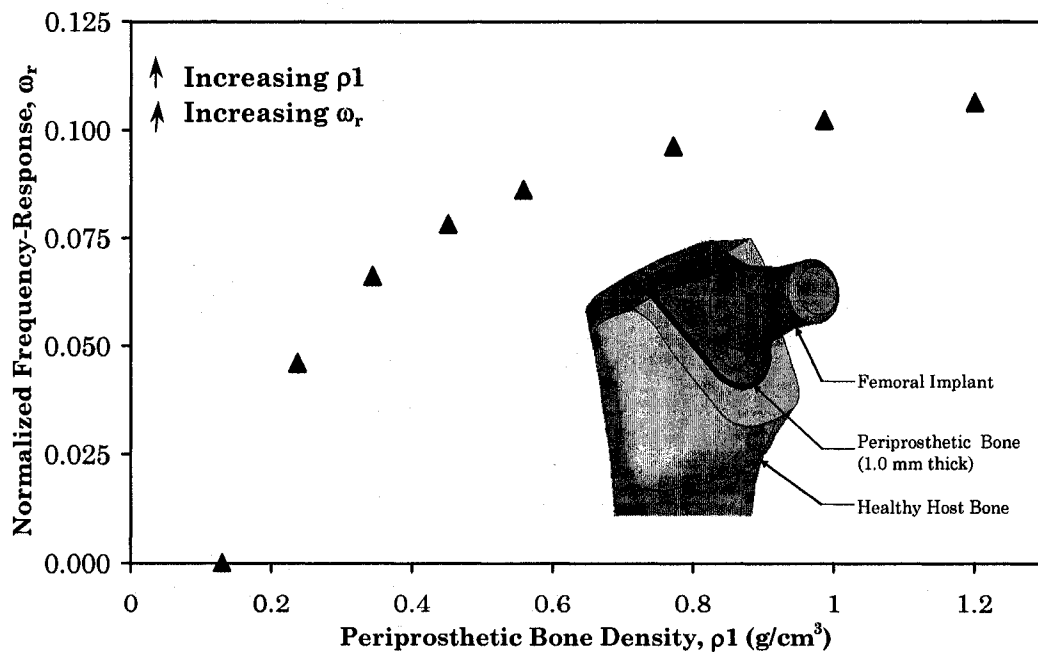


Figure 5.6: Effect of varying periprosthetic bone density (Results normalized). Modal response (Mode #1) of implant with two types of bone layers (see Figure 5.4) (Periprosthetic Bone: $t_1 = 1.0$ mm, $0.13 \text{ g/cm}^3 < \rho_1 < 1.20 \text{ g/cm}^3$, $E = 1310\rho_1^{1.4}$, Cancellous Host Bone: Density = 1.20 g/cm^3 , Elastic Modulus = 1690.9 MPa)

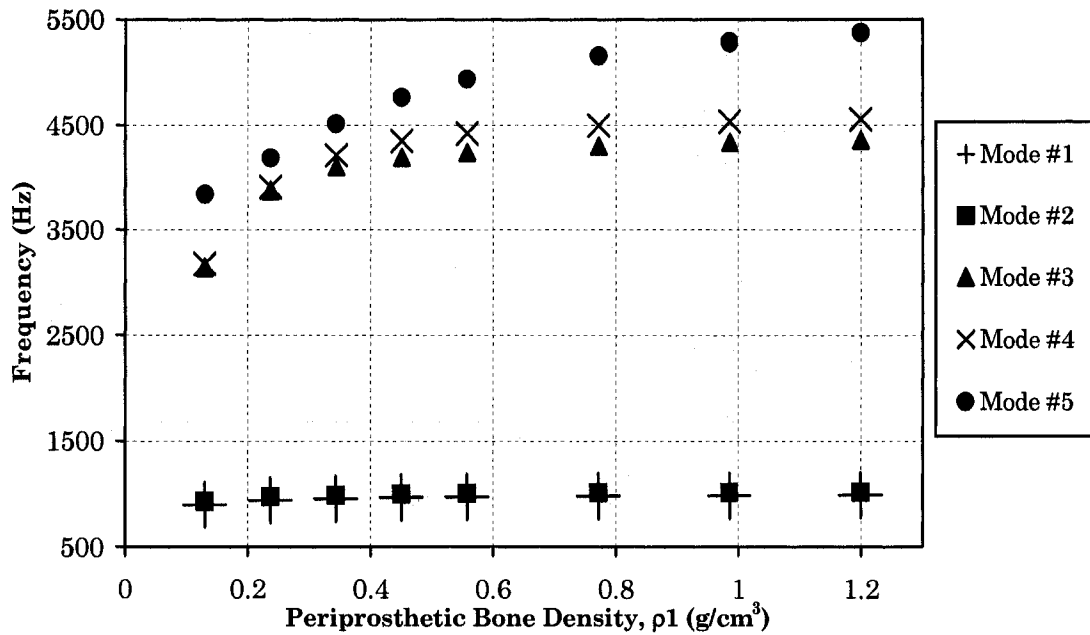


Figure 5.7: Effect of varying periprosthetic bone density and comparison of modal response (first five modes) of implant with two types of bone layers (Figure 5.4) (Periprosthetic Bone: $t_1 = 1.0$ mm, $0.13 \text{ g/cm}^3 \leq \rho_1 \leq 1.20 \text{ g/cm}^3$, $E = 1310\rho^{1.4}$, Cancellous Host Bone: Density = 1.20 g/cm^3 , Elastic Modulus = 1690.9 MPa). Results have NOT been normalized.

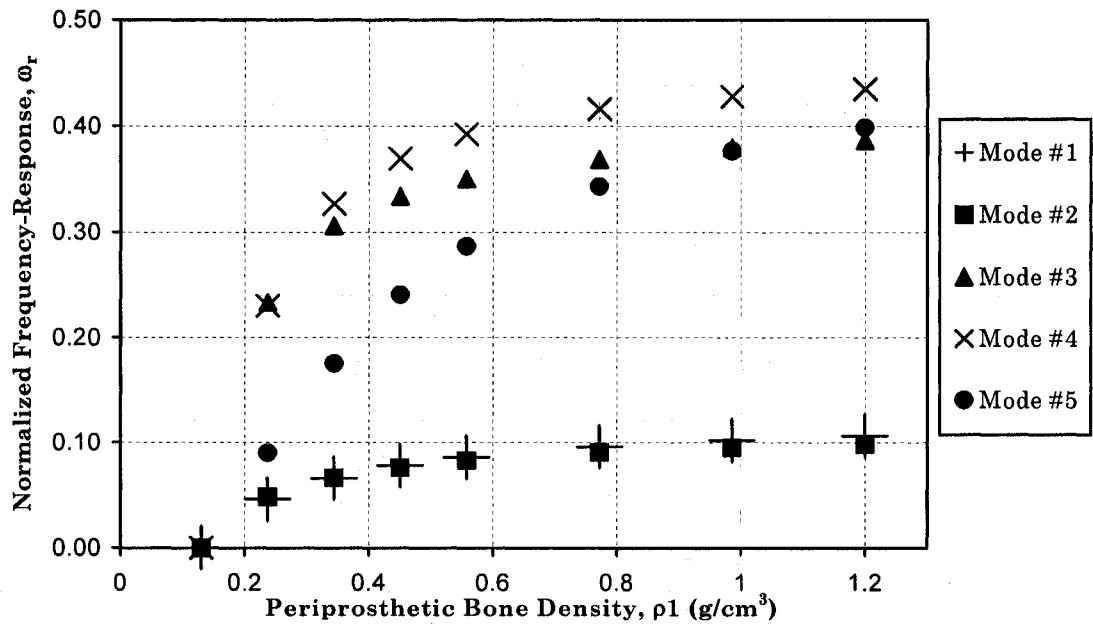


Figure 5.8: Effect of varying periprosthetic bone density and comparison of modal response (first five modes) of implant with two types of bone layers (Figure 5.4) (Periprosthetic Bone: $t_1 = 1.0$ mm, $0.13 \text{ g/cm}^3 < \rho_1 < 1.20 \text{ g/cm}^3$, $E = 1310\rho^{1.4}$, Cancellous Host Bone: Density = 1.20 g/cm^3 , Elastic Modulus = 1690.9 MPa). Results have been normalized with respect to ω at $\rho_1 = 0.13 \text{ g/cm}^3$ of each mode.

A comparison of the overall range of the modal analysis values between $\rho_1 = 0.13 \text{ g/cm}^3$ and $\rho_1 = 1.20 \text{ g/cm}^3$, relative to the frequency-response at $\rho_1 = 0.13 \text{ g/cm}^3$ (Equation 5.4), highlights which mode number produces largest frequency range in response to density variations of a uniformly thick periprosthetic bone stock. As shown in Figure 5.9, the overall percent difference is the highest for Mode #4 (41.1%) and it would seem to indicate that Mode #4 is slightly more responsive in indicating changes in periprosthetic bone density (assuming a constant thickness periprosthetic bone stock) than Mode #3 or #5 (overall percent difference was 37.5% and 38.3% respectively). However, according to Figure 5.10, when comparing the decrease in frequency response relative to the frequency response at $\rho_1 = 1.20 \text{ g/cm}^3$ (Equation 5.5), Mode #5 is more sensitive to detecting early decreases in the density of the periprosthetic bone since the rate of decrease in the frequency is much higher in comparison with the other modes. Therefore, the frequency responses during the fifth mode are more likely to indicate early loosening of the prosthetic.

$$\text{Overall Percent difference} = \frac{\omega_{1.20} - \omega_{0.13}}{\omega_{0.13}} \quad (5.4)$$

Where: $\omega_{1.20}$ = frequency-response at $\rho_1 = 1.20 \text{ g/cm}^3$
 $\omega_{0.13}$ = frequency-response at $\rho_1 = 0.13 \text{ g/cm}^3$

$$\text{Decrease in frequency response} = \frac{\omega_{1.20} - \omega_{\rho}}{\omega_{1.20}} \quad (5.5)$$

Where: $\omega_{1.20}$ = frequency-response at $\rho_1 = 1.20 \text{ g/cm}^3$
 ω_{ρ} = frequency-response at ρ_1 of interest

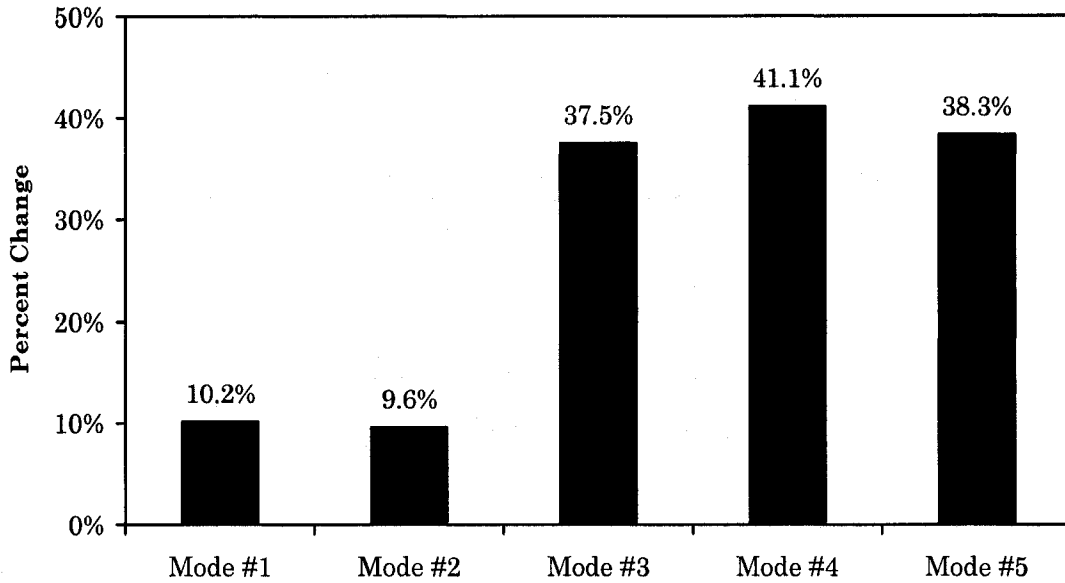


Figure 5.9: Effect of varying periprosthetic bone density -
Percent difference between frequency responses at $\rho_1 = 0.13 \text{ g/cm}^3$ and 1.20 g/cm^3 .
(Periprosthetic Bone: $t_1 = 1.0 \text{ mm}$, $0.13 \text{ g/cm}^3 \leq \rho_1 \leq 1.20 \text{ g/cm}^3$, $E = 1310\rho_1^{1.4}$,
Cancellous Host Bone: Density = 1.20 g/cm^3 , Elastic Modulus = 1690.9 MPa)

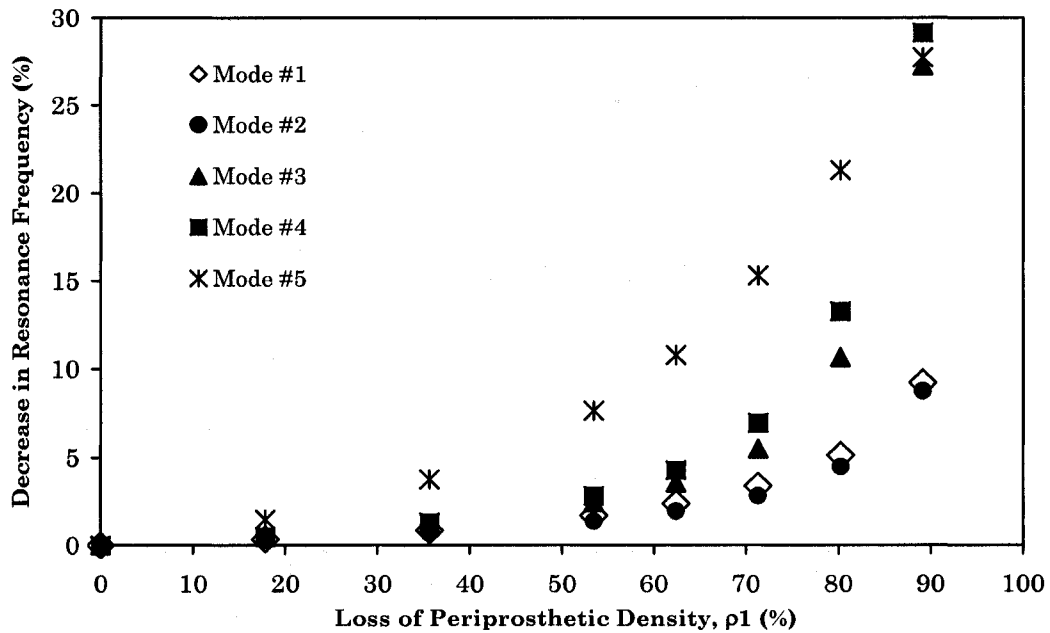


Figure 5.10: Effect of varying periprosthetic bone density -
Decrease in resonance frequency relative to frequency response at $\rho_1 = 1.20 \text{ g/cm}^3$.
(Periprosthetic Bone: $t_1 = 1.0 \text{ mm}$, $0.13 \text{ g/cm}^3 \leq \rho_1 \leq 1.20 \text{ g/cm}^3$, $E = 1310\rho_1^{1.4}$,
Cancellous Host Bone: Density = 1.20 g/cm^3 , Elastic Modulus = 1690.9 MPa)

5.4.2 Range and resolution

Measurement resolution is limited by the noise density (or noise floor) and will also vary with the measurement bandwidth. Equation (5.6) defines the relationship between resolution, noise density and bandwidth.

$$R = N\sqrt{1.6BW} \quad (5.6)$$

Where:

R	=	resolution (mg)
N	=	noise density $\left(\frac{mg}{\sqrt{Hz}}\right)$
BW	=	bandwidth (Hz)

The results in Figure 5.5 were not normalized to illustrate the typical values and range of the computed first-mode frequency-response results of the implant. As indicated by the values of the frequency-response in Figure 5.5, it is reasonable to conclude that a potential *in vivo* sensor with a resolution of 1 Hz (within a bandwidth of 100 Hz) is achievable since existing, commercially available MEMS (Micro-Electro-Mechanical Systems) accelerometers can already resolve signals lower than 1 Hz (within 100 Hz).

For example, Analog Devices (Analog Devices Inc., Norwood, Massachusetts) produces an accelerometer (ADXL202JE/AE) that allows signals below 2 mg (at 60 Hz bandwidth) to be resolved with a noise density of $0.2 \text{ mg}/\sqrt{Hz}$. Another manufacturer, MEMSIC (Memsic Inc., North Andover, Massachusetts), produces the MXR7210GL/ML chip that is capable of a resolution better than 1 mg at 1 Hz at a noise density of $0.4 \text{ mg}/\sqrt{Hz}$. Both of these accelerometers are available in hermetically sealed, LCC (leadless chip carriers) surface mount packages approximately 5mm x 5mm x 2mm and are operational between 0°C to 70°C (normal body temperature range is 36.1 - 37.8 °C [Simmers, 1988]).

5.5 Effects of Periprosthetic Bone Thickness

The variation in periprosthetic bone thickness (as shown in Figure 5.11) was investigated because an increase in the thickness of lower-density periprosthetic bone stock could be indicative of progressive or impending bone loss, due to instability, failed osseointegration and/or atrophy. The potential to mechanically measure and verify increases in periprosthetic bone thickness around the implant would be significant since it is difficult to obtain roentgenograms with beams positioned exactly tangential to the surface of the porous-coated areas along the implant [Engh *et al.*, 1990]. It is especially difficult to situate the patient and the scanning gantry in the same positions during serial roentgenograms. As a result, the state-of-health of the bone surrounding proximally porous-coated implants are difficult to assess since reactive lines around the porous-coated area are difficult to distinguish and measure, especially in the early stages.

The first-mode frequency-response of the implant, as the periprosthetic bone thickness (t_1) uniformly increases, is shown in Figures 5.12 and 5.13. At a given density, as the increase in bone thickness progressed, it corresponded to a lower frequency-response value. This trend is consistent for the first five modes (Figures 5.12 to 5.17). These results are similar to the effects of decreased periprosthetic bone density. This is significant because these results are consistent in suggesting that a descending frequency-response value indicates deteriorating periprosthetic bone, whether it is due to loss of bone density or increases in thickness of affected (or deteriorating) periprosthetic bone at a given density. In addition, Table 5.1 and Figure 5.13 indicate that as the periprosthetic thickness increases, the frequency range between $\rho_1 = 0.13 - 1.20 \text{ g/cm}^3$ also increases.

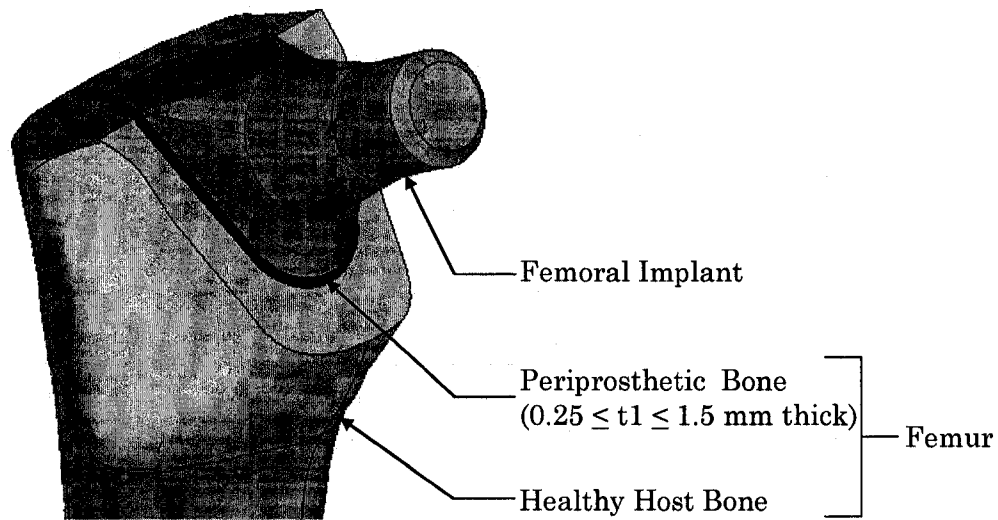


**Figure 5.11: Effect of varying periprosthetic bone thickness:
Analysis Configuration.**

(Periprosthetic Bone: $0.25 \text{ mm} \leq t1 \leq 1.5 \text{ mm}$, $0.13 \text{ g/cm}^3 \leq \rho1 \leq 1.20 \text{ g/cm}^3$, $E = 1310\rho^{1.4}$,
Cancellous Host Bone: Density = 1.20 g/cm^3 , Elastic Modulus = 1690.9 MPa)

**Table 5.1: Varying periprosthetic bone thickness and its effect
on the frequency range (Mode #1) between $\rho1 = 0.13 - 1.20 \text{ g/cm}^3$.**

(Periprosthetic Bone: $0.25 \text{ mm} \leq t1 \leq 1.5 \text{ mm}$, $0.13 \text{ g/cm}^3 \leq \rho1 \leq 1.20 \text{ g/cm}^3$, $E = 1310\rho^{1.4}$,
Cancellous Host Bone: Density = 1.20 g/cm^3 , Elastic Modulus = 1690.9 MPa)

Periprosthetic bone thickness, $t1$ (mm)	Frequency range between $\rho1 = 0.13 - 1.20 \text{ g/cm}^3$ (Hz)	Difference in range, ($\omega_{1.30} - \omega_{0.12}$) (Hz)
0.25	944.6 - 985.0	40.4
0.50	925.4 - 985.3	59.9
1.00	894.4 - 985.3	90.9
1.50	870.0 - 985.4	115.3

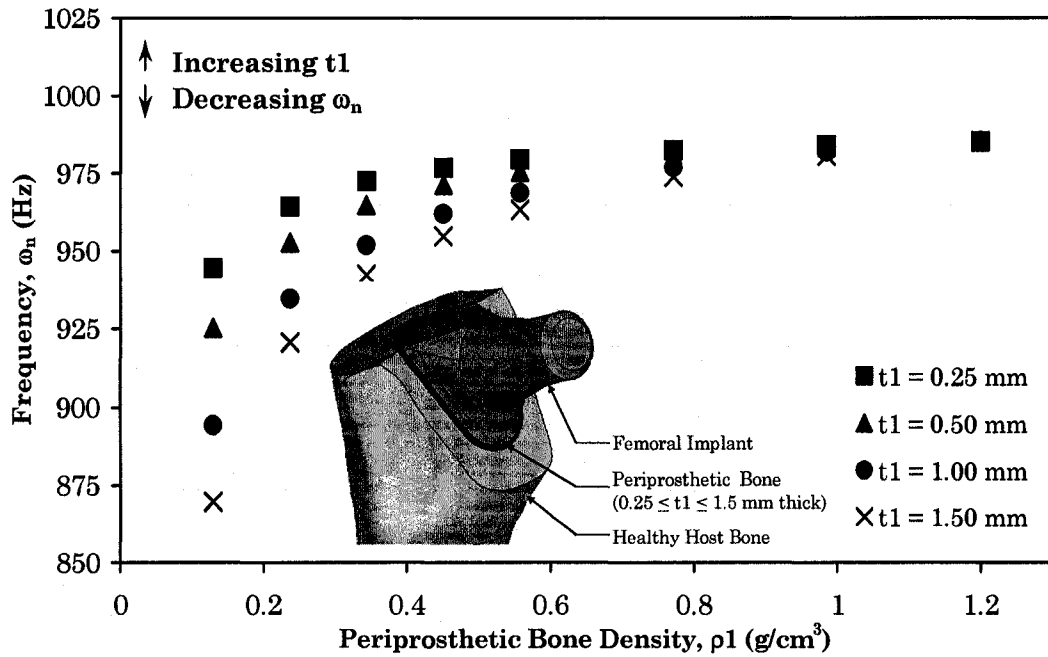


Figure 5.12: Effect of varying periprosthetic bone thickness (NOT normalized). Modal response (Mode #1) of implant with two types of bone layers (Figure 5.11) (Periprosthetic Bone: $0.25 \text{ mm} \leq t_1 \leq 1.5 \text{ mm}$, $0.13 \text{ g/cm}^3 \leq \rho_1 \leq 1.20 \text{ g/cm}^3$, $E = 1310\rho^{1.4}$, Cancellous Host Bone: Density = 1.20 g/cm^3 , Elastic Modulus = 1690.9 MPa)

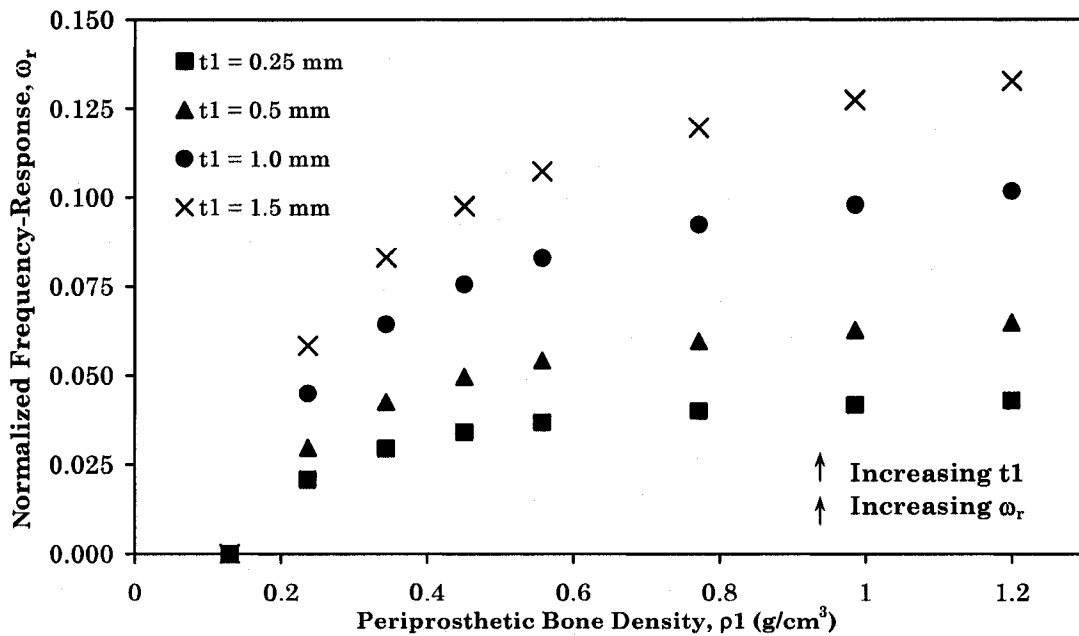


Figure 5.13: Effect of varying periprosthetic bone thickness (Results normalized). Modal response (Mode #1) of implant with two types of bone layers (Figure 5.11) (Periprosthetic Bone: $0.25 \text{ mm} \leq t_1 \leq 1.5 \text{ mm}$, $0.13 \text{ g/cm}^3 \leq \rho_1 \leq 1.20 \text{ g/cm}^3$, $E = 1310\rho^{1.4}$, Cancellous Host Bone: Density = 1.20 g/cm^3 , Elastic Modulus = 1690.9 MPa)

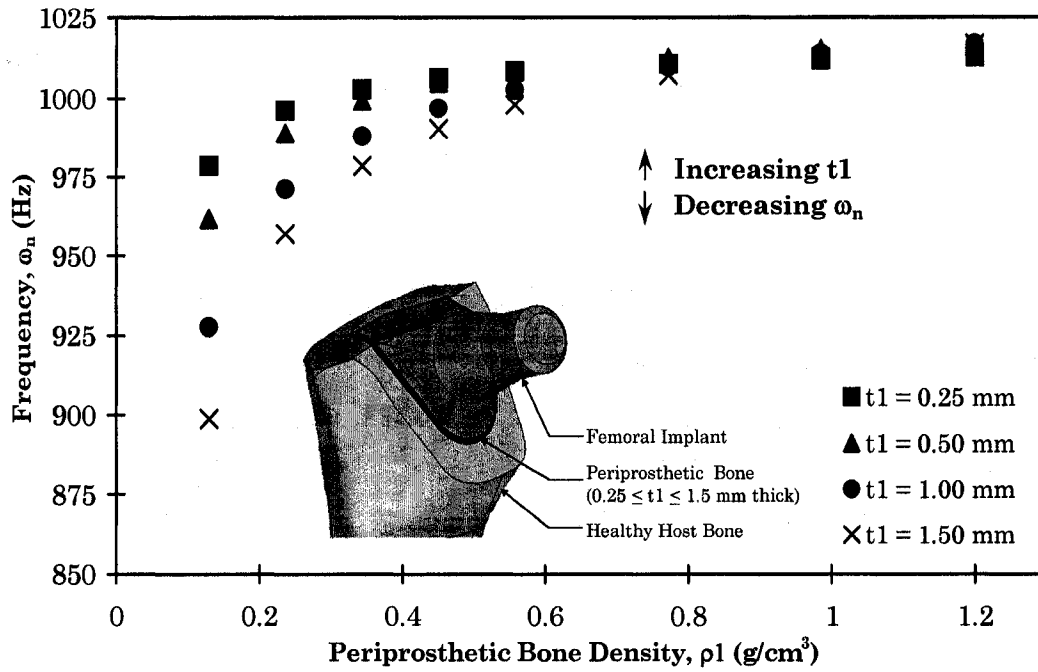


Figure 5.14: Effect of varying periprosthetic bone thickness, t_1 . Modal response (Mode #2) of implant with two types of bone layers (Figure 5.11) (Periprosthetic Bone: $0.25 \text{ mm} \leq t_1 \leq 1.5 \text{ mm}$, $0.13 \text{ g/cm}^3 \leq \rho_1 \leq 1.20 \text{ g/cm}^3$, $E = 1310\rho^{1.4}$, Cancellous Host Bone: Density = 1.20 g/cm^3 , Elastic Modulus = 1690.9 MPa)

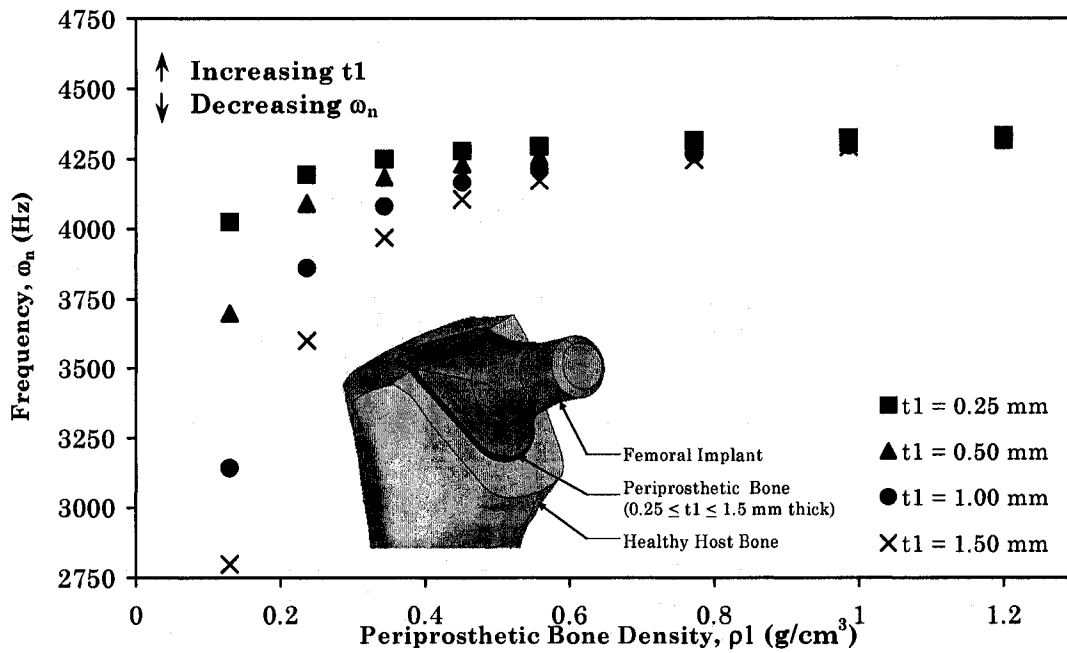


Figure 5.15: Effect of varying periprosthetic bone thickness, t_1 . Modal response (Mode #3) of implant with two types of bone layers (Figure 5.11) (Periprosthetic Bone: $0.25 \text{ mm} \leq t_1 \leq 1.5 \text{ mm}$, $0.13 \text{ g/cm}^3 \leq \rho_1 \leq 1.20 \text{ g/cm}^3$, $E = 1310\rho^{1.4}$, Cancellous Host Bone: Density = 1.20 g/cm^3 , Elastic Modulus = 1690.9 MPa)

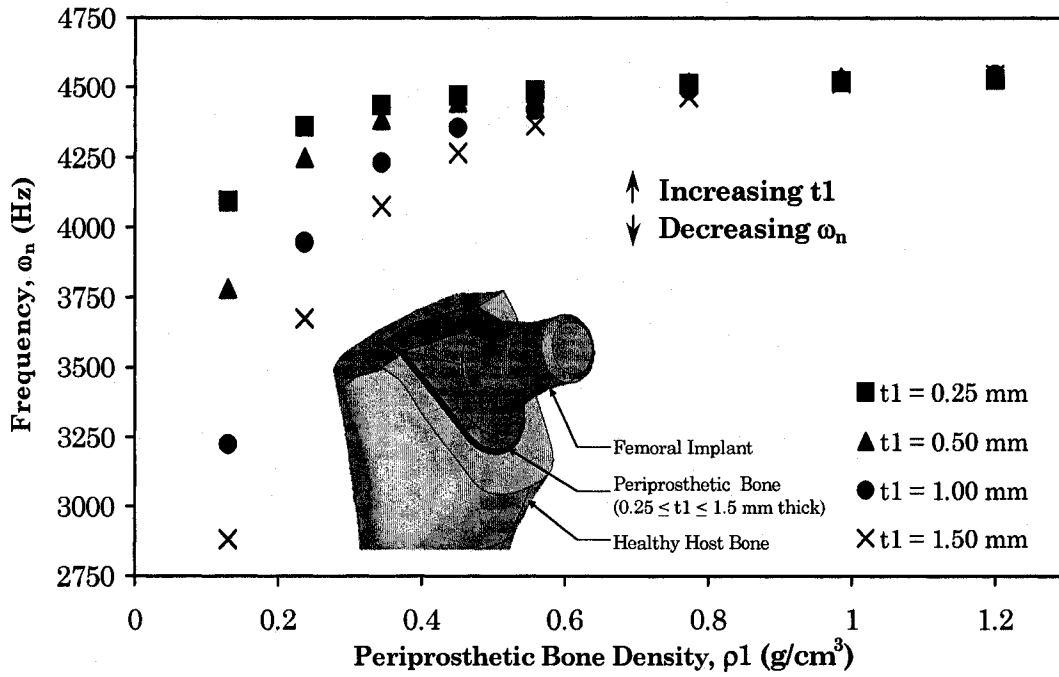


Figure 5.16: Effect of varying periprosthetic bone thickness, t_1 .
 Modal response (Mode #4) of implant with two types of bone layers (Figure 5.11)
 (Periprosthetic Bone: $0.25 \text{ mm} \leq t_1 \leq 1.5 \text{ mm}$, $0.13 \text{ g/cm}^3 \leq \rho_1 \leq 1.20 \text{ g/cm}^3$, $E = 1310\rho^{1.4}$,
 Cancellous Host Bone: Density = 1.20 g/cm^3 , Elastic Modulus = 1690.9 MPa)

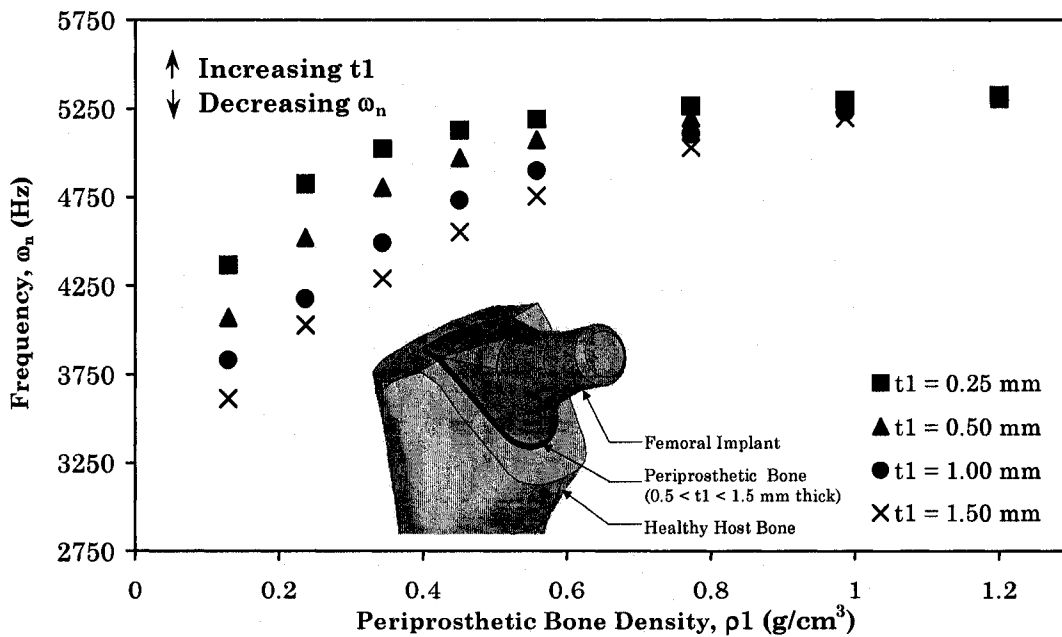


Figure 5.17: Effect of varying periprosthetic bone thickness, t_1 .
 Modal response (Mode #5) of implant with two types of bone layers (Figure 5.11)
 (Periprosthetic Bone: $0.25 \text{ mm} \leq t_1 \leq 1.5 \text{ mm}$, $0.13 \text{ g/cm}^3 \leq \rho_1 \leq 1.20 \text{ g/cm}^3$, $E = 1310\rho^{1.4}$,
 Cancellous Host Bone: Density = 1.20 g/cm^3 , Elastic Modulus = 1690.9 MPa)

It is noteworthy to observe that although an implant's frequency-response may have reached a plateau during serial frequency measurements (as shown conceptually in Figure 5.1), this alone would not necessarily indicate that physiological changes in the bone have ceased. Rather, it may be indicative of increased bone density coupled with the effects of increased periprosthetic bone thickness, or decreases in both density and thickness of the periprosthetic bone. For example, as shown in Figure 5.12, a frequency of approximately 950 Hz corresponds to a range of potential density and thickness permutations (Table 5.2). In these instances, it would appear that the positive effects of increased bone density could negate the unfavorable consequences of increased deteriorating periprosthetic bone thickness.

Table 5.2: Various permutations of periprosthetic bone thickness (t_1) and periprosthetic bone density (ρ_1) that produce a first mode frequency-response of approximately 950 Hz, as shown in Figure 5.11. (Periprosthetic Bone: $0.25 \text{ mm} \leq t_1 \leq 1.50 \text{ mm}$, $E = 1310\rho^{1.4}$, Cancellous Host Bone: Density = 1.20 g/cm^3 , Elastic Modulus = 1690.9 MPa)

Periprosthetic bone thickness, t_1 (mm)	Periprosthetic bone density, ρ_1 (g/cm ³)			
	0.154	0.231	0.326	0.388
0.25	950.0 Hz			
0.50	950.1 Hz			
1.00	950.1 Hz			
1.50	950.0 Hz			

In addition, as shown in Figure 5.18, the overall percent difference increases as the thickness of the periprosthetic bone stock increases. Figure 5.18 also indicates that the highest overall percent difference occurs during Mode #4 for the largest tested thickness value of $t_1 = 1.5$ mm (57.7%) and the overall percent difference of this particular mode is slightly larger when compared to Mode #3 or #5 (overall percent difference was 54.4% and 46.8% respectively for $t_1 = 1.5$ mm). However, when comparing the decrease in frequency response relative to the frequency response at $\rho_1 = 1.20$ g/cm³ (Figures 5.19 to 5.22), Mode #5 is consistently more sensitive to detecting early decreases in the density of the periprosthetic bone since the rate of decrease in the frequency is much higher in comparison with the other modes. Therefore, the fifth mode frequency responses are more likely to indicate early loosening of the prosthetic, regardless of the thickness of the periprosthetic bone.

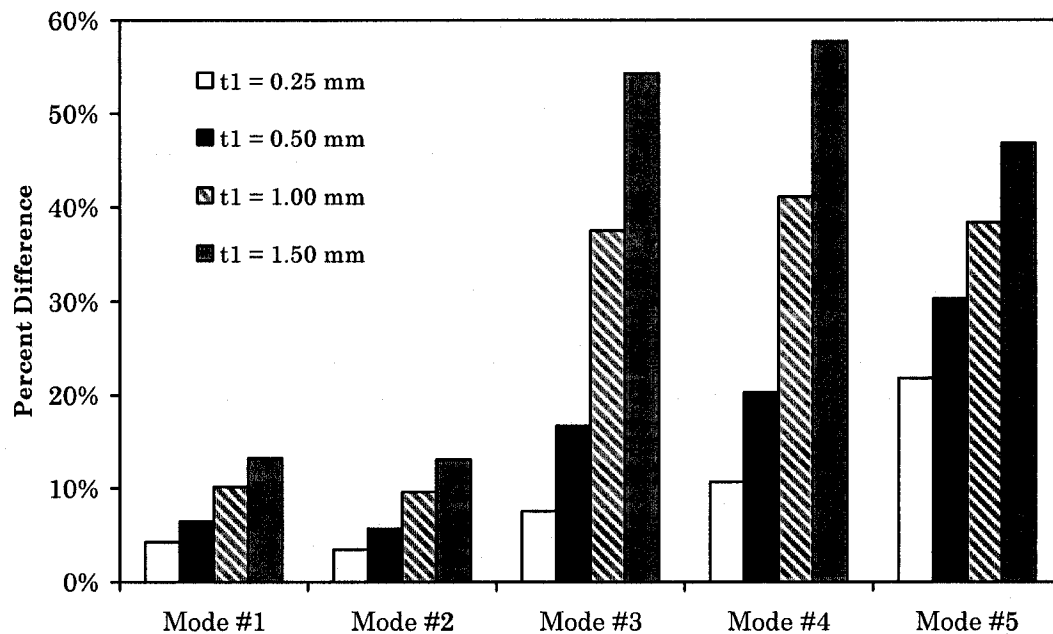


Figure 5.18: Effect of varying periprosthetic bone thickness, t_1 – Percent difference between frequency responses at $\rho_1 = 0.13$ g/cm³ and $\rho_1 = 1.20$ g/cm³. (Periprosthetic Bone: 0.5 mm $\leq t_1 \leq 1.5$ mm, 0.13 g/cm³ $\leq \rho_1 \leq 1.20$ g/cm³, $E = 1310\rho^{1.4}$, Cancellous Host Bone: Density = 1.20 g/cm³, Elastic Modulus = 1690.9 MPa)

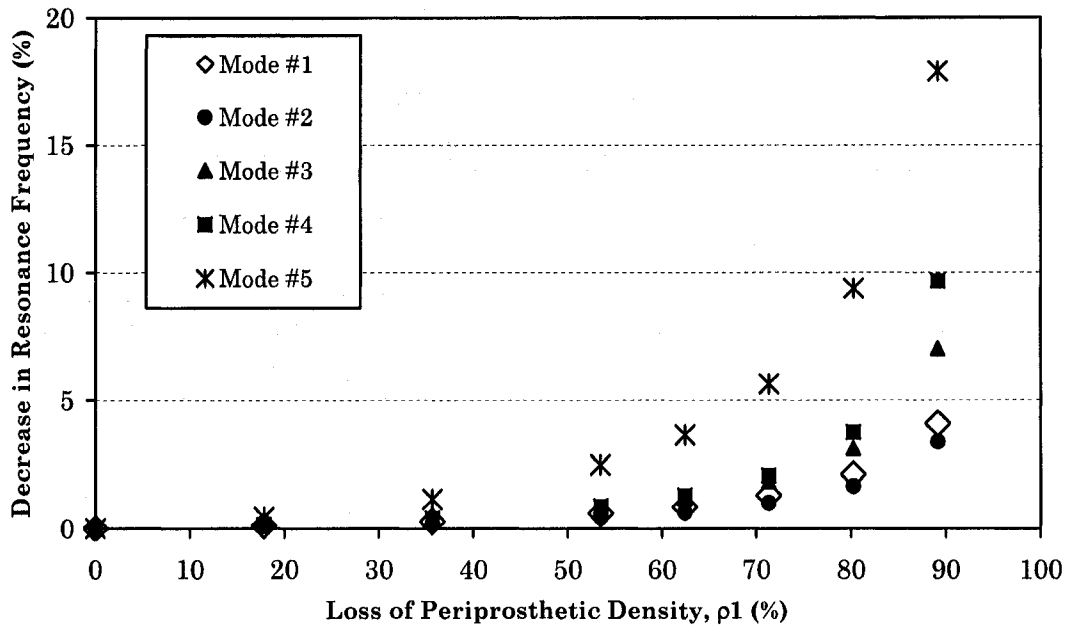


Figure 5.19: Effect of varying periprosthetic bone density ($t_1 = 0.25\text{mm}$) – Decrease in resonance frequency relative to frequency response at $\rho_1 = 1.20\text{ g/cm}^3$. (Periprosthetic Bone: $t_1 = 0.25\text{ mm}$, $0.13\text{ g/cm}^3 \leq \rho_1 \leq 1.20\text{ g/cm}^3$, $E = 1310\rho^{1.4}$, Cancellous Host Bone: Density = 1.20 g/cm^3 , Elastic Modulus = 1690.9 MPa)

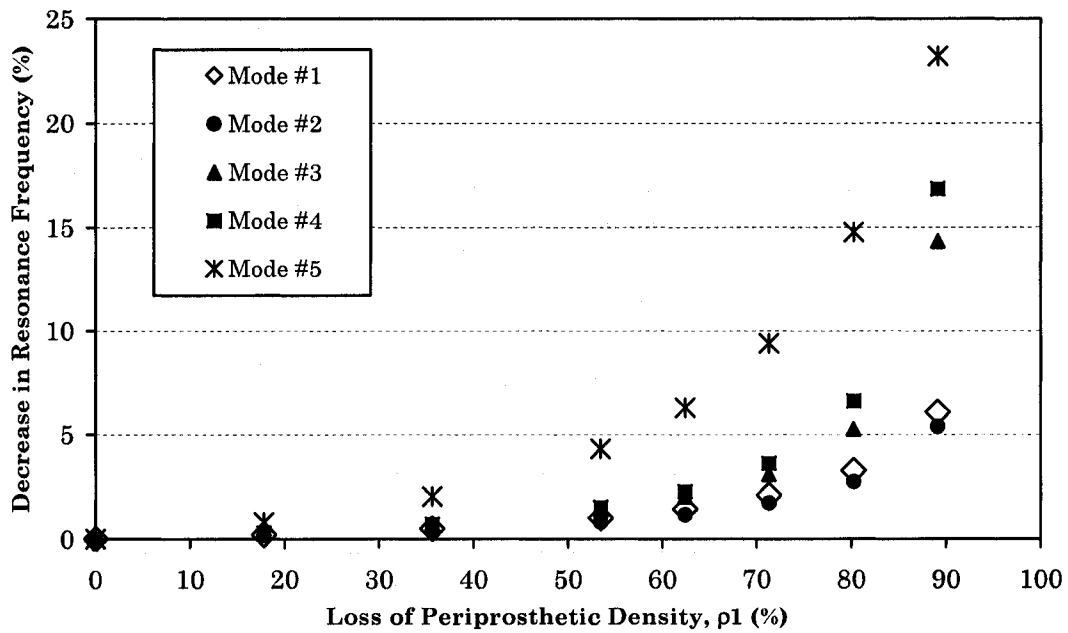


Figure 5.20: Effect of varying periprosthetic bone density ($t_1 = 0.50\text{mm}$) – Decrease in resonance frequency relative to frequency response at $\rho_1 = 1.20\text{ g/cm}^3$. (Periprosthetic Bone: $t_1 = 0.50\text{ mm}$, $0.13\text{ g/cm}^3 \leq \rho_1 \leq 1.20\text{ g/cm}^3$, $E = 1310\rho^{1.4}$, Cancellous Host Bone: Density = 1.20 g/cm^3 , Elastic Modulus = 1690.9 MPa)

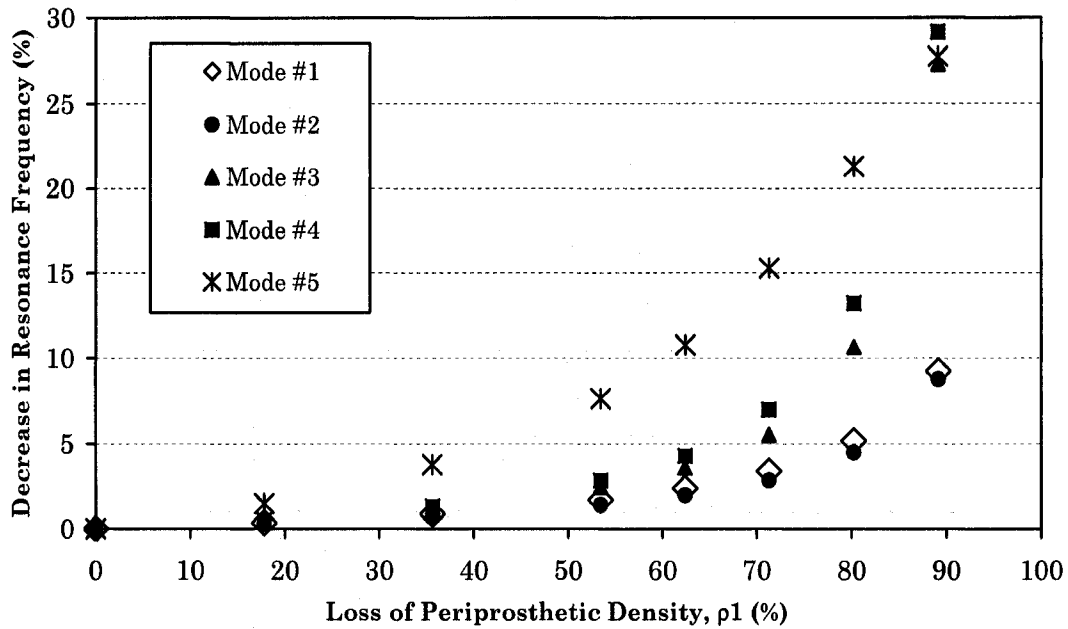


Figure 5.21: Effect of varying periprosthetic bone density ($t_1 = 1.00\text{mm}$) – Decrease in resonance frequency relative to frequency response at $\rho_1 = 1.20 \text{ g/cm}^3$. (Periprosthetic Bone: $t_1 = 1.00 \text{ mm}$, $0.13 \text{ g/cm}^3 \leq \rho_1 \leq 1.20 \text{ g/cm}^3$, $E = 1310\rho_1^{1.4}$, Cancellous Host Bone: Density = 1.20 g/cm^3 , Elastic Modulus = 1690.9 MPa)

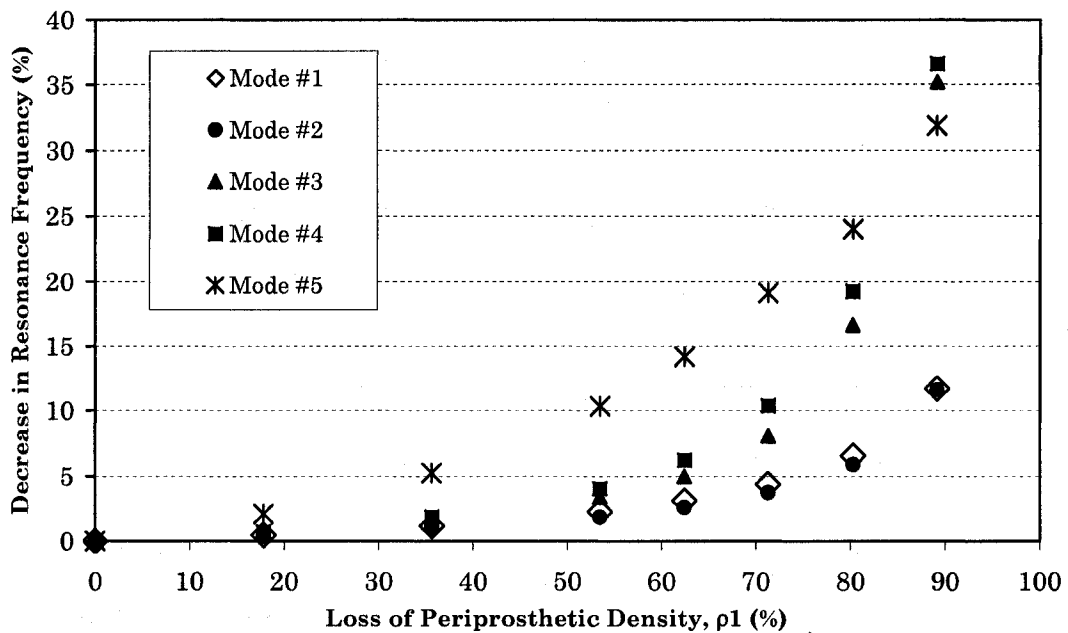


Figure 5.22: Effect of varying periprosthetic bone density ($t_1 = 1.50\text{mm}$) – Decrease in resonance frequency relative to frequency response at $\rho_1 = 1.20 \text{ g/cm}^3$. (Periprosthetic Bone: $t_1 = 1.50 \text{ mm}$, $0.13 \text{ g/cm}^3 \leq \rho_1 \leq 1.20 \text{ g/cm}^3$, $E = 1310\rho_1^{1.4}$, Cancellous Host Bone: Density = 1.20 g/cm^3 , Elastic Modulus = 1690.9 MPa)

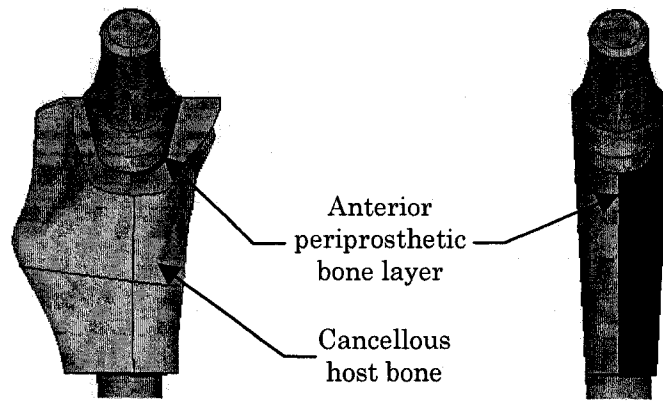
5.6 Effects of Localized Non-Osseointegrated Periprosthetic Bone along the porous-coated body of the implant

Since bone loss does not usually occur uniformly around the implant, an investigation of density changes in different “regions” is necessary to determine if changes in periprosthetic bone density in localized areas along the porous-coated body of the implant are detectable. The effects of proximal non-osseointegrated regions in comparison to distal non-osseointegrated regions along the porous-coated surface of the implant will be examined. In addition, comparisons between the non-osseointegrated anterior and posterior regions as well as the non-osseointegrated lateral and medial regions will also be observed. Furthermore, this section will include the modal analysis results of the implant due to density variations of periprosthetic bone stock located in specific physiologically-significant zones (greater trochanter, calcar, mid-lateral cortex and mid-medial cortex) along the porous-coated surface of the implant.

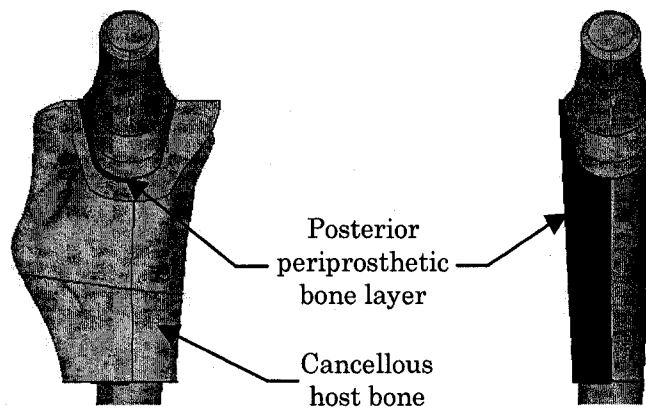
5.6.1 Anterior vs. Posterior Non-Osseointegration

An implant is regarded as osseointegrated when there is no progressive relative movement between the implant and the bone with which it has direct contact [Brånemark, 1983]. Clinically, this means that there is an interlocking mechanism whereby prosthetic components are incorporated into living bone and that the union can persist under all normal conditions of loading. Clearly, osseointegration would not be viable in the presence of bone loss or low-density periprosthetic bone stock.

In the anterior non-osseointegrated condition, the density of the periprosthetic bone on located on the anterior half of the implant (Figure 5.23a) was varied from 0.13 – 1.20 g/cm³, while the density of the healthy posterior half of the implant was 1.20 g/cm³. In the posterior non-osseointegrated situation (Figure 5.23b), the conditions were reversed.



(a) Anterior periprosthetic bone stock – shown with and without host bone stock



(b) Posterior periprosthetic bone stock – shown with and without host bone stock

Figure 5.23: Anterior vs. Posterior Non-Osseointegration

In both cases, periprosthetic bone: $t_1 = 1.0 \text{ mm}$, $0.13 \text{ g/cm}^3 \leq \rho_1 \leq 1.20 \text{ g/cm}^3$, and healthy cancellous host bone: density = 1.20 g/cm^3 , elastic modulus = 1690.9 MPa .

Figure 5.24 indicates that the largest range in frequency-response, between $\rho_1 = 0.13 \text{ g/cm}^3$ and $\rho_1 = 1.20 \text{ g/cm}^3$, occurred in Mode #5 with a percent difference of 17.6% for the anterior half and 16.9% for the posterior half. Comparisons of the modal response of the implant in anterior or posterior non-osseointegrated conditions (Figure 5.28 to 5.32) indicate that the frequency-response of the implant is sensitive to localized density variations. However, during the fifth mode, the width of the frequency range is very similar for both the anterior and posterior non-

osseointegration conditions (804 Hz and 778 Hz respectively, as shown in Figure 5.32). Therefore, the results from Mode #5 would not be very useful for differentiating between the anterior and posterior non-osseointegrated conditions. Instead, the results in Mode #3 are more effective for differentiating between anterior and posterior non-osseointegrated conditions (3.7% and 6.4% respectively), as shown in Figure 5.24. The frequency-response range of the non-osseointegrated anterior periprosthetic bone was approximately 166% larger than the non-osseointegrated posterior condition during Mode #3 (261 Hz vs. 157 Hz respectively).

A comparison of the decrease in frequency response relative to the frequency response at $\rho_1 = 1.20 \text{ g/cm}^3$ (Figures 5.25 to 5.26) reveals that the rate of decrease in the frequency is much higher during Mode #5 than the other modes and therefore more sensitive to detecting early decreases in the density of the periprosthetic bone for both anterior and posterior halves. Therefore, the fifth mode frequency responses are more likely to indicate early loosening of the prosthetic in these regions. A similar analysis of the Mode #3 results (Figure 5.27) indicates that the rate of decrease in the frequency results is slightly higher for the anterior half.

In summary, Figures 5.25 to 5.32 show that the frequency-response to density variations, between the non-osseointegrated anterior and posterior halves, are difficult to distinguish and it would be hard to uniquely identify between the anterior and posterior halves within only one mode of results. Rather, the results from Mode #5 and Mode #3 would need to be concurrently assessed to determine the absence of osseointegration and to establish which side of the implant is more likely to be non-osseointegrated. Once again, the results in Mode #5 are more likely to indicate early loosening, although not able to distinctly identify which half.

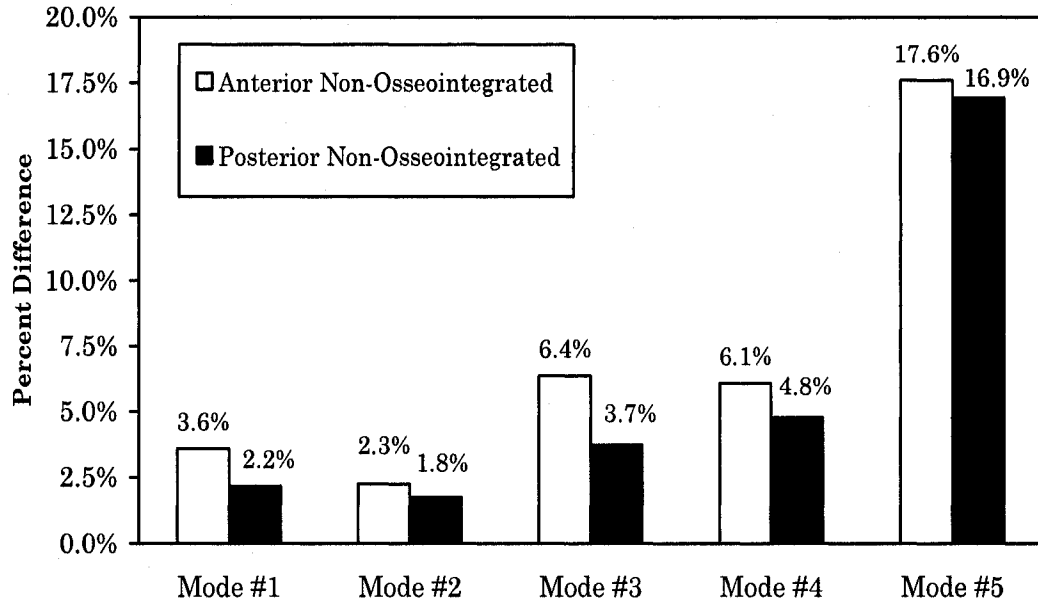


Figure 5.24: Anterior vs. Posterior Non-Osseointegration – Percent difference between frequency responses at $\rho_1 = 0.13 \text{ g/cm}^3$ and $\rho_1 = 1.20 \text{ g/cm}^3$ (Periprosthetic Bone: $t_1 = 1.0 \text{ mm}$, $0.13 \text{ g/cm}^3 \leq \rho_1 \leq 1.20 \text{ g/cm}^3$, $E = 1310\rho^{1.4}$, Cancellous Host Bone: Density = 1.20 g/cm^3 , Elastic Modulus = 1690.9 MPa)

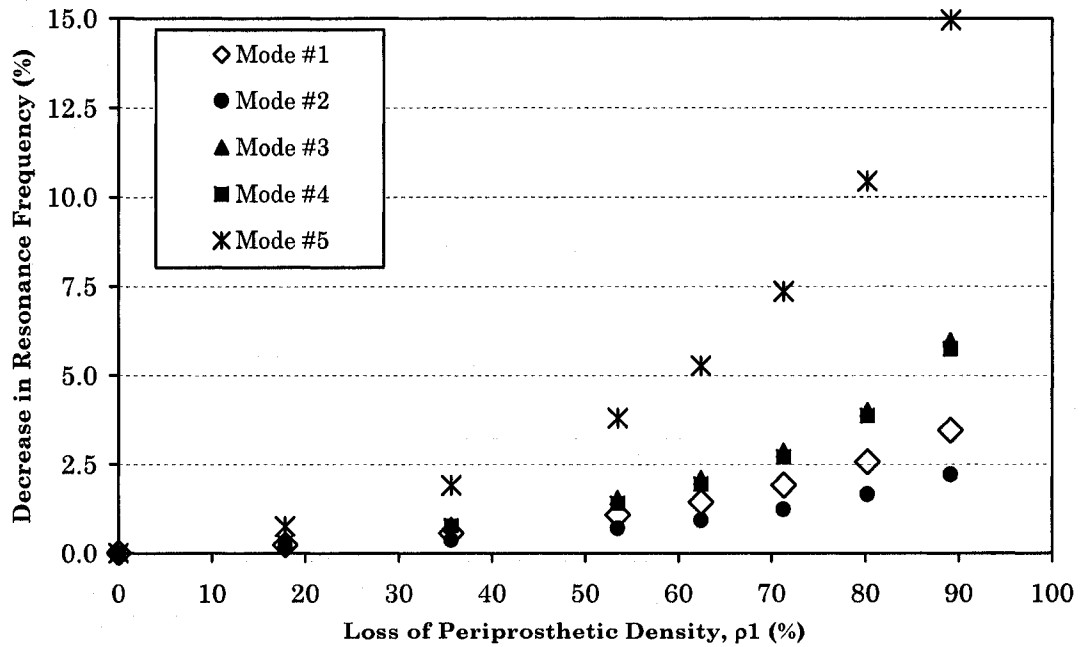


Figure 5.25: Anterior Non-Osseointegration – Decrease in resonance frequency relative to frequency response at $\rho_1 = 1.20 \text{ g/cm}^3$. (Periprosthetic Bone: $t_1 = 1.00 \text{ mm}$, $0.13 \text{ g/cm}^3 \leq \rho_1 \leq 1.20 \text{ g/cm}^3$, $E = 1310\rho^{1.4}$, Cancellous Host Bone: Density = 1.20 g/cm^3 , Elastic Modulus = 1690.9 MPa)

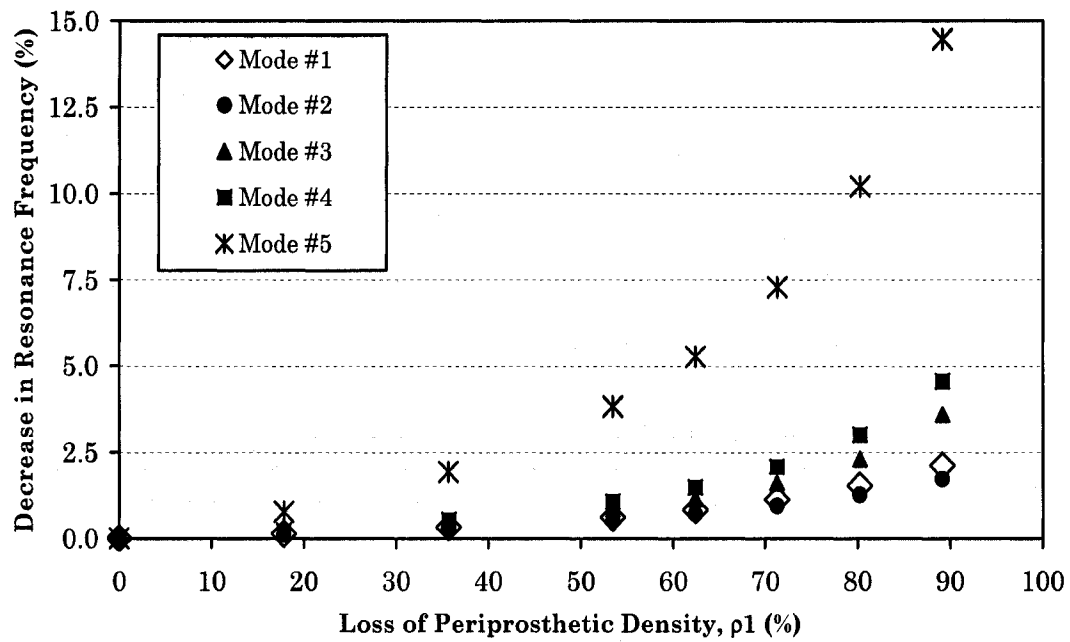


Figure 5.26: Posterior Non-Osseointegration –
 Decrease in resonance frequency relative to frequency response at $\rho_1 = 1.20 \text{ g/cm}^3$.
 (Periprosthetic Bone: $t_1 = 1.00 \text{ mm}$, $0.13 \text{ g/cm}^3 \leq \rho_1 \leq 1.20 \text{ g/cm}^3$, $E = 1310\rho^{1.4}$,
 Cancellous Host Bone: Density = 1.20 g/cm^3 , Elastic Modulus = 1690.9 MPa)

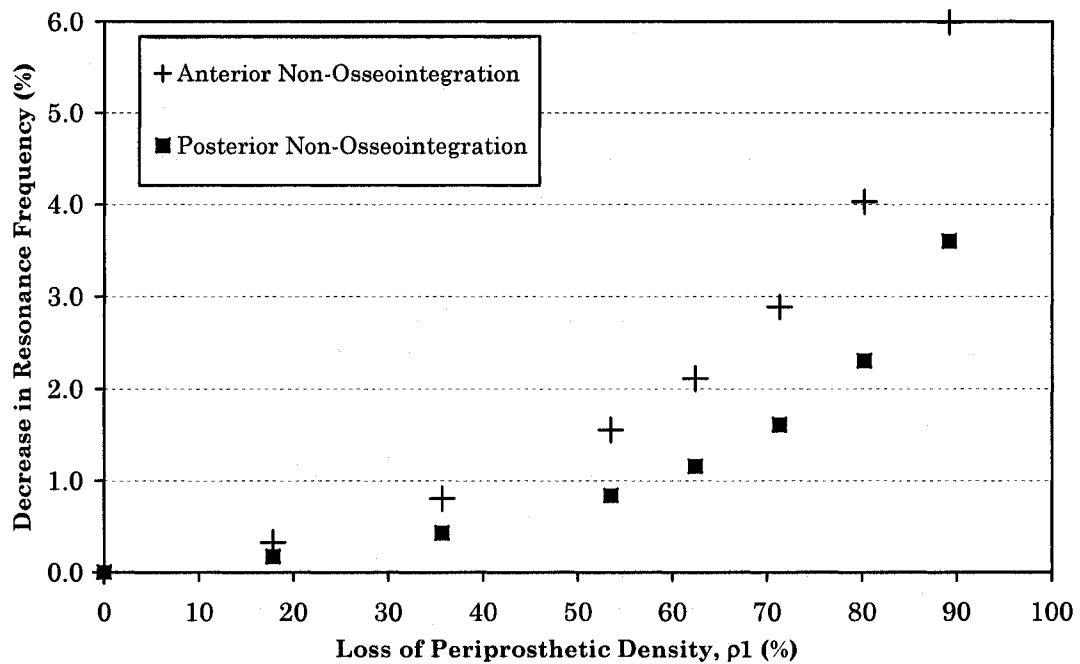


Figure 5.27: Anterior vs. Posterior Non-Osseointegration (Mode #3) –
 Decrease in resonance frequency relative to frequency response at $\rho_1 = 1.20 \text{ g/cm}^3$.
 (Periprosthetic Bone: $t_1 = 1.00 \text{ mm}$, $0.13 \text{ g/cm}^3 \leq \rho_1 \leq 1.20 \text{ g/cm}^3$, $E = 1310\rho^{1.4}$,
 Cancellous Host Bone: Density = 1.20 g/cm^3 , Elastic Modulus = 1690.9 MPa)

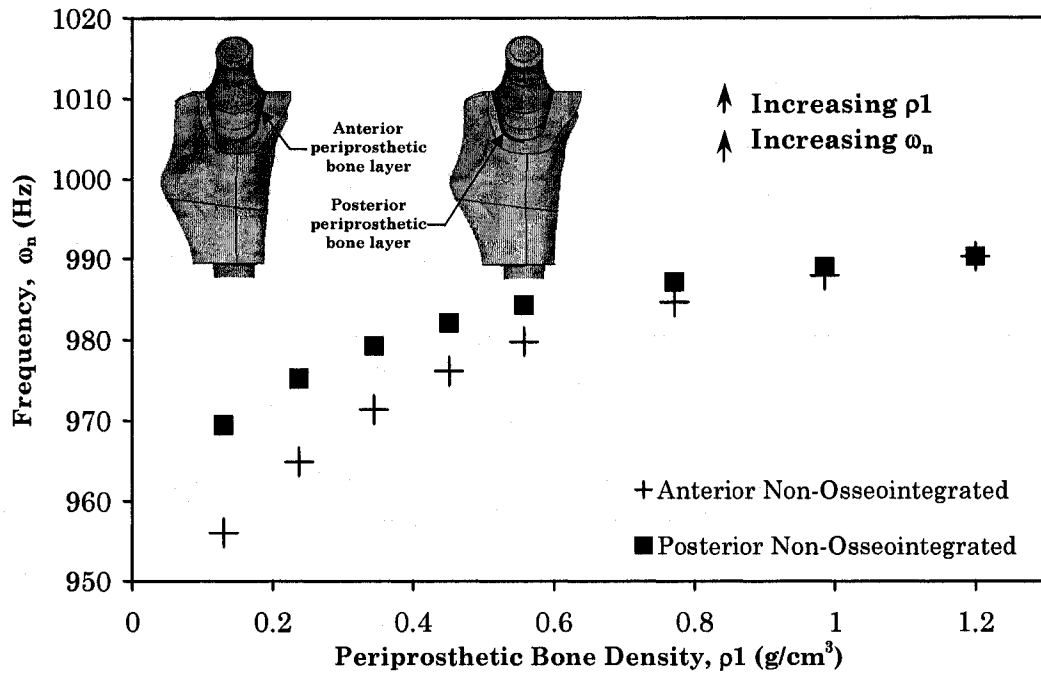


Figure 5.28: Anterior vs. Posterior Non-Osseointegration – Modal Analysis (Mode #1)
 (Periprosthetic Bone: $t_1 = 1.0$ mm, $0.13 \text{ g/cm}^3 \leq \rho_1 \leq 1.20 \text{ g/cm}^3$, $E = 1310\rho^{1.4}$,
 Cancellous Host Bone: Density = 1.20 g/cm^3 , Elastic Modulus = 1690.9 MPa)

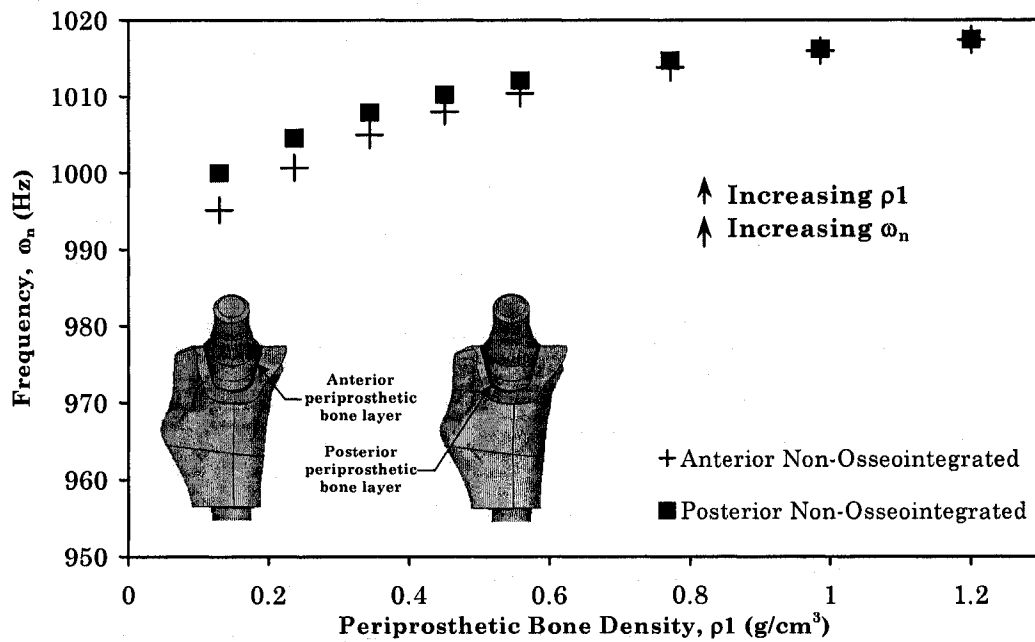


Figure 5.29: Anterior vs. Posterior Non-Osseointegration – Modal Analysis (Mode #2)
 (Periprosthetic Bone: $t_1 = 1.0$ mm, $0.13 \text{ g/cm}^3 \leq \rho_1 \leq 1.20 \text{ g/cm}^3$, $E = 1310\rho^{1.4}$,
 Cancellous Host Bone: Density = 1.20 g/cm^3 , Elastic Modulus = 1690.9 MPa)

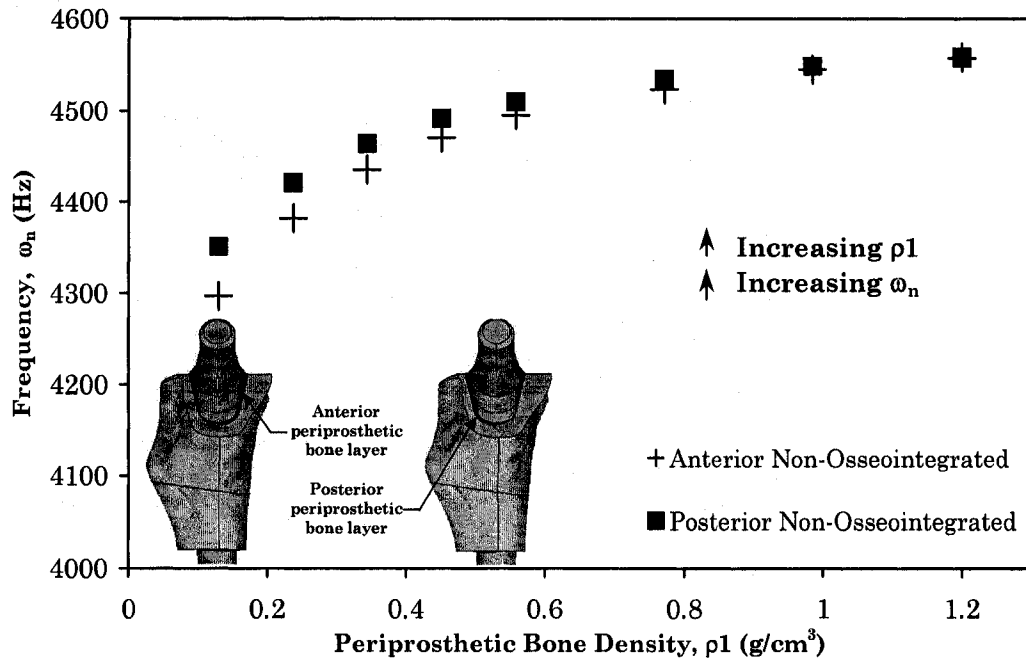


Figure 5.30: Anterior vs. Posterior Non-Osseointegration – Modal Analysis (Mode #3)
 (Periprosthetic Bone: $t_1 = 1.0$ mm, $0.13 \text{ g/cm}^3 \leq \rho_1 \leq 1.20 \text{ g/cm}^3$, $E = 1310\rho_1^{1.4}$, Cancellous Host Bone: Density = 1.20 g/cm^3 , Elastic Modulus = 1690.9 MPa)

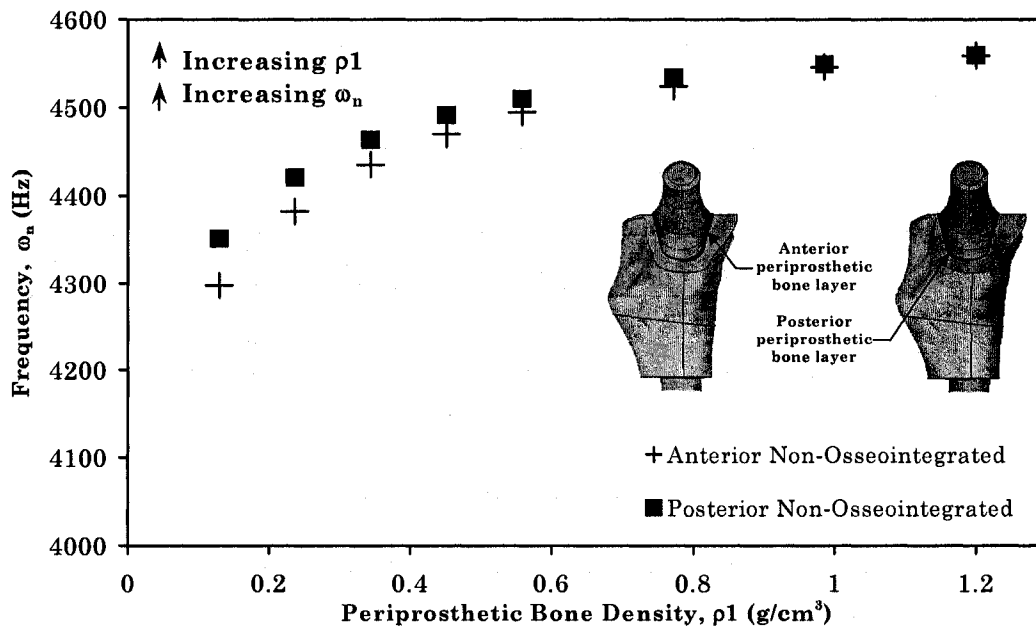


Figure 5.31: Anterior vs. Posterior Non-Osseointegration – Modal Analysis (Mode #4)
 (Periprosthetic Bone: $t_1 = 1.0$ mm, $0.13 \text{ g/cm}^3 \leq \rho_1 \leq 1.20 \text{ g/cm}^3$, $E = 1310\rho_1^{1.4}$, Cancellous Host Bone: Density = 1.20 g/cm^3 , Elastic Modulus = 1690.9 MPa)

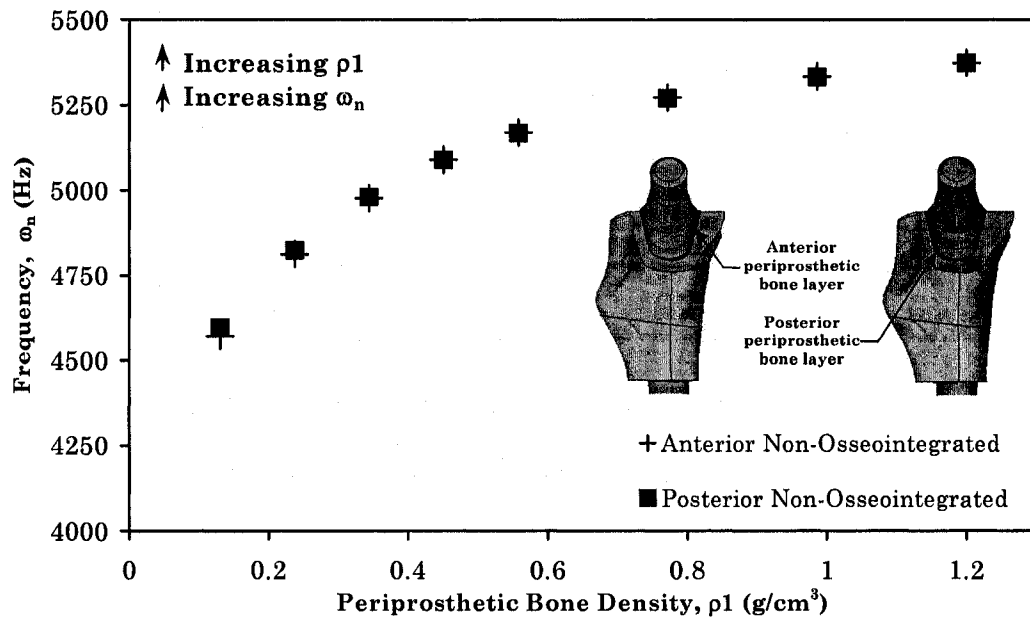


Figure 5.32: Anterior vs. Posterior Non-Osseointegration – Modal Analysis (Mode #5)
 (Periprosthetic Bone: $t_1 = 1.0$ mm, $0.13 \text{ g/cm}^3 \leq \rho_1 \leq 1.20 \text{ g/cm}^3$, $E = 1310\rho_1^{1.4}$,
 Cancellous Host Bone: Density = 1.20 g/cm^3 , Elastic Modulus = 1690.9 MPa)

5.6.2 Medial vs. Lateral Non-Osseointegration

In the medial non-osseointegrated case, the density of the periprosthetic bone on located on the predominately medial half of the implant (Figure 5.33a) was varied from 0.13 – 1.20 g/cm³, while the density of the posterior half of the implant was healthy ($\rho_1 = 1.20$ g/cm³). In the lateral non-osseointegrated situation (Figure 5.33b), the conditions were reversed.

Although the volumes of medial and lateral sections are not equal (0.20970E-05 m³ and 0.15883E-05 m³ respectively), it is more physiologically accurate to consider these sections in this manner since the implant has been designed correspondingly to achieve maximum fixation and to minimize the local or systemic rejection response.

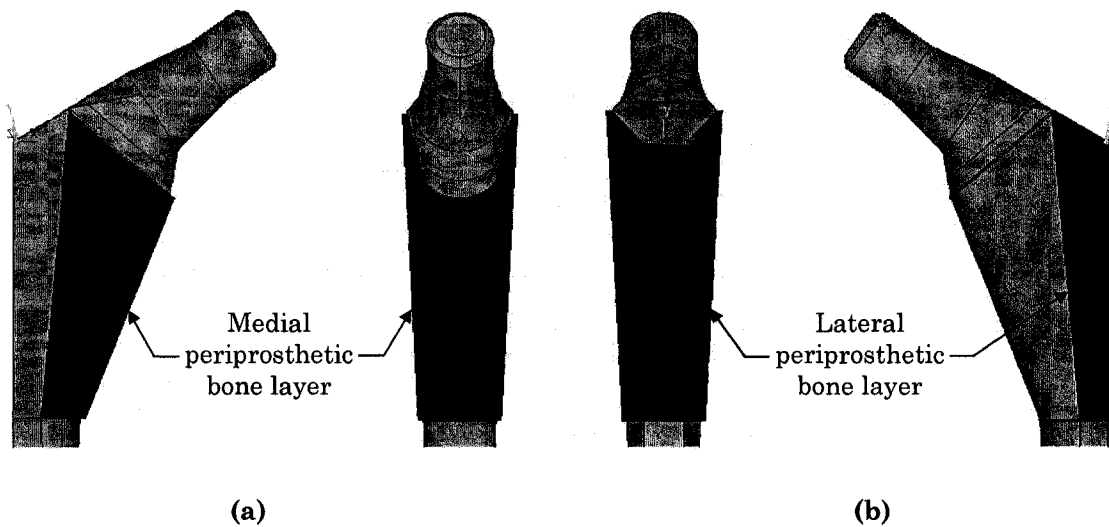


Figure 5.33: Medial vs. Lateral Non-Osseointegration

(a) Medial periprosthetic bone stock

(b) Lateral periprosthetic bone stock

In both cases, periprosthetic bone: $t_1 = 1.0$ mm, 0.13 g/cm³ $\leq \rho_1 \leq 1.20$ g/cm³, and healthy cancellous host bone: density = 1.20 g/cm³, elastic modulus = 1690.9 MPa.

According to the results shown in Figure 5.34, between $\rho_1 = 0.13$ g/cm³ and $\rho_1 = 1.20$ g/cm³, modes #1, 3, 4 and 5 show that the percent difference of the frequency-response of non-osseointegration of the medial periprosthetic bone is

larger than the percent difference of the frequency-response of the non-osseointegrated lateral periprosthetic bone. The largest percent difference occurred for the medial non-osseointegrated case during Mode #5 with a percent difference of 28.4%. The Mode #3, 4 and 5 results (Figures 5.34) indicate that the frequency-responses of the non-osseointegration of the predominately medial side varies significantly (11.0%, 13.5% and 28.4% respectively) between $\rho_1 = 0.13 \text{ g/cm}^3$ and $\rho_1 = 1.20 \text{ g/cm}^3$.

For the lateral non-osseointegrated case, the largest percent difference was 5.1%, which occurred during the fourth mode. These results indicate that the non-osseointegration of the predominately lateral side does not produce frequency-responses that are highly distinguishable between $\rho_1 = 0.13 \text{ g/cm}^3$ and $\rho_1 = 1.20 \text{ g/cm}^3$.

A comparison of the decrease in frequency response relative to the frequency response at $\rho_1 = 1.20 \text{ g/cm}^3$ (Figures 5.35) reveals that the rate of decrease in the frequency is much higher during Mode #5 than the other modes for the non-osseointegrated medial case. Therefore, the results in Mode #5 are more sensitive to detecting early decreases in the density of the predominately medially-located periprosthetic bone. In contrast, the frequency change of the laterally-located periprosthetic bone is nominal as indicated by Figure 5.34 and 5.36.

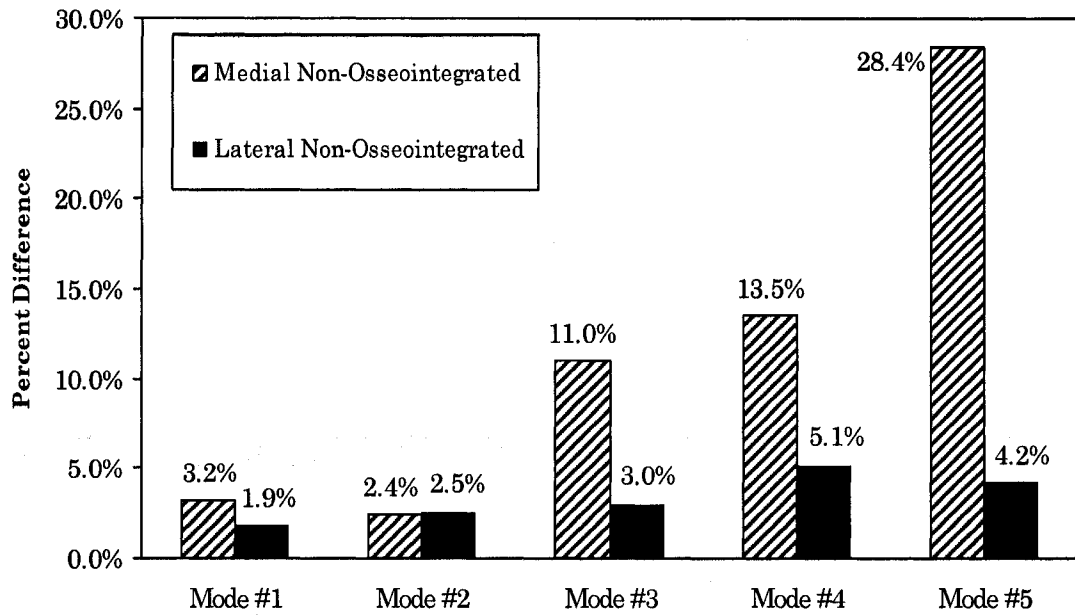


Figure 5.34: Medial vs. Lateral Non-Osseointegration – Percent difference between frequency responses at $\rho_1 = 0.13 \text{ g/cm}^3$ and $\rho_1 = 1.20 \text{ g/cm}^3$ (Periprosthetic Bone: $t_1 = 1.0 \text{ mm}$, $0.13 \text{ g/cm}^3 \leq \rho_1 \leq 1.20 \text{ g/cm}^3$, $E = 1310\rho_1^{1.4}$, Cancellous Host Bone: Density = 1.20 g/cm^3 , Elastic Modulus = 1690.9 MPa)

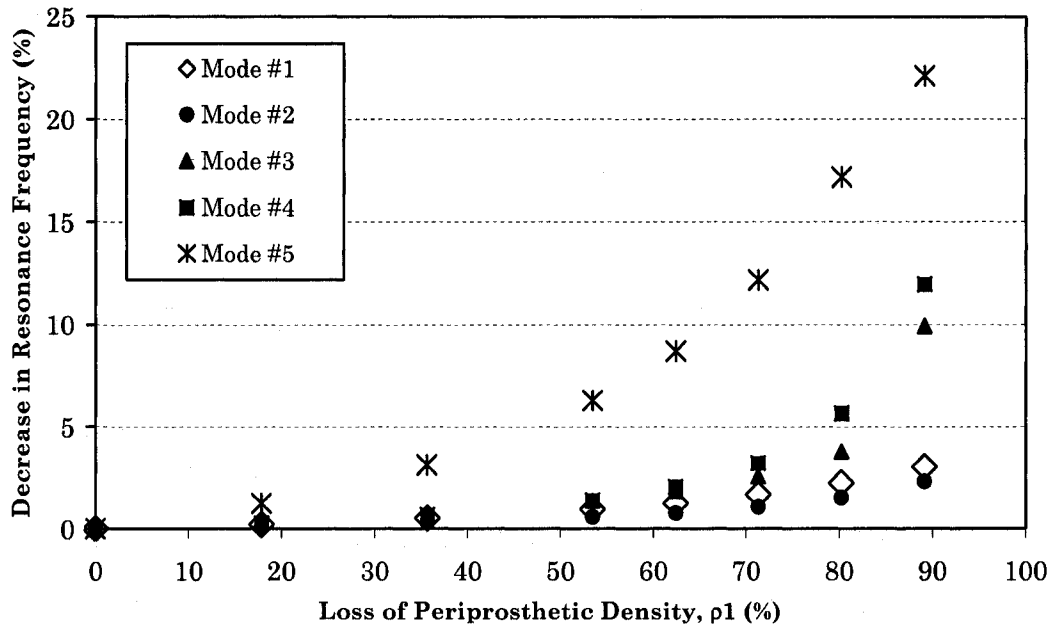


Figure 5.35: Medial Non-Osseointegration – Decrease in resonance frequency relative to frequency response at $\rho_1 = 1.20 \text{ g/cm}^3$. (Periprosthetic Bone: $t_1 = 1.00 \text{ mm}$, $0.13 \text{ g/cm}^3 \leq \rho_1 \leq 1.20 \text{ g/cm}^3$, $E = 1310\rho_1^{1.4}$, Cancellous Host Bone: Density = 1.20 g/cm^3 , Elastic Modulus = 1690.9 MPa)

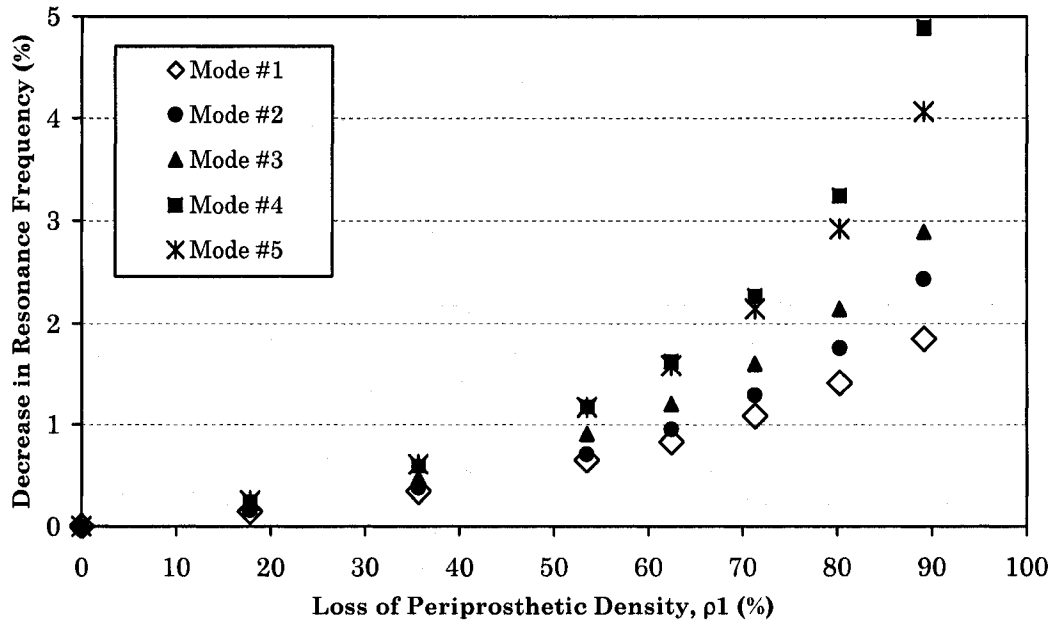


Figure 5.36: Lateral Non-Osseointegration –
 Decrease in resonance frequency relative to frequency response at $\rho_1 = 1.20 \text{ g/cm}^3$.
 (Periprosthetic Bone: $t_1 = 1.00 \text{ mm}$, $0.13 \text{ g/cm}^3 \leq \rho_1 \leq 1.20 \text{ g/cm}^3$, $E = 1310\rho_1^{1.4}$,
 Cancellous Host Bone: Density = 1.20 g/cm^3 , Elastic Modulus = 1690.9 MPa)

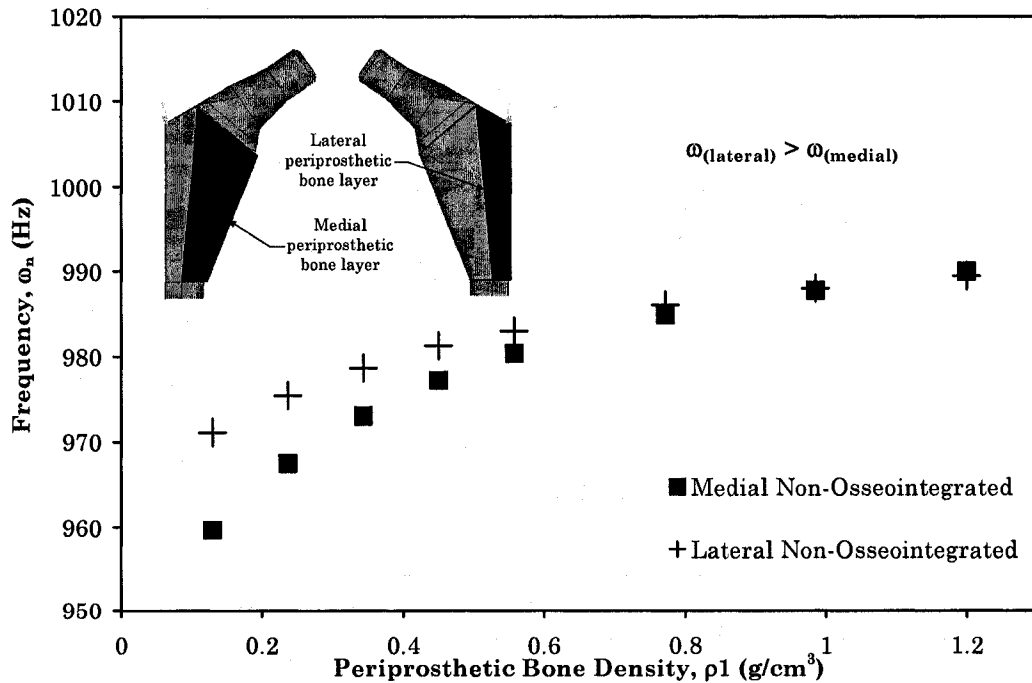


Figure 5.37: Medial vs. Lateral Non-Osseointegration – Modal Analysis (Mode #1).
 (Periprosthetic Bone: $t_1 = 1.0 \text{ mm}$, $0.13 \text{ g/cm}^3 \leq \rho_1 \leq 1.20 \text{ g/cm}^3$, $E = 1310\rho_1^{1.4}$,
 Cancellous Host Bone: Density = 1.20 g/cm^3 , Elastic Modulus = 1690.9 MPa)

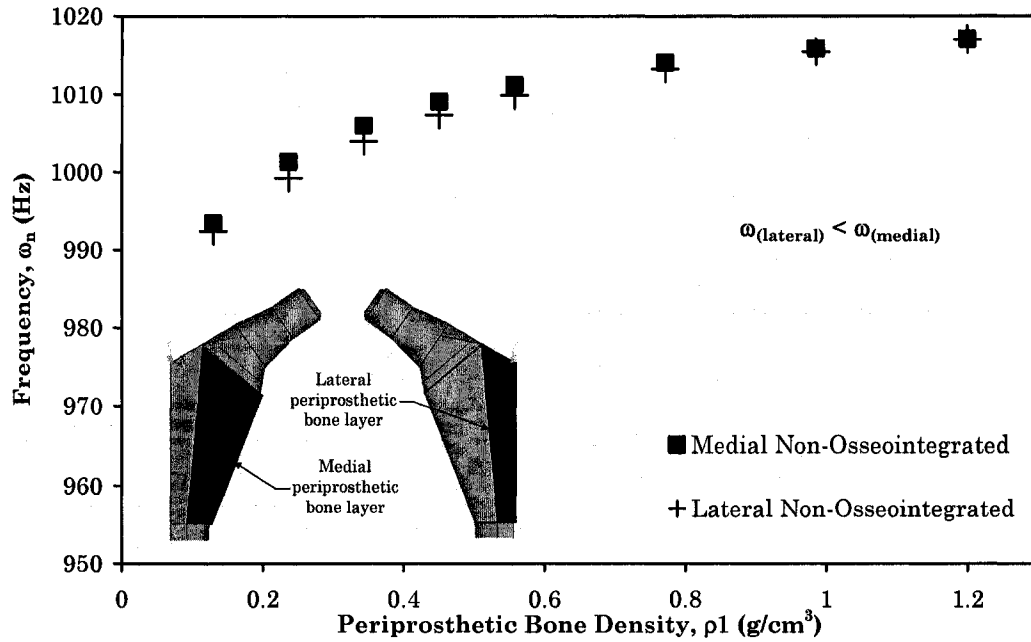


Figure 5.38: Medial vs. Lateral Non-Osseointegration – Modal Analysis (Mode #2).
 (Periprosthetic Bone: $t_1 = 1.0$ mm, $0.13 \text{ g/cm}^3 \leq \rho_1 \leq 1.20 \text{ g/cm}^3$, $E = 1310\rho^{1.4}$,
 Cancellous Host Bone: Density = 1.20 g/cm^3 , Elastic Modulus = 1690.9 MPa)

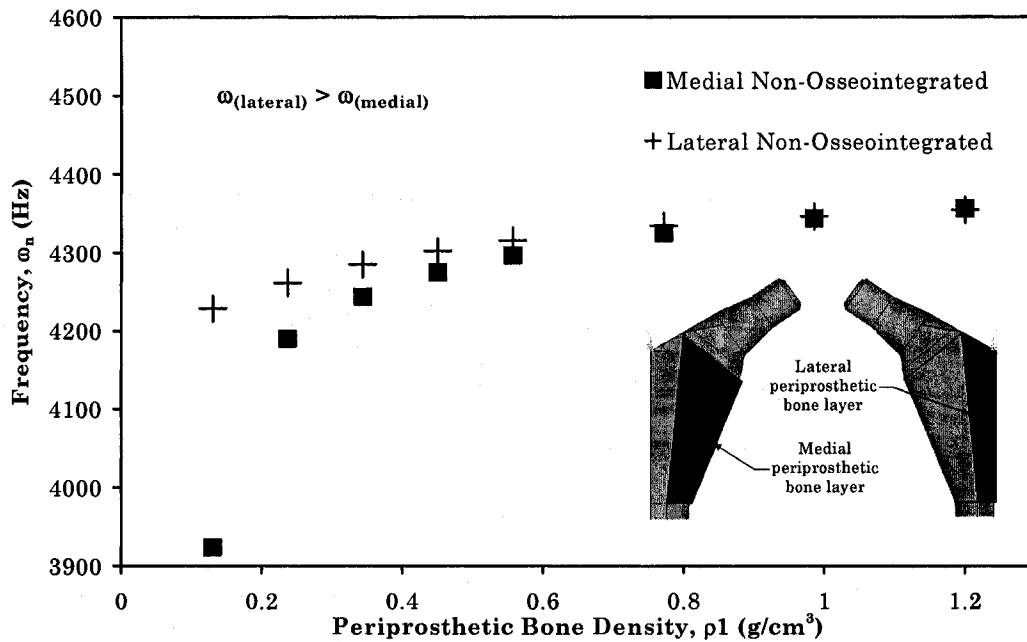


Figure 5.39: Medial vs. Lateral Non-Osseointegration – Modal Analysis (Mode #3).
 (Periprosthetic Bone: $t_1 = 1.0$ mm, $0.13 \text{ g/cm}^3 \leq \rho_1 \leq 1.20 \text{ g/cm}^3$, $E = 1310\rho^{1.4}$,
 Cancellous Host Bone: Density = 1.20 g/cm^3 , Elastic Modulus = 1690.9 MPa)

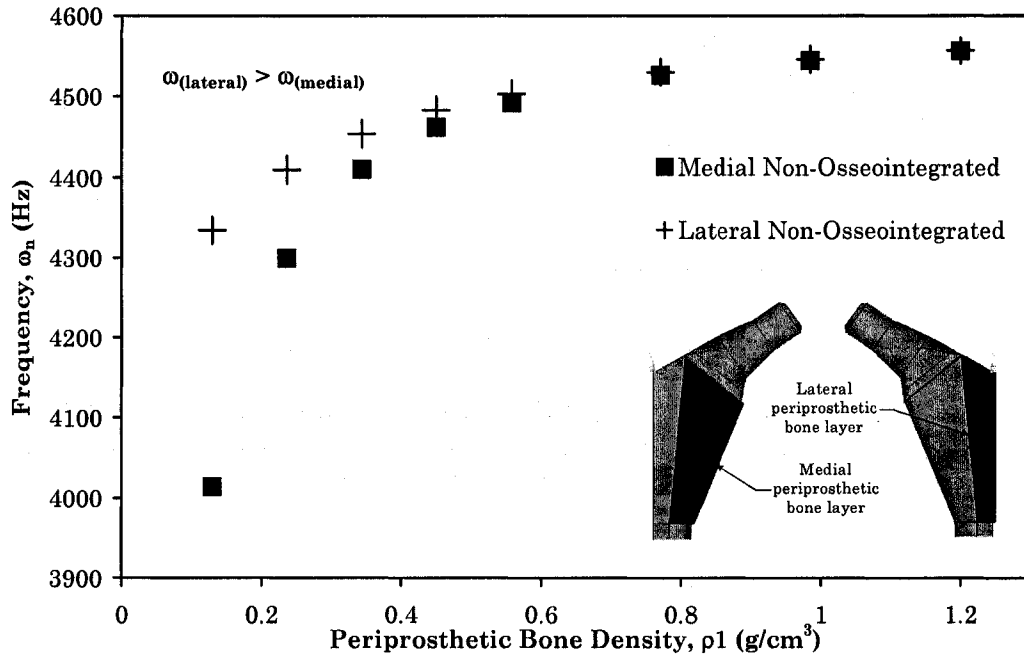


Figure 5.40: Medial vs. Lateral Non-Osseointegration – Modal Analysis (Mode #4).
 (Periprosthetic Bone: $t_1 = 1.0$ mm, $0.13 \text{ g/cm}^3 \leq \rho_1 \leq 1.20 \text{ g/cm}^3$, $E = 1310\rho^{1.4}$,
 Cancellous Host Bone: Density = 1.20 g/cm^3 , Elastic Modulus = 1690.9 MPa)

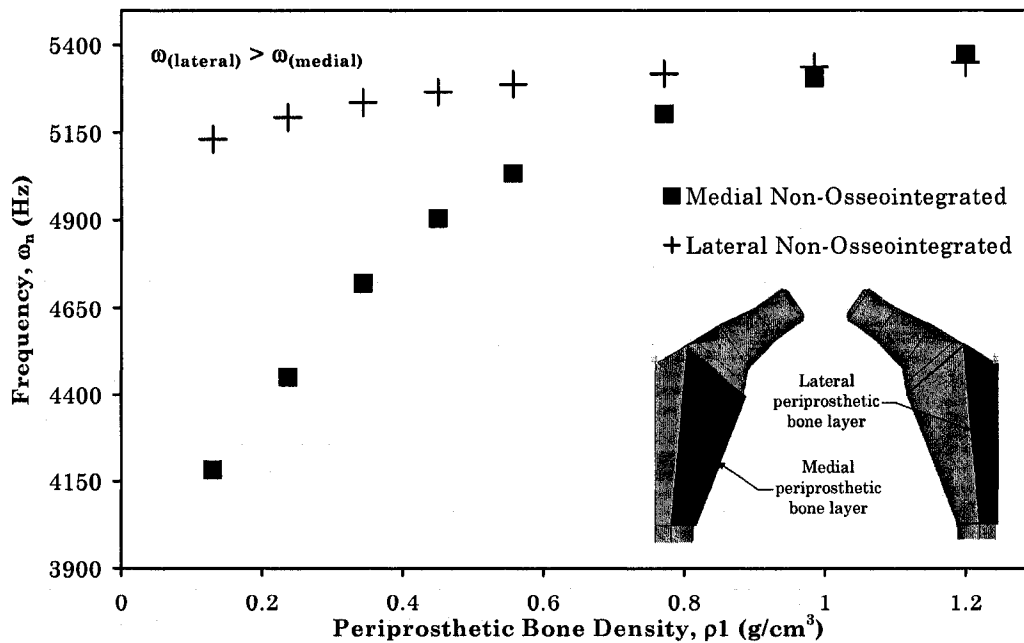


Figure 5.41: Medial vs. Lateral Non-Osseointegration – Modal Analysis (Mode #5).
 (Periprosthetic Bone: $t_1 = 1.0$ mm, $0.13 \text{ g/cm}^3 \leq \rho_1 \leq 1.20 \text{ g/cm}^3$, $E = 1310\rho^{1.4}$,
 Cancellous Host Bone: Density = 1.20 g/cm^3 , Elastic Modulus = 1690.9 MPa)

5.6.3 Proximal vs. Distal Non-Osseointegration

To examine the effects of proximal or distal non-osseointegration, the periprosthetic bone layer was divided into two sections. Each section enclosed approximately one-half of the volume of the porous-coated body of the implant (Figure 5.42). The division of the two sections corresponded to a distance of 126.4 mm measured from the distal tip of the femoral stem and the geometric properties are listed in Table 5.3.

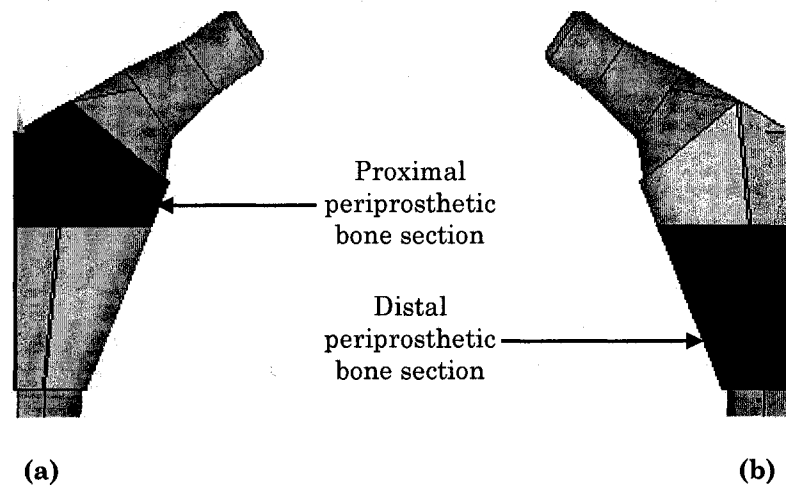


Figure 5.42: Proximal vs. Distal Non-Osseointegration
 (a) Proximal periprosthetic bone stock
 (b) Distal periprosthetic bone stock

In both cases, periprosthetic bone: $t_1 = 1.0 \text{ mm}$, $0.13 \text{ g/cm}^3 \leq \rho_1 \leq 1.20 \text{ g/cm}^3$, and healthy cancellous host bone: density = 1.20 g/cm^3 , elastic modulus = 1690.9 MPa .

Table 5.3: Geometric Properties of Proximal and Distal sections

Section	Volume of Section (m ³)	Volume of implant enclosed by section (m ³)
Proximal	1.57e-06	8.86e-06
Distal	2.14e-06	8.91e-06

The results shown in Figure 5.43 indicate that percent difference of the frequency-response of the distal half is higher than the proximal half during the first four modes. Among the first four modes, the largest percent difference was 17.3% during the fourth mode for the non-osseointegrated distal portion. However, the largest percent difference, of all five modes, occurred during the fifth mode (23.2%) for the proximal half.

Based on the results shown in Figure 5.43, although the fourth mode produced the highest range for the distal portion, the results of mode #1 indicate that the first mode is approximately 46 times more sensitive to density variations of the distal portion than the proximal portion (9.6% vs. 0.2% respectively). However, to confirm proximal non-osseointegration, the fifth mode frequency-response appears to be more sensitive to density variations of the proximal portion. The fifth mode percent difference of the frequency-response, between $\rho_1 = 0.13 \text{ g/cm}^3$ and $\rho_1 = 1.20 \text{ g/cm}^3$, was 23.2% for the proximal portion and 3.7% for the distal portion.

A comparison of the decrease in frequency response relative to the frequency response at $\rho_1 = 1.20 \text{ g/cm}^3$ (Figures 5.44) reveals that the rate of decrease in the frequency is much higher during Mode #5 than the other modes for the non-osseointegrated proximal portion. Therefore, these results further support the observation that frequency-response in Mode #5 is more sensitive to detecting early decreases in the density of the proximal periprosthetic bone. For the distally-located periprosthetic bone case, the frequency change is slightly larger in Mode #4 than the other modes, as indicated by Figure 5.45.

To attempt to differentiate between proximally- or distally- located non-integrated periprosthetic bone, the frequency response results from Mode #1, 2 and 5 would need to be concurrently assessed in order to aid in determining which part of the implant is more likely to be loosened.

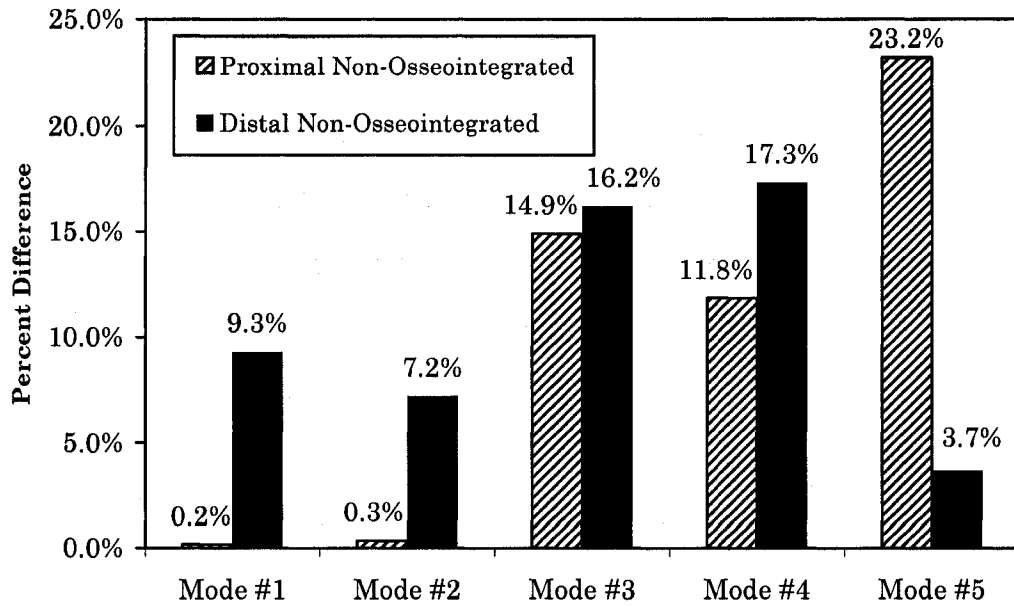


Figure 5.43: Proximal vs. Distal Non-Osseointegration – Percent difference between frequency responses at $\rho_1 = 0.13 \text{ g/cm}^3$ and $\rho_1 = 1.20 \text{ g/cm}^3$ (Periprosthetic Bone: $t_1 = 1.0 \text{ mm}$, $0.13 \text{ g/cm}^3 \leq \rho_1 \leq 1.20 \text{ g/cm}^3$, $E = 1310\rho_1^{1.4}$, Cancellous Host Bone: Density = 1.20 g/cm^3 , Elastic Modulus = 1690.9 MPa)

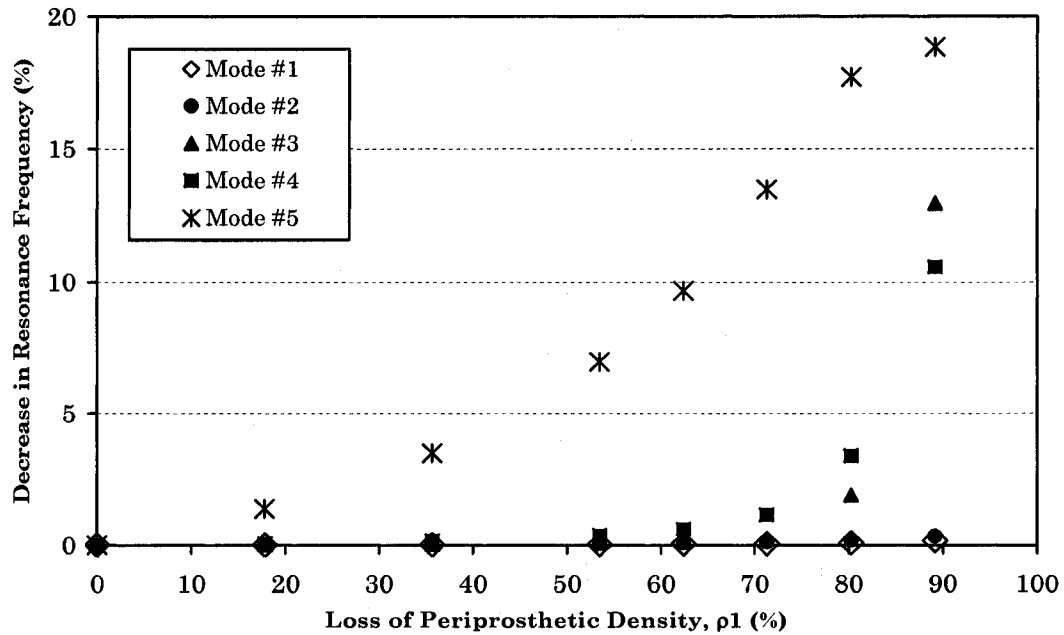


Figure 5.44: Proximal Non-Osseointegration – Decrease in resonance frequency relative to frequency response at $\rho_1 = 1.20 \text{ g/cm}^3$. (Periprosthetic Bone: $t_1 = 1.00 \text{ mm}$, $0.13 \text{ g/cm}^3 \leq \rho_1 \leq 1.20 \text{ g/cm}^3$, $E = 1310\rho_1^{1.4}$, Cancellous Host Bone: Density = 1.20 g/cm^3 , Elastic Modulus = 1690.9 MPa)

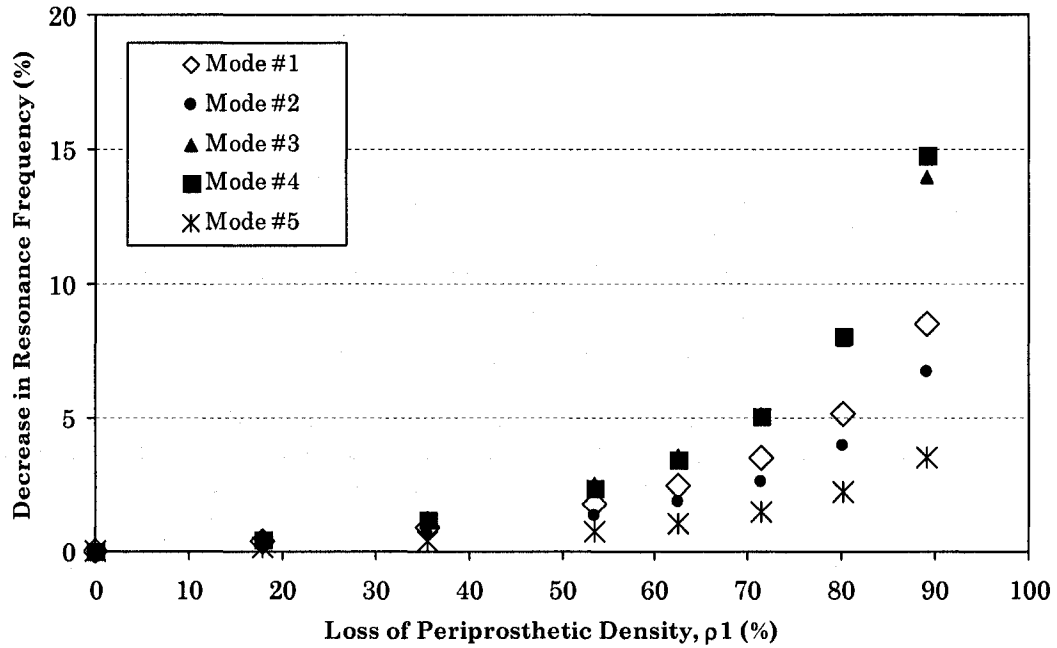


Figure 5.45: Distal Non-Osseointegration -
 Decrease in resonance frequency relative to frequency response at $\rho_1 = 1.20 \text{ g/cm}^3$.
 (Periprosthetic Bone: $t_1 = 1.00 \text{ mm}$, $0.13 \text{ g/cm}^3 \leq \rho_1 \leq 1.20 \text{ g/cm}^3$, $E = 1310\rho^{1.4}$,
 Cancellous Host Bone: Density = 1.20 g/cm^3 , Elastic Modulus = 1690.9 MPa)

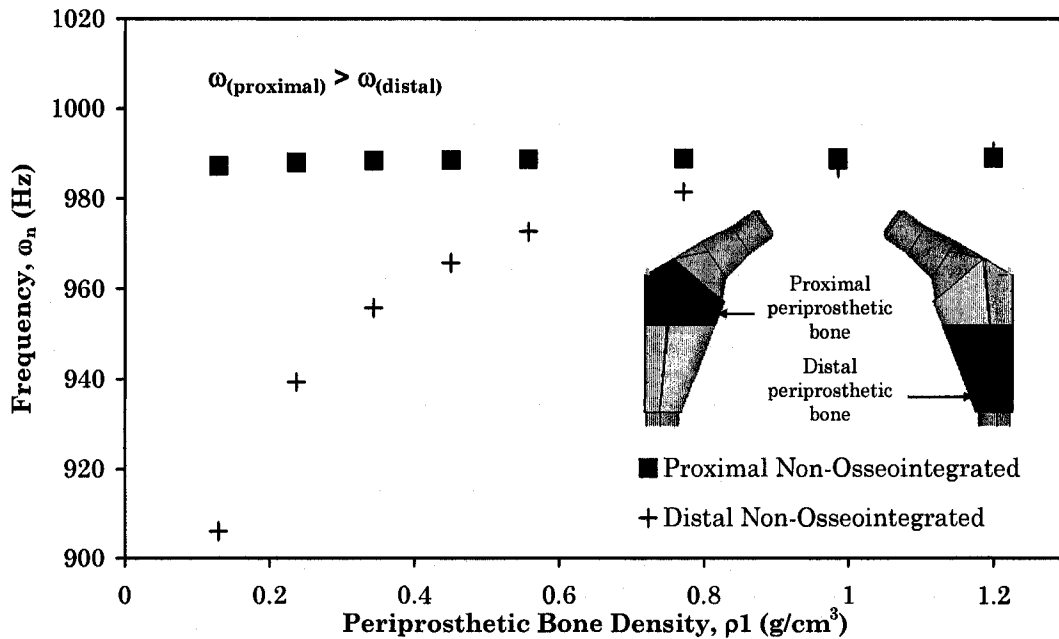


Figure 5.46: Proximal vs. Distal Non-Osseointegration- Modal Analysis (Mode #1)
 (Periprosthetic Bone: $t_1 = 1.0 \text{ mm}$, $0.13 \text{ g/cm}^3 \leq \rho_1 \leq 1.20 \text{ g/cm}^3$, $E = 1310\rho^{1.4}$,
 Cancellous Host Bone: Density = 1.20 g/cm^3 , Elastic Modulus = 1690.9 MPa)

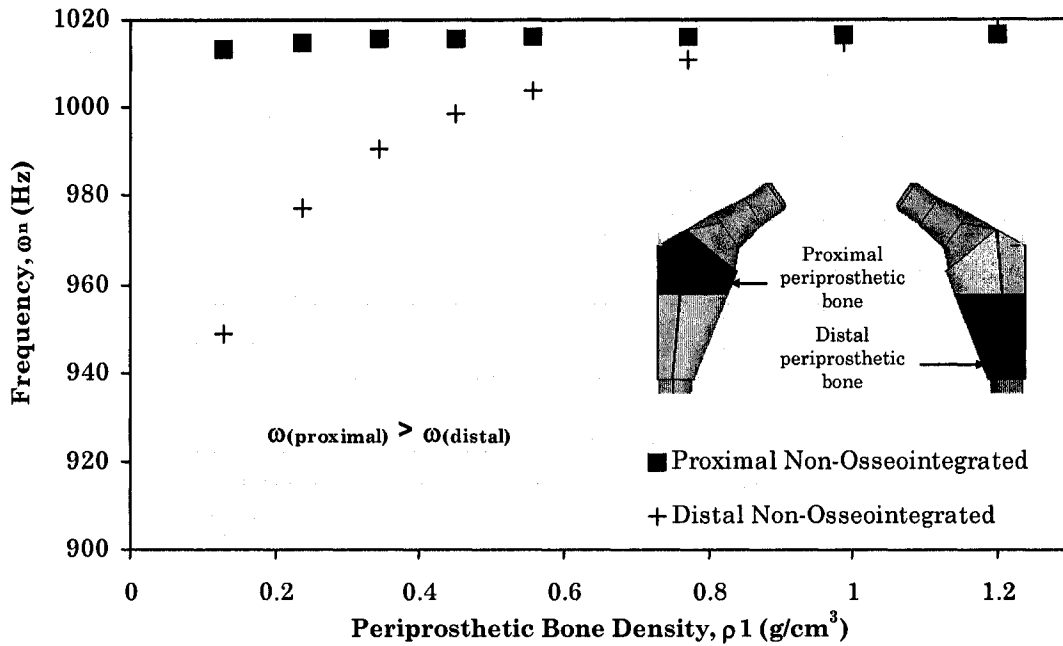


Figure 5.47: Proximal vs. Distal Non-Osseointegration- Modal Analysis (Mode #2)
 (Periprosthetic Bone: $t_1 = 1.0$ mm, $0.13 \text{ g/cm}^3 \leq \rho_1 \leq 1.20 \text{ g/cm}^3$, $E = 1310\rho^{1.4}$,
 Cancellous Host Bone: Density = 1.20 g/cm^3 , Elastic Modulus = 1690.9 MPa)

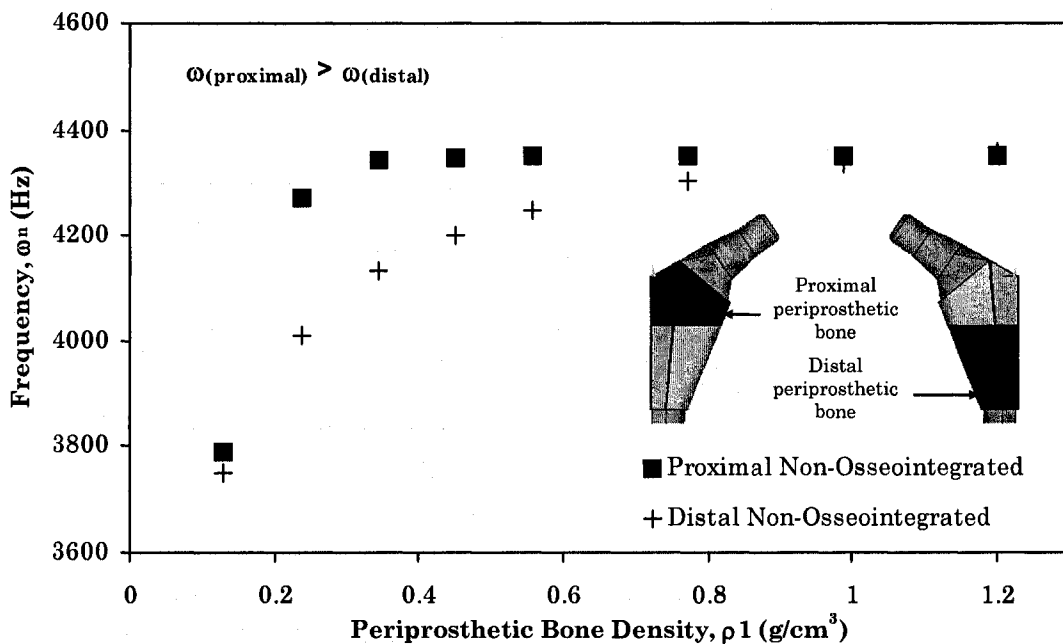


Figure 5.48: Proximal vs. Distal Non-Osseointegration- Modal Analysis (Mode #3)
 (Periprosthetic Bone: $t_1 = 1.0$ mm, $0.13 \text{ g/cm}^3 \leq \rho_1 \leq 1.20 \text{ g/cm}^3$, $E = 1310\rho^{1.4}$,
 Cancellous Host Bone: Density = 1.20 g/cm^3 , Elastic Modulus = 1690.9 MPa)

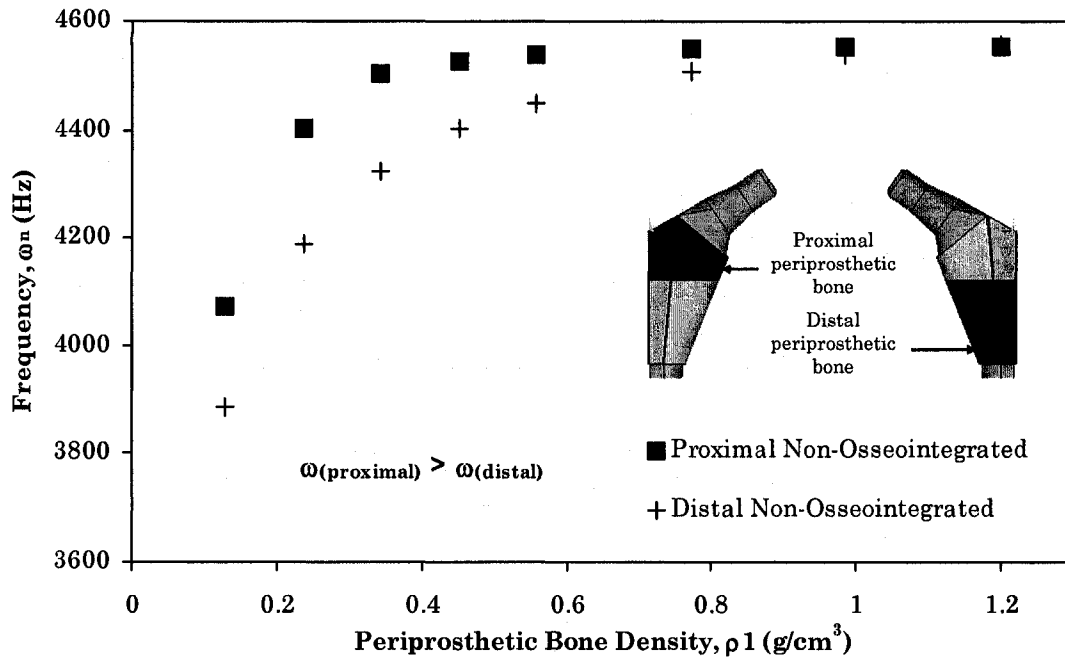


Figure 5.49: Proximal vs. Distal Non-Osseointegration- Modal Analysis (Mode #4)
 (Periprosthetic Bone: $t_1 = 1.0$ mm, $0.13 \text{ g/cm}^3 \leq \rho_1 \leq 1.20 \text{ g/cm}^3$, $E = 1310\rho^{1.4}$,
 Cancellous Host Bone: Density = 1.20 g/cm^3 , Elastic Modulus = 1690.9 MPa)

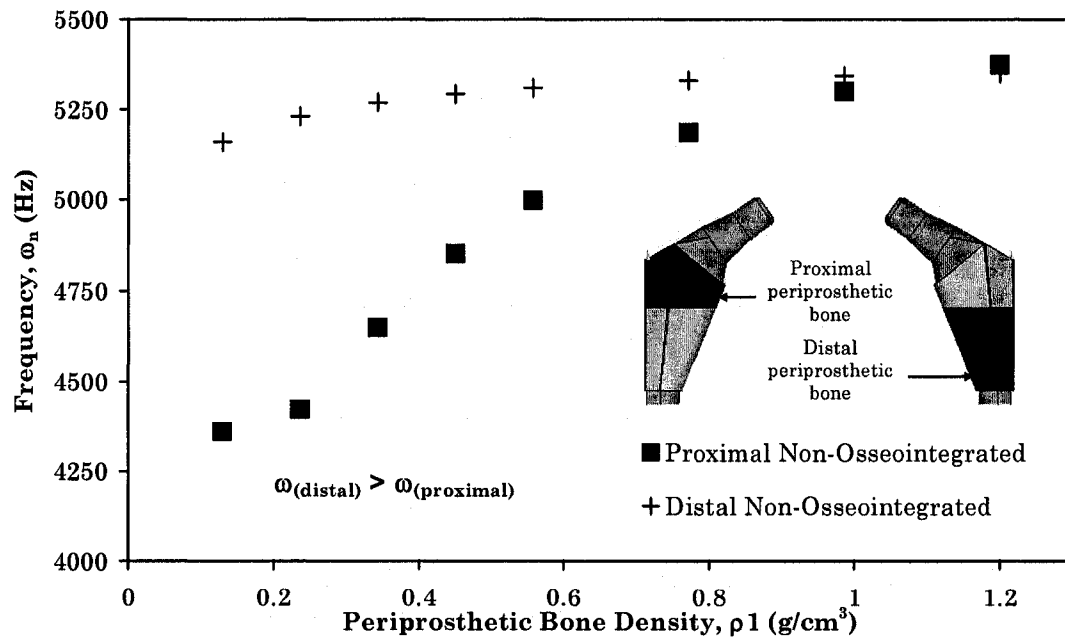


Figure 5.50: Proximal vs. Distal Non-Osseointegration- Modal Analysis (Mode #5)
 (Periprosthetic Bone: $t_1 = 1.0$ mm, $0.13 \text{ g/cm}^3 \leq \rho_1 \leq 1.20 \text{ g/cm}^3$, $E = 1310\rho^{1.4}$,
 Cancellous Host Bone: Density = 1.20 g/cm^3 , Elastic Modulus = 1690.9 MPa)

5.6.4 Osseointegration in Physiologically Significant Regions (variation of the Gruen Zones)

This section includes results of the modal response of the implant due to density variations in specific physiologically-significant quadrants. For the purposes of this study, the original seven Gruen zones protocol [Gruen *et al.*, 1979] (Figure 5.51) were modified and four regions of interest were considered for this particular study: the greater trochanter, the calcar, the mid-lateral cortex and the mid-medial cortex, as shown in Figure 5.52.

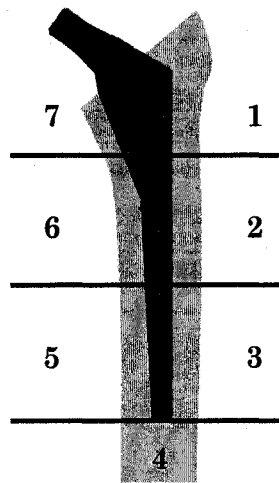


Figure 5.51: Gruen Zones- (1) Greater Trochanter (2) Lateral Metaphysis (3) Lateral Diaphysis (4) Diaphysis distal to the femoral implant (5) Medial Diaphysis (6) Medial Metaphysis (7) Lesser Trochanter or Calcar [Gruen *et al.*, 1979]

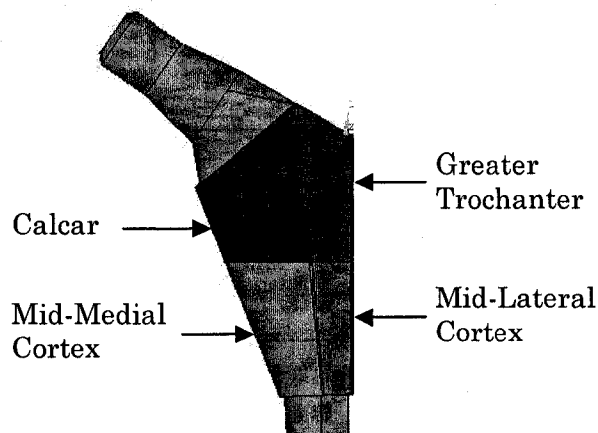


Figure 5.52: Four physiologically-significant regions: Greater Trochanter, Calcar, Mid-Lateral Cortex and Mid-Medial Cortex

The results shown in Figure 5.53 show that the largest percent difference occurs during the fifth mode (20.6%), for the calcar region. These results are significant because some implants with fully-covered porous stems can fail to osseointegrate around the calcar region since fixation of the distal stem is usually favored with these types of implants. In addition the ability to measure calcar region fixation is also important since proximal osseointegration, especially along the medial cortex, is highly desirable and also enhances stability of the implant near the neck of the implant, Figure 5.53 also indicates that the other three regions are not as sensitive to volumetric bone density variations and it would be difficult to differentiate the frequency-response results between each of these regions. The results for all five modes are shown in Figures 5.57 to 5.61.

The largest frequency range of all five modes occurs during Modes # 3, 4 and 5 (as shown in Figure 5.53). A closer examination of decrease in frequency response relative to the frequency response at $\rho_1 = 1.20 \text{ g/cm}^3$ (Figures 5.54 to 5.56) reveals that the rate of decrease in the frequency is slightly higher for the mid-medial cortex during Mode #3, even though the overall width of the range is higher for the calcar. The same trend is also indicated in Mode #4. These fourth mode results also suggest that the rate of frequency changes of the mid-lateral and mid-medial cortex are higher in comparison to the calcar region, although the overall frequency range for the calcar area is slightly larger than the other two regions. However, given that the overall decrease in frequency during Mode #3 and 4 are very low (approximately 4%), these modes would not be ideal for monitoring early loosening in these areas.

In contrast, the decrease in frequency responses is the highest during Mode #5 for the calcar region. Therefore, these results further support the observation that the frequency-responses in Mode #5 are more likely to indicate early decreases in the periprosthetic density of the calcar region.

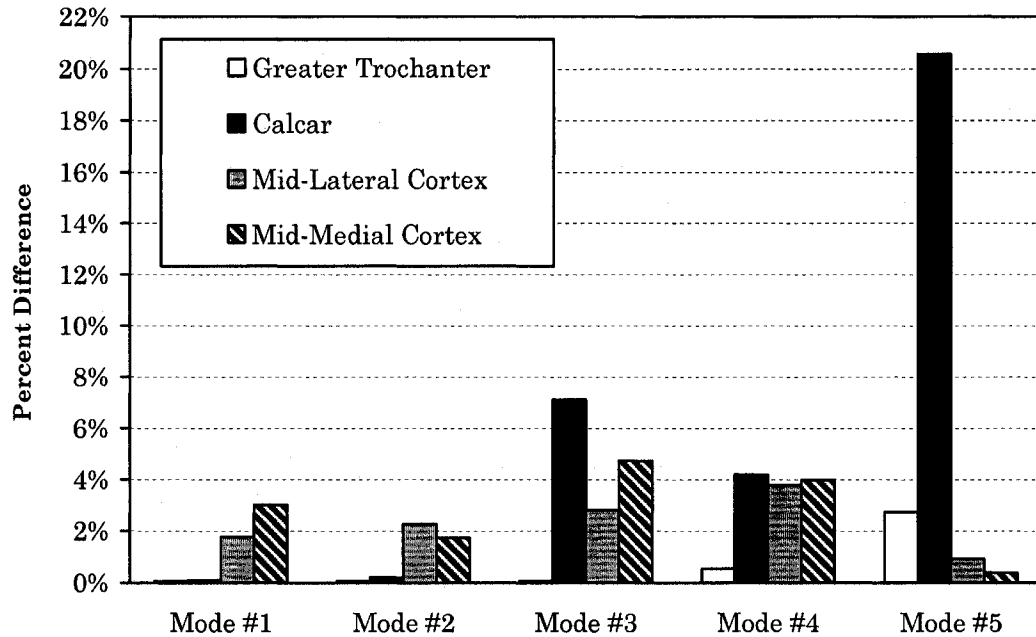


Figure 5.53: Non-osseointegration of the four physiologically-significant regions – Percent difference between frequency responses at $\rho_1 = 0.13 \text{ g/cm}^3$ and 1.20 g/cm^3 (Periprosthetic Bone: $t_1 = 1.0 \text{ mm}$, $0.13 \text{ g/cm}^3 \leq \rho_1 \leq 1.20 \text{ g/cm}^3$, $E = 1310\rho^{1.4}$, Cancellous Host Bone: Density = 1.20 g/cm^3 , Elastic Modulus = 1690.9 MPa)

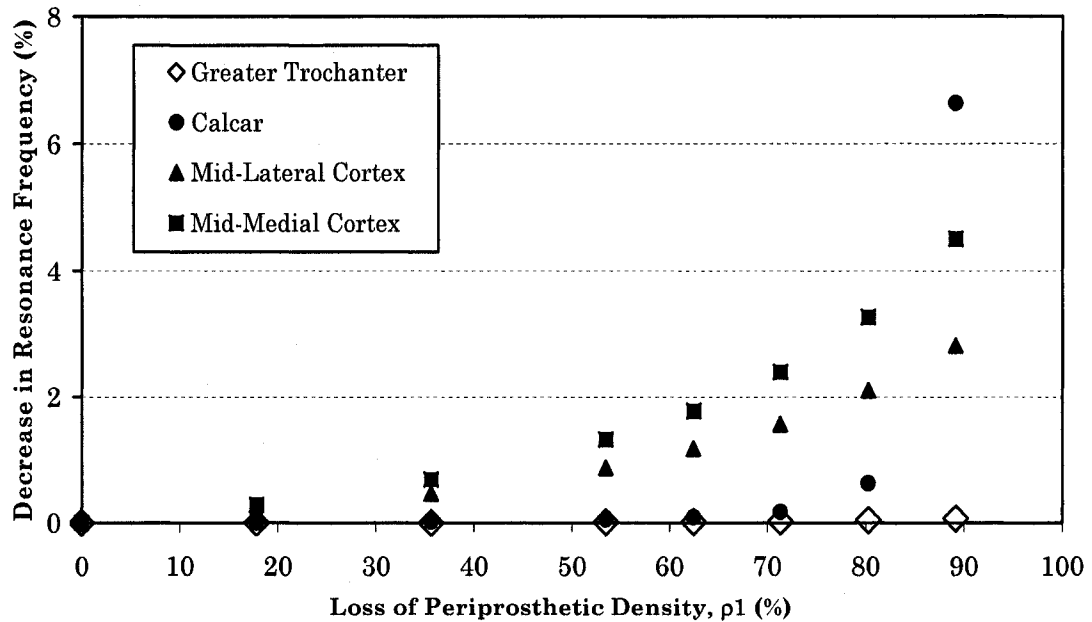


Figure 5.54: Non-osseointegration of the four physiologically-significant regions – Decrease in Mode #3 resonance frequency relative to frequency response at $\rho_1 = 1.20 \text{ g/cm}^3$. (Periprosthetic Bone: $t_1 = 1.00 \text{ mm}$, $0.13 \text{ g/cm}^3 \leq \rho_1 \leq 1.20 \text{ g/cm}^3$, $E = 1310\rho^{1.4}$, Cancellous Host Bone: Density = 1.20 g/cm^3 , Elastic Modulus = 1690.9 MPa)

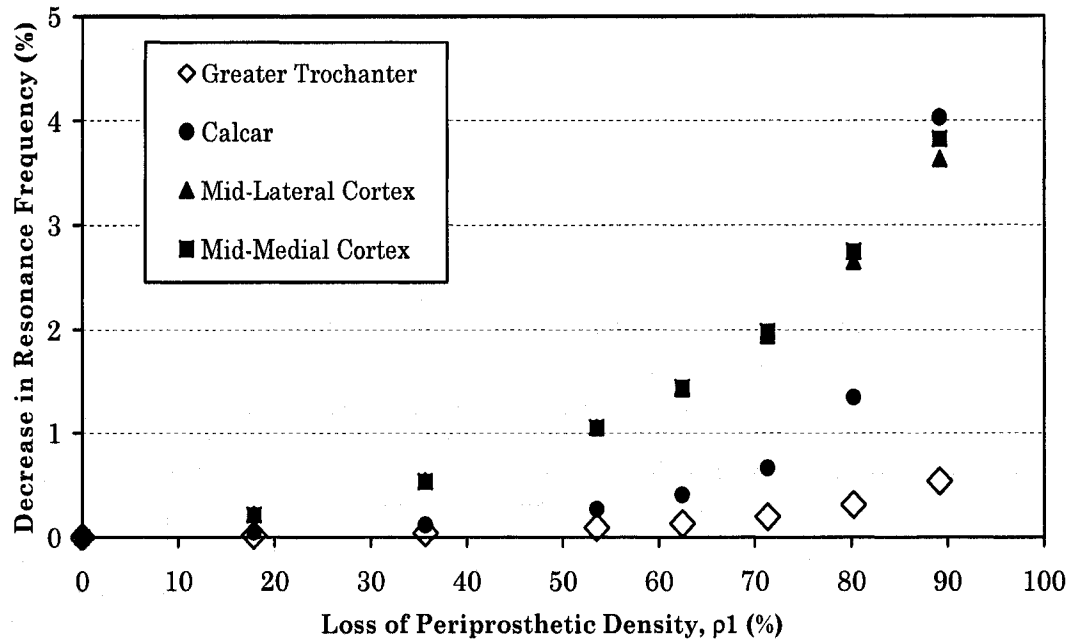


Figure 5.55: Non-osseointegration of the four physiologically-significant regions – Decrease in Mode #4 resonance frequency relative to frequency response at $\rho_1 = 1.20 \text{ g/cm}^3$. (Periprosthetic Bone: $t_1 = 1.00 \text{ mm}$, $0.13 \text{ g/cm}^3 \leq \rho_1 \leq 1.20 \text{ g/cm}^3$, $E = 1310\rho^{1.4}$, Cancellous Host Bone: Density = 1.20 g/cm^3 , Elastic Modulus = 1690.9 MPa)

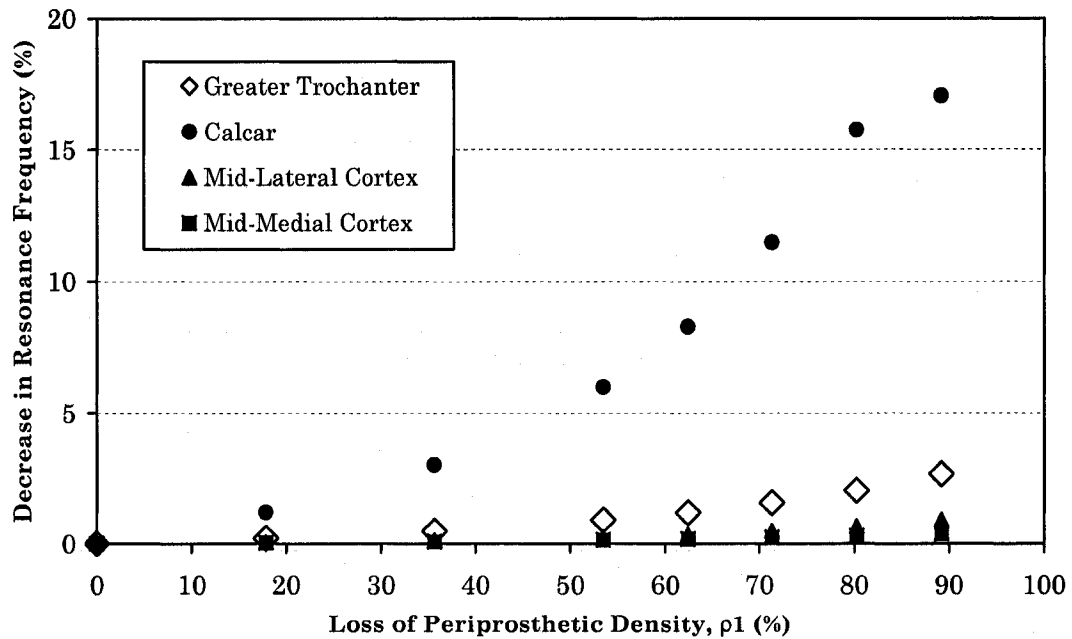


Figure 5.56: Non-osseointegration of the four physiologically-significant regions – Decrease in Mode #5 resonance frequency relative to frequency response at $\rho_1 = 1.20 \text{ g/cm}^3$. (Periprosthetic Bone: $t_1 = 1.00 \text{ mm}$, $0.13 \text{ g/cm}^3 \leq \rho_1 \leq 1.20 \text{ g/cm}^3$, $E = 1310\rho^{1.4}$, Cancellous Host Bone: Density = 1.20 g/cm^3 , Elastic Modulus = 1690.9 MPa)

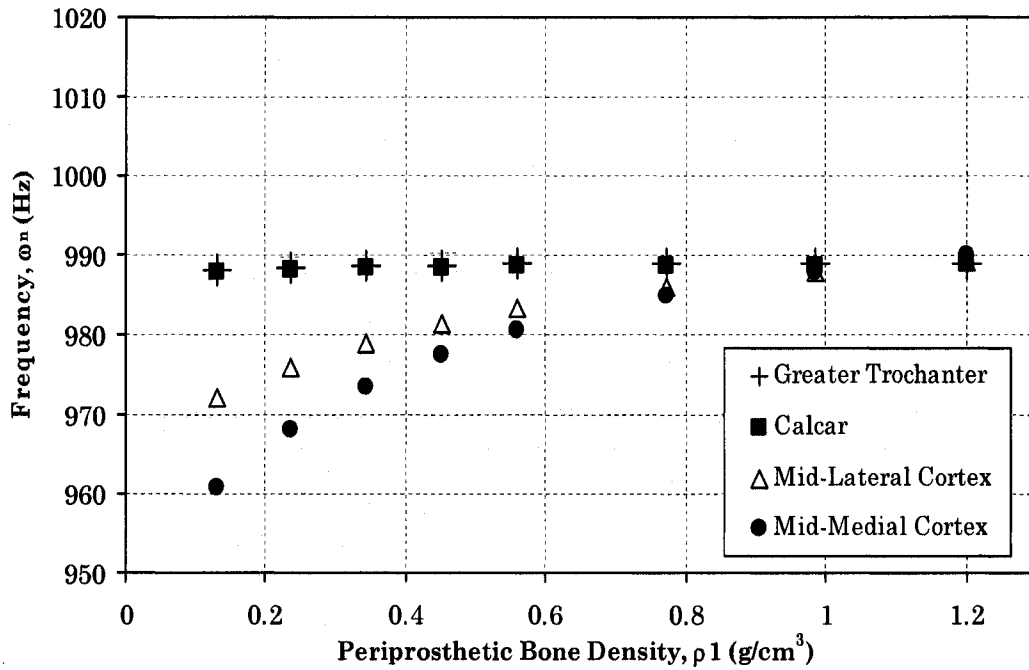


Figure 5.57: Non-osseointegration of the four physiologically-significant regions (Greater Trochanter, Calcar, Mid-Lateral Cortex and Mid-Medial Cortex)-(Mode #1) (Periprosthetic Bone: $t_1 = 1.0$ mm, $0.13 \text{ g/cm}^3 \leq \rho_1 \leq 1.20 \text{ g/cm}^3$, $E = 1310\rho^{1.4}$, Cancellous Host Bone: Density = 1.20 g/cm^3 , Elastic Modulus = 1690.9 MPa)

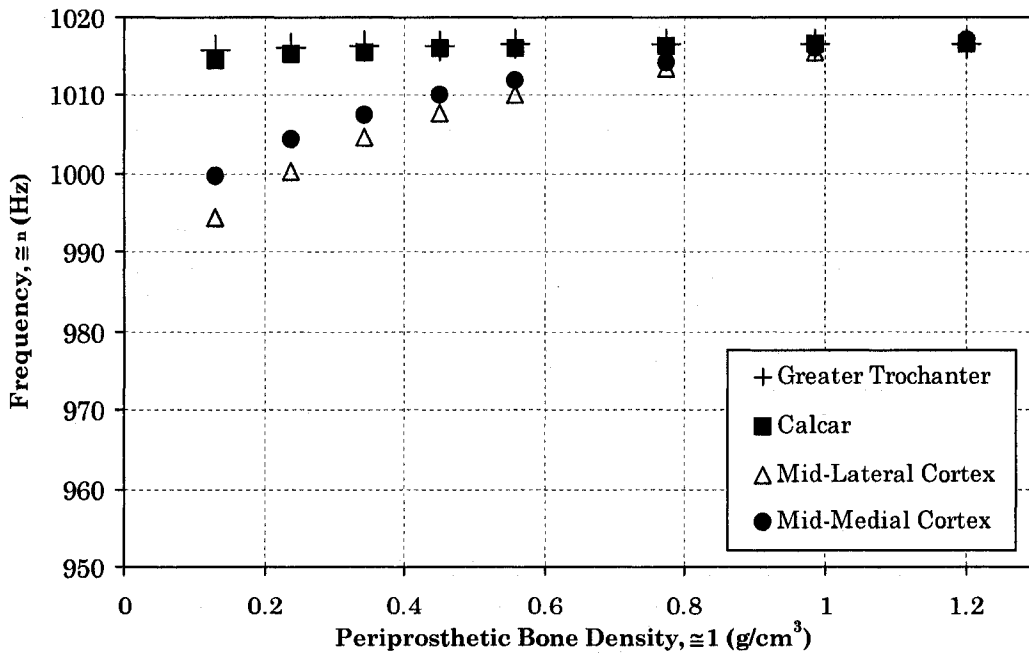


Figure 5.58: Non-osseointegration of the four physiologically-significant regions (Greater Trochanter, Calcar, Mid-Lateral Cortex and Mid-Medial Cortex)-(Mode #2) (Periprosthetic Bone: $t_1 = 1.0$ mm, $0.13 \text{ g/cm}^3 \leq \rho_1 \leq 1.20 \text{ g/cm}^3$, $E = 1310\rho^{1.4}$, Cancellous Host Bone: Density = 1.20 g/cm^3 , Elastic Modulus = 1690.9 MPa)

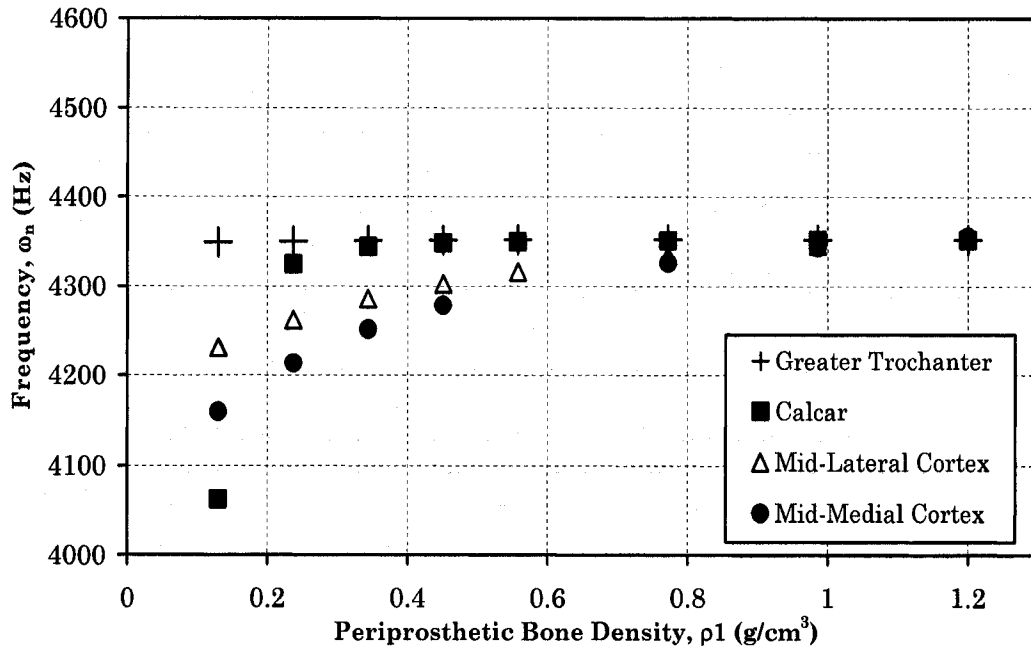


Figure 5.59: Non-osseointegration of the four physiologically-significant regions (Greater Trochanter, Calcar, Mid-Lateral Cortex and Mid-Medial Cortex)-(Mode #3) (Periprosthetic Bone: $t_1 = 1.0$ mm, $0.13 \text{ g/cm}^3 \leq \rho_1 \leq 1.20 \text{ g/cm}^3$, $E = 1310\rho^{1.4}$, Cancellous Host Bone: Density = 1.20 g/cm^3 , Elastic Modulus = 1690.9 MPa)

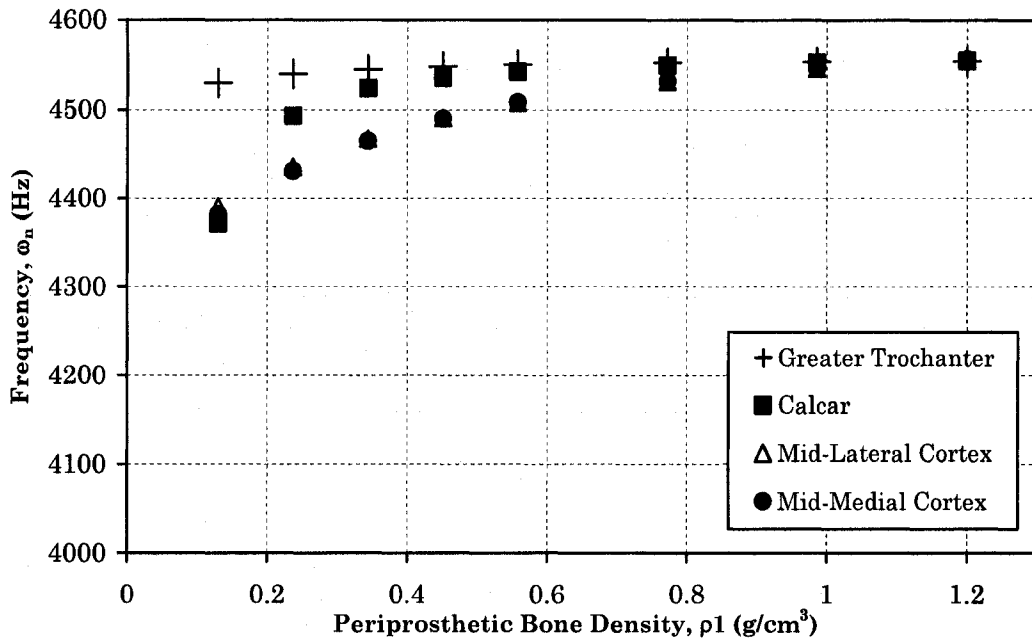


Figure 5.60: Non-osseointegration of the four physiologically-significant regions (Greater Trochanter, Calcar, Mid-Lateral Cortex and Mid-Medial Cortex)-(Mode #4) (Periprosthetic Bone: $t_1 = 1.0$ mm, $0.13 \text{ g/cm}^3 \leq \rho_1 \leq 1.20 \text{ g/cm}^3$, $E = 1310\rho^{1.4}$, Cancellous Host Bone: Density = 1.20 g/cm^3 , Elastic Modulus = 1690.9 MPa)

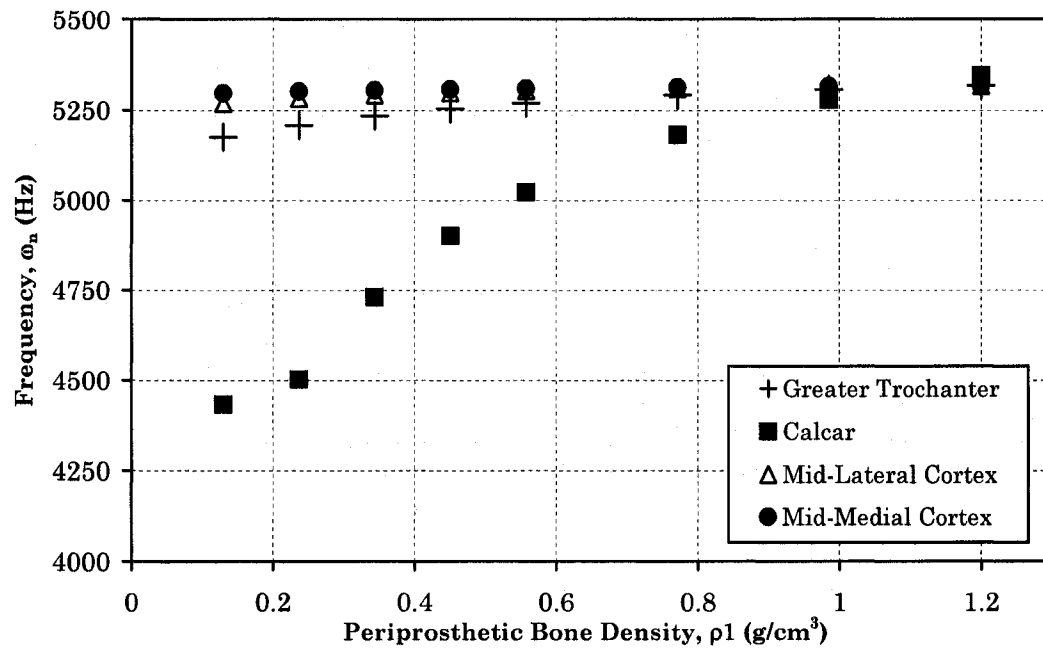
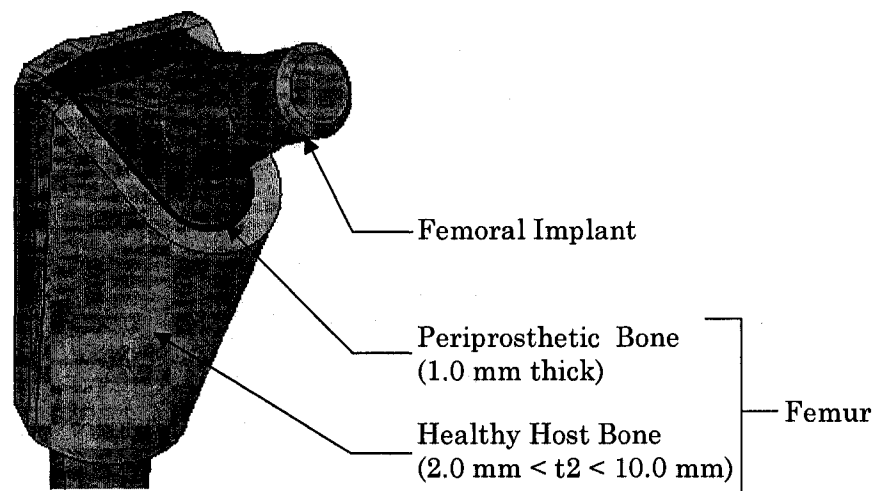


Figure 5.61: Non-osseointegration of the four physiologically-significant regions (Greater Trochanter, Calcar, Mid-Lateral Cortex and Mid-Medial Cortex)-(Mode #5) (Periprosthetic Bone: $t_1 = 1.0$ mm, $0.13 \text{ g/cm}^3 \leq \rho_1 \leq 1.20 \text{ g/cm}^3$, $E = 1310\rho_1^{1.4}$, Cancellous Host Bone: Density = 1.20 g/cm^3 , Elastic Modulus = 1690.9 MPa)

5.7 Effects of varying Cancellous Host Bone Thickness

The variation in cancellous host bone thickness was investigated because increasing thickness of cancellous host bone stock is reflective of the effect of different bone sizes, due to the variability of typical THR patients. The thickness of the cancellous host bone (t_2) varied uniformly in 2.0 mm increments from 2.0 mm to 10.0 mm, as shown in Figure 5.62. The density of the cancellous host bone was constant at $\rho_2 = 1.20 \text{ g/cm}^3$. The thickness of the periprosthetic bone was constant at $t_1 = 1.0 \text{ mm}$ thick and the density of the periprosthetic bone (ρ_1) varied between 0.13 g/cm^3 to 1.20 g/cm^3 .



**Figure 5.62: Effect of varying cancellous host bone thickness, t_2 :
Analysis Configuration.**

**(Periprosthetic Bone: $t_1 = 1.0 \text{ mm}$, $0.13 \text{ g/cm}^3 \leq \rho_1 \leq 1.20 \text{ g/cm}^3$, $E = 1310\rho^{1.4}$,
Cancellous Bone: $2 \text{ mm} \leq t_2 \leq 10 \text{ mm}$, $\rho_2 = 1.20 \text{ g/cm}^3$, Elastic Modulus = 1690.9 MPa)**

The frequency-response of the implant, as the thickness of the cancellous host bone layer (t_2) increases, is shown in Figures 5.63 to 5.68. The results from the first five modes all indicate that as the thickness of the cancellous bone layer increased, it corresponded to a lower frequency-response value. These results are consistent with

Equation 5.3, which indicates that the natural frequency is inversely proportional to the square root of the mass. Therefore, as the mass increases, the natural frequency would be decreased, which is reflected in the results.

It is interesting to note that it would appear that the increase of the cancellous bone thickness does not seem to detrimentally affect the effectiveness of the this monitoring technique, The results from the first four modes (as shown in Figure 5.63), show that the percent difference of the frequency-response of the implant, between $\rho_1 = 0.13 \text{ g/cm}^3$ and $\rho_1 = 1.20 \text{ g/cm}^3$, did not vary significantly within each mode. Although the percent difference of the frequency-response of the implant decreased (as t_2 increased) during the fifth mode, the overall results in Figure 5.63 would seem to indicate that patients with larger bone structure could also benefit from the same monitoring technique.

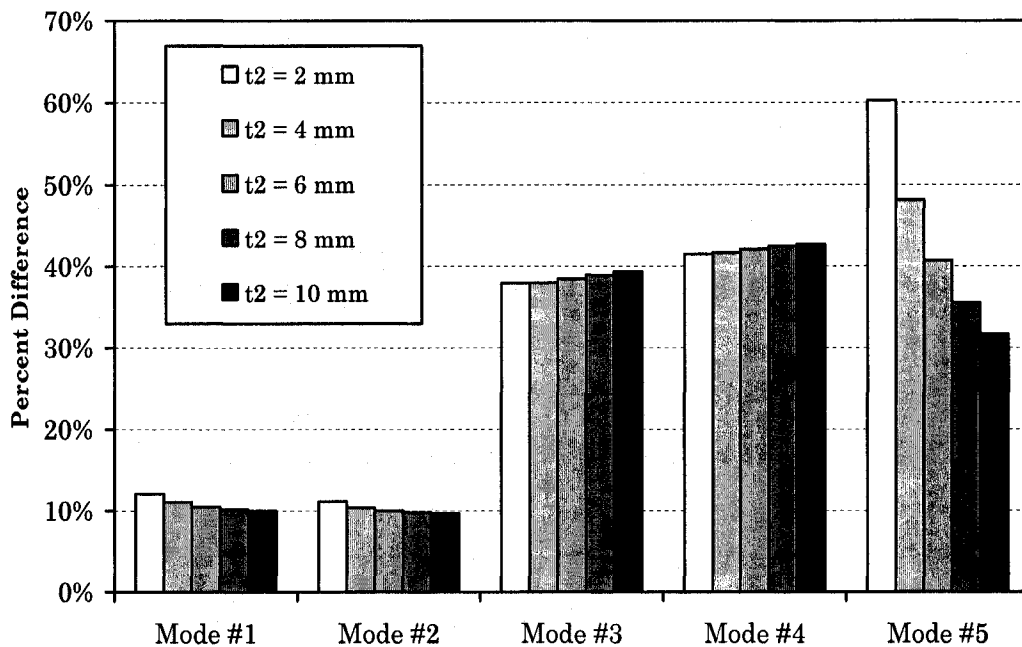


Figure 5.63: Effect of varying cancellous host bone thickness, t_2 – Percent difference between frequency responses at $\rho_1 = 0.13 \text{ g/cm}^3$ and $\rho_1 = 1.20 \text{ g/cm}^3$ (Periprosthetic Bone: $t_1 = 1.0 \text{ mm}$, $0.13 \text{ g/cm}^3 \leq \rho_1 \leq 1.20 \text{ g/cm}^3$, $E = 1310\rho^{1.4}$, Cancellous Bone: $2 \text{ mm} \leq t_2 \leq 10 \text{ mm}$, $\rho_2 = 1.20 \text{ g/cm}^3$, Elastic Modulus = 1690.9 MPa)

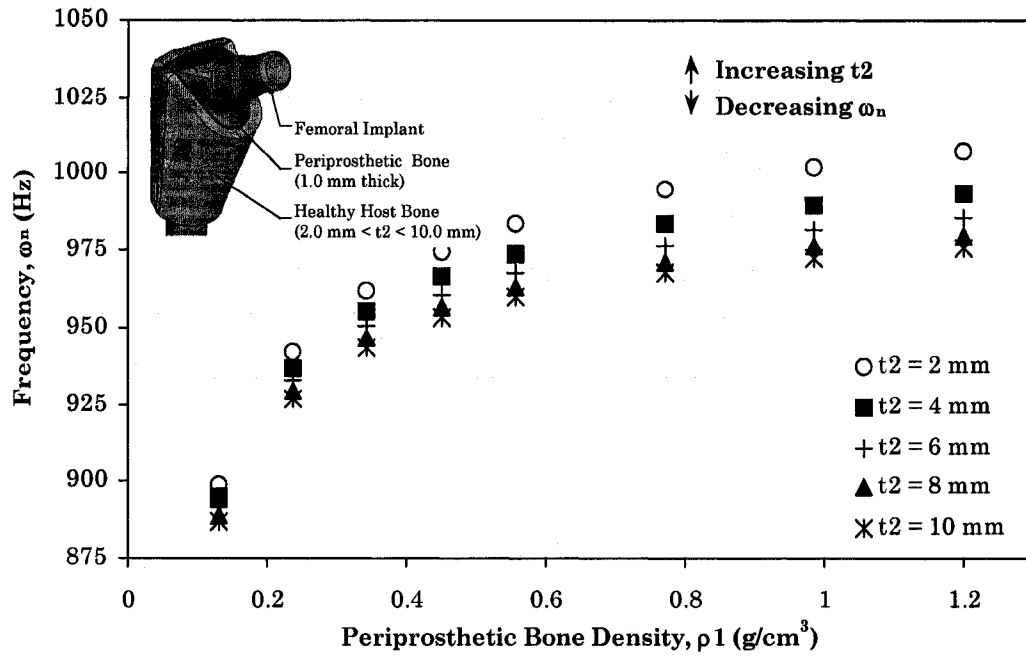


Figure 5.64: Effect of varying cancellous host bone thickness, t_2 . Modal response (Mode #1) of implant with two types of bone layers (Figure 5.56) (Periprosthetic Bone: $t_1 = 1.0$ mm, $0.13 \text{ g/cm}^3 \leq \rho_1 \leq 1.20 \text{ g/cm}^3$, $E = 1310\rho^{1.4}$, Cancellous Bone: $2 \text{ mm} \leq t_2 \leq 10 \text{ mm}$, $\rho_2 = 1.20 \text{ g/cm}^3$, Elastic Modulus = 1690.9 MPa)

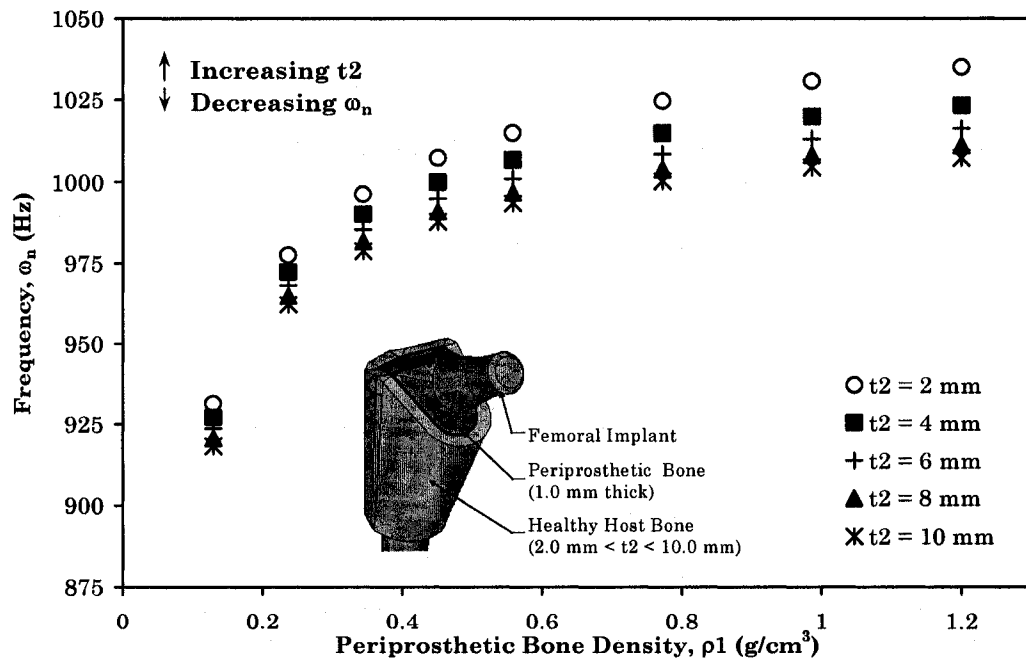


Figure 5.65: Effect of varying cancellous host bone thickness, t_2 . Modal response (Mode #2) of implant with two types of bone layers (Figure 5.56) (Periprosthetic Bone: $t_1 = 1.0$ mm, $0.13 \text{ g/cm}^3 \leq \rho_1 \leq 1.20 \text{ g/cm}^3$, $E = 1310\rho^{1.4}$, Cancellous Bone: $2 \text{ mm} \leq t_2 \leq 10 \text{ mm}$, $\rho_2 = 1.20 \text{ g/cm}^3$, Elastic Modulus = 1690.9 MPa)

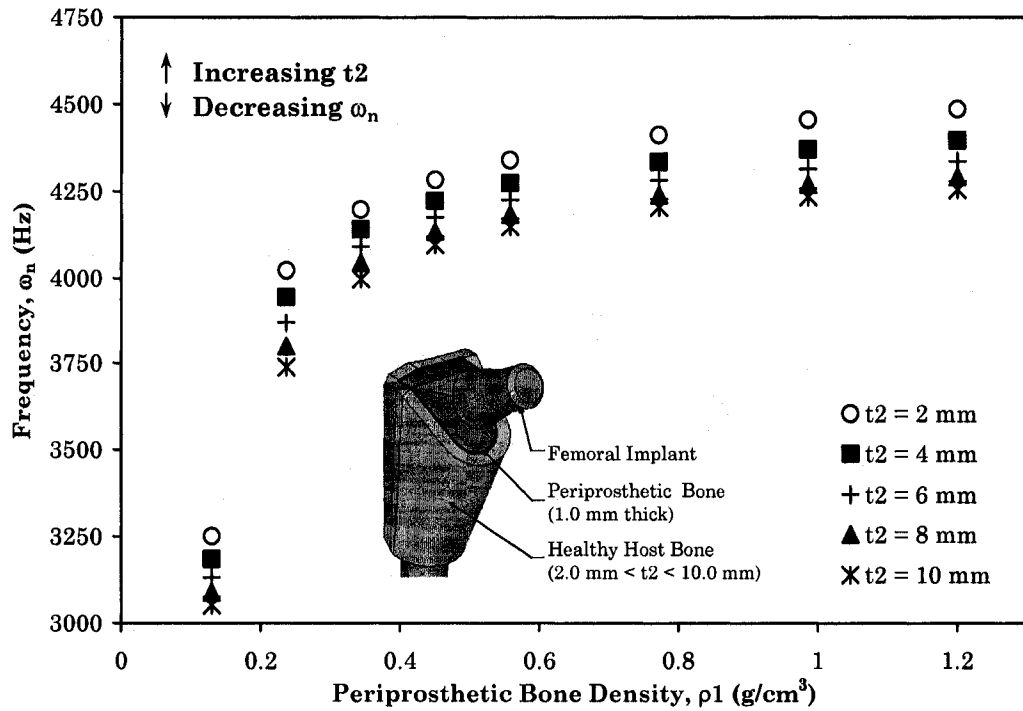


Figure 5.66: Effect of varying cancellous host bone thickness, t_2 .
 Modal response (Mode #3) of implant with two types of bone layers (Figure 5.56)
 (Periprosthetic Bone: $t_1 = 1.0$ mm, $0.13 \text{ g/cm}^3 \leq \rho_1 \leq 1.20 \text{ g/cm}^3$, $E = 1310\rho^{1.4}$,
 Cancellous Bone: $2 \text{ mm} \leq t_2 \leq 10 \text{ mm}$, $\rho_2 = 1.20 \text{ g/cm}^3$, Elastic Modulus = 1690.9 MPa)

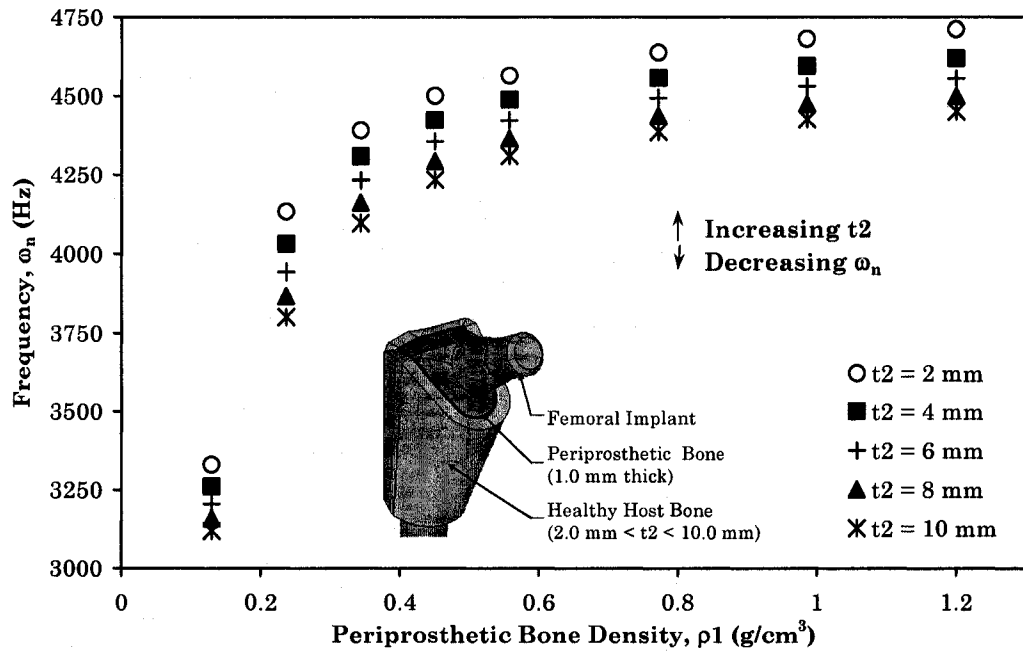


Figure 5.67: Effect of varying cancellous host bone thickness, t_2 .
 Modal response (Mode #4) of implant with two types of bone layers (Figure 5.56)
 (Periprosthetic Bone: $t_1 = 1.0$ mm, $0.13 \text{ g/cm}^3 \leq \rho_1 \leq 1.20 \text{ g/cm}^3$, $E = 1310\rho^{1.4}$,
 Cancellous Bone: $2 \text{ mm} \leq t_2 \leq 10 \text{ mm}$, $\rho_2 = 1.20 \text{ g/cm}^3$, Elastic Modulus = 1690.9 MPa)

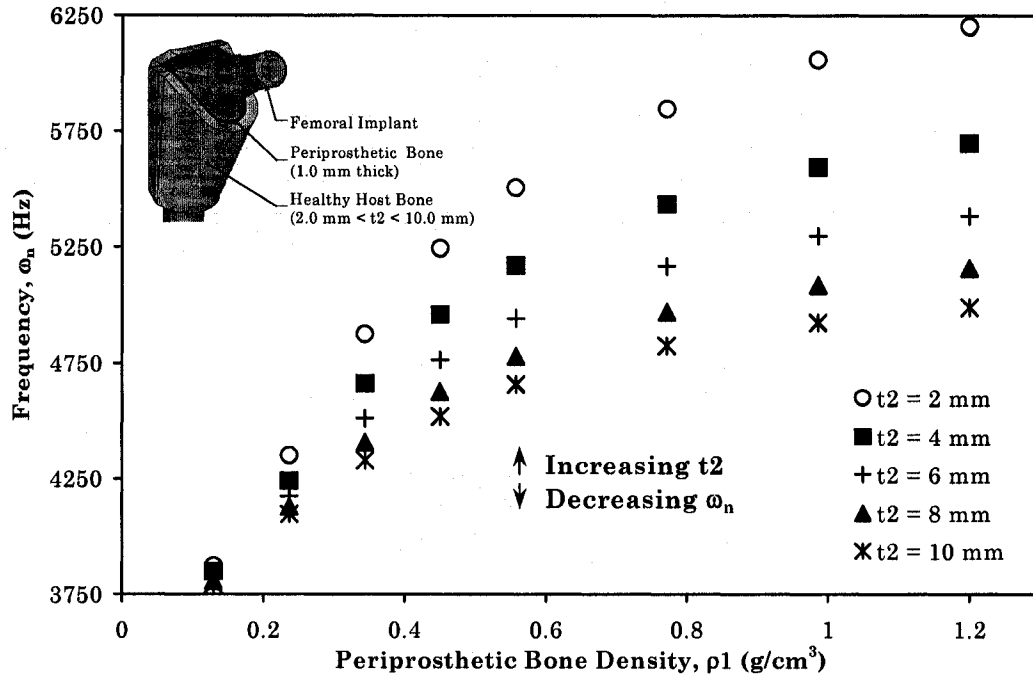


Figure 5.68: Effect of varying cancellous host bone thickness, t_2 .
Modal response (Mode #5) of implant with two types of bone layers (Figure 5.56)
(Periprosthetic Bone: $t_1 = 1.0 \text{ mm}$, $0.13 \text{ g}/\text{cm}^3 \leq \rho_1 \leq 1.20 \text{ g}/\text{cm}^3$, $E = 1310\rho_1^{1.4}$,
Cancellous Bone: $2 \text{ mm} \leq t_2 \leq 10 \text{ mm}$, $\rho_2 = 1.20 \text{ g}/\text{cm}^3$, Elastic Modulus = 1690.9 MPa)

Chapter 6

Conclusions and Future Work

6.1 Summary and Conclusions

Hip replacement procedures have become a very common procedure in the treatment of degenerative hip and joint disease due mainly to arthritis, as discussed in Chapter 1. Time-related variations of periprosthetic bone density after total hip arthroplasty reflect the physiological condition of the bone and implant interface. The ability to quantitatively assess periprosthetic bone density may be clinically relevant in the early diagnosis of pathologic bone deterioration or delayed fracture union and as a means of evaluating potential prosthetic designs and facilitate design improvements.

A parametric study was conducted to determine whether variations in the physiological status of periprosthetic bone, surrounding a femoral stem, would correspond to a relative change of the frequency-response of the implant. This study analyzed the effects of varying geometric and material properties of periprosthetic and host bone. Utilizing modal analysis, a comparison of the results indicate that some forms of non-osseointegrated periprosthetic bone would be detectable using this type of non-destructive, *in vivo* diagnostic technique.

The concept of utilizing vibrational techniques to identify physiological or structural deficiencies is not novel. Chapter 2 summarizes other investigators who have examined the validity of using vibration techniques to characterize the physical properties of long bones, the detection of prosthetic loosening or fracture healing. Vibrational frequency analysis was later applied to femurs with implanted hip

prostheses (both experimental and FE studies) and results indicated that the vibrational technique could possibly be used to differentiate between loose and fixed implants. However, these particular studies focused mainly on fixed or catastrophic loosening of the implant. Rather, this particular study specifically focuses on other variables such as density and stiffness of periprosthetic bone and its affect on the early detection of non-osseointegration of an implant using vibrational frequency analysis.

Bone physiology was discussed in Chapter 3, as well as the material properties of the cortical and cancellous bone of the human femur. The cortical bone properties were adopted from the results of an intensive investigation by Ashman *et al.* [1984] and the cancellous bone properties were based on a power law relationship reported by Lotz *et al.* [1990]. In addition, Chapter 3 also introduced the type of femoral stem utilized (Stryker® Howmedica Osteonics' Secur-Fit™ HA) as well as its material properties.

Chapter 4 discussed the implementation of the finite element method to numerically facilitate of the modal analysis of the implant and bone continuum. In addition, the challenges of creating and implementing a compatible finite element model of the femur, periprosthetic bone volume and implant were addressed. To establish the validity of the implant model, comparisons of geometrically similar cantilever beams was considered. This analysis confirmed that simple beam theory was not applicable for determining the natural frequencies of the distal stem, due to the low aspect ratio (9.2). In addition, the inclusion of the cortical bone layer during the FE analysis was determined to be unnecessary, as the cortical bone layer did not dramatically alter the frequency response of the implant. It was also determined that the implementation of a constant-thickness bone layer can be used to substitute and simulate the effect of the regular topography of the cancellous bone, without much degradation to the frequency results. This proved to be significant as it provided a method to parametrically simulate different bone sizes due to the variability in hip replacement patients. A sensitivity analysis of different element sizes helped to determine that an element size of 2.5 mm would be the best compromise between accuracy and computational time.

The modal analysis results of various case studies were presented in Chapter 5. The scope of the analysis protocol included examining the effects of varying periprosthetic bone density and thickness, periprosthetic bone density in localized regions and varying the thickness of the cancellous host bone layer. The results indicate that variations in periprosthetic density do indeed affect the frequency response of the implant. As the quality of the bone decreases, so does the frequency response. This trend was observed in all the cases. Early detection of decreases in periprosthetic density is most likely to be observed during Mode #5, at the higher frequency ranges. According to Figures 5.7 and 5.8, Mode #1 and #2 were also not likely to provide any significant indications of loosening.

An examination of varying the thickness of periprosthetic bone increased, indicated that an increase in thickness also decreased the values of the frequency responses and resulted in producing a response within a larger frequency range. The results of this particular case study also revealed that a periprosthetic bone thickness as thin as 0.25 mm could be detectable in certain cases. Figure 5.20 shows that an overall catastrophic loss of 0.25 mm thick bone would vary the Mode #5 frequency response by almost 25%. It is also significant to note that although the frequency response value may remain relatively unchanged during serial measurements, Table 5.2 indicates that this phenomenon may not solely indicate that physiological changes have ceased.

A comparison of the non-osseointegration of the anterior and posterior halves along the implant reveal that that variations in the density of the anterior-located bone is a little more likely to affect the frequency-response of the system. However, it would be difficult to determine which side is affected based on this data alone. In contrast, the frequency response due to variations of the medially-located periprosthetic bone was much more pronounced in comparison with the lateral side (Figure 5.34). The results from the comparison of proximal and distal volumes indicate that non-osseointegration of the proximal half is more likely to be detectable.

This vibrational technique appears to be very effective for detecting density variations in periprosthetic bone around the calcar region, as shown in Figure 5.53.

This is significant as proximal fixation of the implant in this area is crucial for enhancing stability.

A parametric increase in the thickness of the cancellous bone also indicates that bone size does not detrimentally affect the effectiveness of the vibrational frequency technique as shown in Figure 5.64.

6.2 Future Work

Now that it has been parametrically established that the vibrational frequency response of an implant can be affected by variations in the periprosthetic bone density, a closer examination of this phenomenon would be the next step. A more detailed FE model could be used to develop a better understanding of the validity and limitations of the vibrational analysis approach. The implementation of anisotropic material properties would need to be applied. The influence of including the acetabular components would also need to be explored.

Other physiologically relevant permutations should also be examined. This includes instances such as when fibrous tissue forms around the implant. This type of tissue is not osseointegrated into the implant, yet can provide some form of stability in some cases.

In addition, an amplitude analysis of along the various parts of the implant may aid in determining the best placement of input and output accelerometers to measure the frequency responses. Depending on the location of excitation and measurement, an examination of the effects of damping due to surrounding soft tissue such as fat, muscle and skin would also need to be explored.

References

- Allcock S., Ali M.A. (1997). Early failure of a carbon-fiber composite femoral component. *Journal of Arthroplasty*, Vol.12(3), pp. 356-58.
- American Academy of Orthopaedic Surgeons (2004). *Facts about Total Hip and Total Knee Replacement*. Rosemont, Illinois, American Academy of Orthopaedic Surgeons, Department of Research and Scientific Affairs.
- Analog Devices (2005). [online]. Available from: http://www.analog.com/UploadedFiles/Data_Sheets/53728567227477ADXL202E_a.pdf [accessed June 10, 2005].
- Arpaia, P., Bruno, V., Clemente, F., Zanesco, A. (2005). Low-Invasive Diagnosis of Prosthesis Osseointegration by Electrical Impedance Spectroscopy. *IEEE Instrumentation and Measurement Technology Conference. May 17-19, 2005, Ottawa, Ontario, Canada*, IEEE Publishing Services, pp. 929-933.
- Ashman, R.B., Cowin, S.C., Buskirk, W.C.V., Rice, J.C. (1984). A continuous wave technique for the measurement of the elastic properties of cortical bone. *Journal of Biomechanics*, Vol. 17(5), pp. 349-361.
- Ashman, R.B., Rho, J.Y. (1988). Elastic Modulus of trabecular bone material. *Journal of Biomechanics*, Vol. 20, pp. 177-181.
- Augat, P., Link, T., Lang, T.F., Lin, J.C., Majumdar, S., Genant, H.K. (1998). Anisotropy of the elastic modulus of trabecular bone specimens from different anatomical locations. *Medical and Engineering Physics*, Vol. 20, pp. 124-131
- Bhandari, M., Guyatt, G.H., Swiontkowski, M.F., Tornetta, P. 3rd., Sprague, S., Schemitsch, E.H. (2002). A lack of consensus in the assessment of fracture healing among orthopaedic surgeons. *Journal of Orthopaedic Trauma*, Vol. 16, pp. 562-566.
- Brånemark, P.I. (1983). Osseointegration and its experimental studies. *Journal of Prosthetic Dentistry*, Vol. 50, pp. 399-410.

- Brown, T.D., Ferguson, A.B. (1980). Mechanical property distributions in the cancellous bone of the human proximal femur. *Acta Orthopaedica Scandinavica*, Vol. 51, pp. 429-437.
- Browne, M., Roques, A., Taylor, A. (2005). The acoustic emission technique in orthopaedics – a review. *Journal of Strain Analysis for Engineering Design*, Vol. 40(1), pp. 59-79.
- Canadian Institute for Health Information (CIHI) (2002). *Canadian Joint Replacement Registry (CJRR) Bulletin: Surgical and Orthopaedic Implant Information for Total Hip and Total Knee Replacement Procedures Performed in Canada, May 2001-March 2002*. Toronto, Ontario, Canadian Institute for Health Information.
- Canadian Institute for Health Information (2005). *Canadian Joint Replacement Registry (CJRR) Report. Total Hip and Total Knee Replacements in Canada, 2005*. Ottawa, Ontario, Canadian Institute for Health Information.
- Carter, D.R., Hayes, W.C. (1977). The compressive behaviour of bone as a two-phase porous structure. *The Journal of Bone and Joint Surgery (Am)*, Vol. 59A, pp. 954-962.
- Carter, D.R., Spendlger, D.M. (1978). Mechanical Properties and Composition of Cortical Bone. *Clinical Orthopaedics and Related Research*, Vol. 135, pp. 192-217.
- Cheal, E.J., Spector, M., Hayes, W.C. (1992). Role of loads and prosthesis material properties on the mechanics of the proximal femur after total hip arthroplasty. *Journal of Orthopaedic Research*, Vol. 10(3), pp. 405-422.
- Chung, J.K., Pratt, G.W., Babyn, P.S. (1979). A new diagnostic technique for the evaluation of prosthetic fixation. *Proceedings of the 1st IEEE/Eng in Medicine and Biology Society Annual Conference, Frontiers of engineering in health care: IEEE/Engineering in Medicine and Biology Society, October 6-7, 1979, Denver Hilton Hotel, Denver, Colorado, IEEE Publishing Services*, pp. 158-160.

- Ciarelli, M.J., Goldstein, S.A., Kuhn, J.L., Cody, D.D., Brown, M.B. (1991). Evaluation of Orthogonal Mechanical Properties and Density of Human Trabecular Bone From the Major Metaphyseal Regions with Materials Testing and Computed Tomography. *Journal of Orthopaedic Research*, Vol. 9 (5), pp. 674-682.
- Cohen, B., Rushton, N. (1995). Accuracy of DEXA measurement of bone mineral density after total hip arthroplasty. *The Journal of Bone and Joint Surgery (Br)*, Vol. 77B, pp. 815-819.
- Cristofolini, L., Viceconti, M., Cappello, A., Toni, A. (1996). Mechanical validation of whole bone composite femur models. *Journal of Biomechanics*, Vol. 29, pp. 525-535.
- Cuppone, M., Seedhom, B.B., Berry, E., Ostel, A.E. (2004). The longitudinal Young's modulus of cortical bone in the midshaft of human femur and its correlation with CT scanning data. *Calcified Tissue International*, Vol. 74, pp. 302-309.
- Currey, J.D. (1984). *The Mechanical Adaptation of Bones*. Princeton University Press, Princeton, New Jersey, USA.
- Currey, J.D. (1988). The Effect of Porosity and Mineral Content on the Young's Modulus of Elasticity of Compact Bone. *Journal of Biomechanics*, Vol. 21(2), pp. 131-139
- Doherty, W.P., Bovill, E.G., Wilson, E.L. (1974). Evaluation of the use of resonant frequencies to characterize physical properties of human long bones. *Journal of Biomechanics*, Vol. 7, pp. 559-561.
- Dorr, L.D., Arnala, I., Faugere, M.C., Malluche, H.H. (1990). Five-year postoperative results of cemented femoral arthroplasty in patients with systemic bone disease. *Clinical Orthopaedics and Related Research*, Vol. 259, pp. 114-121.
- Ducheyne, P., Heymans, L., Martens, M., Aernoudt, E., Meester, P.D., Mulier, J.C. (1977). The mechanical behaviour of intracondylar cancellous bone of the femur at different loadin rates. *Journal of Biomechanics*, Vol. 10, pp. 747-762.
- Engh, C.A., Massin, P., Suthers, K.E. (1990). Roentgenographic assessment of the biologic fixation of porous-surface femoral components. *Clinical Orthopaedics and Related Research*, Vol. 257, pp. 107-128.

- Evans S.L., Gregson P.J. (1998) Composite technology in load-bearing orthopaedic implants. *Biomaterials*, Vol. 19, pp. 1329-1342.
- Felippa, C.A. (2004). *Introduction to Finite Element Methods*, [online] Department of Aerospace Engineering Sciences and Center for Aerospace Structures, University of Colorado, Boulder, Colorado.
Available from:
<http://caswww.colorado.edu/courses.d/IFEM.d/IFEM.Ch02.d/IFEM.Ch02.Slides.d/IFEM.Ch02.Slides.pdf> [accessed June 20, 2005].
- Forwood, M.R., & Turner, C.H. (1995). Skeletal adaptations to mechanical usage. *Bone*, Vol. 17, pp. S197-S205.
- Fredin, H.O., Lindberg, H., Carlsson, A.S. (1987). Femoral fracture following hip arthroplasty. *Acta Orthopaedica Scandinavica*, Vol. 50, pp. 20-22.
- Furlong, R.J., Osborn, J.F. (1991). Fixation of Hip Prosthesis by Hydroxyapatite Ceramic Coating. *The Journal of Bone and Joint Surgery (Br)*, Vol. 73B, pp. 741-745.
- Galante, J., Rostoker, W., Ray, R.D. (1970). Physical properties of trabecular bone. *Calcified Tissue Research*, Vol. 5, pp. 236-246.
- Georgiou, A.P., Cunningham, J.L. (2001). Accurate diagnosis of hip prosthesis loosening using a vibrational technique. *Clinical Biomechanics*, Vol. 16, pp. 315-323.
- Glassman, A.H., Crowninshield, R.D., Schenck, R., Herberts, P. (2001). A Low Stiffness Composite Biologically Fixed Prosthesis. *Clinical Orthopaedics and Related Research*, Vol. 393, pp. 128-136.
- Greer, B.B. (1999). *Finite Element Modeling and Analysis of the Proximal Femur*. MS thesis, Department of Mechanical Engineering, University of Nevada, Reno.
- Goldstein, S.A. (1987). The Mechanical Properties of Trabecular Bone: Dependence on anatomic location and function. *Journal of Biomechanics*, Vol. 20(11/12), pp. 1055-1067.
- Gruen, T.A., McNeice, G.M., Amstutz, H.C. (1979). Modes of failure of cemented stem-type femoral components. *Clinical Orthopaedics and Related Research*, Vol. 141, pp. 17-27.

- Gustilo, R.B. (1988). Bias Femoral Ingrowth Prosthesis with Two to Five Years Follow-Up. Non-Cemented Total Hip Arthroplasty. Chapter 35, pp. 414. New York, NY, Raven Press, Ltd.
- Harrigan, T.P., Carter, D.R., Mann, R.W., Harris, W.H. (1981). The influence of apparent density and trabecular orientation on the elastic modulus of cancellous bone. *Transactions of the 27th Annual Meeting of the Orthopaedic Research Society*. Las Vegas, Nevada. Vol. 6, pp. 277.
- Heiner, A. and Brown, T. (2001). Structural properties of a new design of composite replicate femurs and tibias. *Journal of Biomechanics*, Vol. 34, pp. 773-782.
- Houghton Mifflin Company (2000). *American Heritage Dictionary of the English Language, Fourth Edition*. Boston, MA, Houghton Mifflin Company.
- Houghton Mifflin Company (2002). *American Heritage Stedman's Medical Dictionary*. Boston, MA, Houghton Mifflin Company.
- Huiskes, R., Weinans, H., van Rietbergen, B. (1992). The Relationship Between Stress Shielding and Bone Resorption Around Total Hip Stems and the Effects of Flexible Materials. *Clinical Orthopaedics and Related Research*, Vol. 274, pp. 124-134.
- Jaecques, S.V.N., Pastrav, C., Zahariuc, A., Van der Perre, G. (2004). Analysis of the fixation quality of cementless hip prostheses using a vibrational technique. *International Conference on Noise & Vibrational Engineering*, September, pp. 443-456.
- Katz, J. and Meunier, A. (1987). The elastic anisotropy of bone. *Journal of Biomechanics*, Vol. 20(11/12), pp.1063-1070.
- Keaveny, T.M., Morgan, E.F., Niebur, G.L., Yeh, O.C. (2001). Biomechanics of Trabecular Bone. *Annual Review of Biomedical Engineering*, Vol. 3, pp. 307-33.
- Khalil, T.B., Viano, D.C., Taber, L.A. (1981). Vibrational Characteristics of the embalmed human femur. *Journal of Sound and Vibration*, Vol. 75(3), pp. 417-436.

- Kiratli, B.J., Heiner, J.P., McBeath, A.A., et al. (1992). Determination of bone mineral density by dual energy X-ray absorptiometry in patients with uncemented total hip arthroplasty. *Journal of Orthopaedic Research*, Vol. 10, pp. 836-844.
- Kroger, H., Miettinen, H., Arnala, I., et al. (1996). Evaluation of periprosthetic bone using dual-energy X-ray absorptiometry: Precision of the method and effect of operation on bone mineral density. *Journal of Bone Mineral Research*, Vol. 10, pp. 1526-1530.
- Kuiper, J.W., van Kuijk, C., Grashuis, J.L. (1997). Distribution of Trabecular and Cortical Bone Related to Geometry: A Quantitative Computed Tomography Study of the Femoral Neck. *Investigative Radiology*, Vol. 32(2), pp. 83-89.
- Lasaygues, P., Ouedraogo, E., Lefebvre, J.P., Gindre, M., Talmant, M., Laugier, P. (2005). Progress towards *in vitro* quantitative imaging of human femur using compound quantitative ultrasonic tomography. *Physics in Medicine and Biology*, Vol. 50, pp. 2633-2649.
- Lee, R.W., Volz, R.G., Sheridan, D.C. (1991). The role of fixation and bone quality on the mechanical stability of tibial knee components. *Clinical Orthopaedics and Related Research*, Vol. 273, pp. 177-189.
- Li, C., Granger, C., Schutte Jr., H.D., Biggers Jr., S.B., Kennedy, J.M., Latour Jr., R.A. (2003). Failure analysis of composite femoral components for hip arthroplasty. *Journal of Rehabilitation Research and Development*, Vol. 40(2), pp. 131-146.
- Li, P.L., Jones, N.B., Gregg, P.J. (1995). Loosening of total hip arthroplasty. *The Journal of Bone and Joint Surgery (Br)*, Vol. 77B, pp. 640-644.
- Li, P.L., Jones, N.B., Gregg, P.J. (1996). Vibration analysis in the detection of total hip prosthetic loosening. *Medical Engineering and Physics*, Vol. 18 (7), pp. 596-600.
- Lieven, N.A.J., Clayton, J., Hoyle, C. (2001). Identification of Damaged Hip Prostheses. *Proceedings of the International Modal Analysis Conference - IMAC*, Vol, 2, pp. 1099-1105.

- Lotz, J.C., Gerhart, T.N., Hayes, W.C. (1990). Mechanical Properties of Trabecular Bone from the Proximal Femur: A Quantitative CT Study. *Journal of Computer Assisted Tomography*, Vol. 14(1), pp. 107-114.
- Magee, F.P., Weinstein, A.M., Longo, J.A., Koeneman, J.B., Yapp, R.A. (1988). A canine composite femoral stem - an in vivo study. *Clinical Orthopaedics and Related Research*, Vol. 235, pp. 237-252.
- Maloney, W.J., Jasty, M., Rosenbery, A., Harris, W.H. (1990a). Bone lysis in well-fixed cemented femoral components. *The Journal of Bone and Joint Surgery (Br)*, Vol. 72B(6), pp. 966-970.
- Maloney, W.J., Jasty, M., Harris, W.H., Galante, J.O., Callaghan, J.J. (1990b). Endosteal erosion in association with stable uncemented femoral components. *The Journal of Bone and Joint Surgery (Am)*, Vol. 72A(7), pp. 1025-1034.
- Maloney, W.J., Sychterz, C., Bragdon, C., McGovern, T., Jasty, M., Engh, C.A., Harris, W.H. (1996). Skeletal Response to Well Fixed Femoral Components Inserted With and Without Cement (Hip). *Clinical Orthopaedic and Related Research*, Vol. 333, pp. 15-26.
- Martens, M., Van Audekercke, R., Delpont, P., De Meester, P., Mulier, J.C. (1983). The mechanical characteristics of cancellous bone at the upper femoral region. *Journal of Biomechanics*, Vol. 16(12), pp. 971-983.
- Memsic (2005). [online]. Available from: <http://www.ditrobotics.com/ICs/BR857210DataSheetMXR7210ML.pdf> [accessed June 10, 2005].
- Merriam-Webster, Inc. (2002). *Merriam-Webster's Medical Dictionary*. Springfield, MA, Merriam-Webster, Inc.
- Morgan, E.F., Bayraktar, H.H., Keaveny, T.M. (2003). Trabecular bone modulus-density relationships depend on anatomic site. *Journal of Biomechanics*, Vol. 36, pp. 897-904.
- Nakamura, K. (1996). Measurement of periprosthetic bone mineral density after cementless hip arthroplasty by dual energy x-ray absorptiometry. Longitudinal and cross-sectional evaluation. *Journal of orthopaedic science*, Vol. 1, pp. 113-122.

- Nordin, M., Frankel, V.H. (2001) *Basic Biomechanics of the Musculoskeletal System*. 3rd edition, Chapter 1, Philadelphia, PA, Lippincott Williams & Wilkins.
- Okano, T., Hagino, H., Otsuka, T., Teshima, R., Yamamoto, K., Hirano, Y., Nakamura, K. (2002). Measurement of periprosthetic bone mineral density by dual-energy x-ray absorptiometry is useful for estimating fixation between the bone and the prosthesis in an early stage. *Journal of Arthroplasty*, Vol. Jan. 17(1), pp. 49-55.
- Ouedraogo, E., Lasaygues, P., Lefebvre, J.P., Gindre, M., Talmant, M., Laugier, P. (2002). Contrast and velocity ultrasonic tomography of long bones. *Ultrasonic Imaging*, Vol. 24(3), pp. 139-160.
- Park, J.B. (1984). *Biomaterials Science and Engineering*. New York, NY, Plenum Press.
- Pearson, J., Dequeker, J., Reeve, J., Felsenber, D., Henley, M., Bright, J., Lunt, M., Adams, J., Diaz Curiel, M., Galan, F. *et al.* (1995). Dual X-Ray absorptiometry of the proximal femur: normal European values standardized with the European Spine Phantom. *Journal of Bone and Mineral Research*, Vol. Feb 10(2), pp. 315-324.
- Pope, M.H., Outwater, J.O. (1974). Mechanical Properties of Bone as a function of position and orientation. *Journal of Biomechanics*, Vol. 7(3), pp. 61-66.
- Poss R., (1992). Natural factors that affect the shape and strength of the aging human femur. *Clinical Orthopaedics and Related Research*, Vol. 274, pp. 194-201.
- Puers, R., Catrysee, M., Vandevoorde, G., Collier, R.J., Louridas, E., Burny, F., Donkerwolcke, M., Moulart, F. (2000). A telemetry system for the detection of hip prosthesis loosening by vibration analysis. *Sensors and Actuators*, Vol. 85, pp. 42-47.
- Reilly, D.T., Burstein, A.H., Frankel, V.H. (1974). The Elastic Modulus for Bone. *Journal of Biomechanics*, Vol. 7, pp. 271-275.
- Reilly, D.T., Burstein, A. H., (1975). The Elastic and Ultimate Properties of Compact bone tissue.. *Journal of Biomechanics*, Vol. 8(6), pp. 393-405.

- Rho, J.Y., Habatho, M.C., Ashman, R.B. (1991). Relations of mechanical properties to density and CT numbers in human bone. *Medical and Engineering Physics*, Vol. 17(5), pp. 347-355.
- Rho, J.Y., Ashman, R.B., Turner, C.H. (1993). Young's Modulus of Trabecular and Cortical Bone Material: Ultrasonic and Microtensile Measurements. *Journal of Biomechanics*, Vol. 26(2), pp. 111-119.
- Rho, J.Y. (1996). An ultrasonic method for measuring the elastic properties of human tibial cortical and cancellous bone. *Ultrasonics*, Vol. 36, pp. 777-783.
- Rice, J.C., Cowin, S.C., Bowman, J.A. (1988). On the dependence of the elasticity and Strength of Cancellous Bone on apparent density. *Journal of Biomechanics*, Vol. 21(2), pp. 155-168.
- Rosenstein, A.D., McCoy, G.F., Bulstrode, C.J., McLardy-Smith, P.D., Cunningham, J.L., Turner-Smith, A.R. (1989). The differentiation of loose and secure femoral implants in total hip replacements using a vibrational technique: an anatomical and pilot clinical study. *Proceedings of the Institution of Mechanical Engineers*, Vol. 203, pp.77-81.
- Qi, G., Mouchon, P.M., Tan, T.E. (2003). How much can a vibrational diagnostic tool reveal in total hip arthroplasty loosening? *Clinical Biomechanics*, Vol. 18, pp. 444-458.
- Rosenstein, A.D., McLardy-Smith, P.D., Cunningham, J.L. (1989). The differentiation of loose and secure femoral implants in total hip replacement using a vibrational technique: an anatomical and pilot clinical study. *Proceedings of the Institution of Mechanical Engineers. Part H, Journal of Engineering in Medicine (London)*, Vol. 203, pp. 77-81.
- Pugh, J.W., Rose, R.M., Radin, E.L. (1973). A Structural Model for the Mechanical Behaviour of Trabecular Bone. *Journal of Biomechanics*, Vol. 6(6), pp. 657-670.
- Salter, R.B. (1999). *Textbook of Disorders and Injuries of the Musculoskeletal System*. 3rd edition, Chapter 1, pp.11. Media, PA, Lippincott Williams & Wilkins.

- Sawbones Pacific Research Laboratories (2004). Sawbones, Biomechanical Test Materials. [online] Vashon, Washington. Available from: <https://secure.sawbones.com/products/bio/default.asp> [accessed June 20, 2005].
- Schaffler, M.B., and Burr, D.B. (1988). Stiffness of Compact Bone: Effects of Porosity and Density. *Journal of Biomechanics*, Vol. 21(1), pp. 13-16.
- Senapati, S.K., Pall, S. (2002). Uhmwpe-Alumina Ceramic Composite, An Improved Prosthesis Materials for an Artificial Cemented Hip Joint. *Trends in Biomaterials and Artificial Organs*, Vol. 16(1), pp. 5-7.
- Shier, D., Butler, D., Lewis, R., (1996). Hole's Human Anatomy & Physiology. 7th edition. Dubuque, Iowa: Wm C Brown Publishers.
- Simmers, L., (1988). Diversified Health Occupations. 2nd ed. Canada: Delmar, pp. 150-151.
- Singh, S. (1989). Ultrasonic non-destructive measurements of cortical bone thickness in human cadaver femur. *Ultrasonics*, Vol. Mar. 27(2), pp. 107-113.
- Starr, C., Taggart, R. (2001). *Biology: The Unity and Diversity of Life*, 7th edition. Belmont, CA., Wadsworth Publishing Co.
- Strelitzki, R., Nicholson, P.H.F., Evans, J.A. (1997). Low-frequency ultrasonic velocity measurements in human calcaneal trabecular bone. *Physiological Measurement*, Vol. 18, pp. 119-127.
- Stryker Howmedica Osteonics. (2004) *Primary Stems*. [online]. Available from: <http://www.stryker.com/jointreplacements/sites/primarysystems/securefitpl.us.php> [accessed July 14, 2004].
- Stryker Howmedica Osteonics. *TMZF™ A Beta Titanium Alloy for Orthopaedic Implants*. [On file at Stryker Orthopaedics].
- Sumner, D.R., Turner, T.M., Igloria, R., Urban, R.M., Galante, J.O. (1998). Functional adaptation and ingrowth of bone vary as a function of hip implant stiffness. *Journal of Biomechanics*, Vol. 31, pp. 909-917.
- Szivek, J.A., Weng, M. and Karpman, R. (1990). Variability in the torsional and bending response of a commercially available composite femur. *Journal of Applied Biomaterials*, Vol. 1, pp. 183-186.

- Trevisan, C., Bigoni, M., Randelli, G., Marinoni, E.C., Peretti, G., Ortolani, S. (1997) Periprosthetic Bone Density Around Fully Hydroxyapatite Coated Femoral Stem. *Clinical Orthopaedics & Related Research. The Rheumatoid Foot*, Vol. 340, pp. 109-117.
- Turner, T.M., Sumner, D.R., Urban, R.M., Galante, J.O. (1997). Maintenance of proximal cortical bone with use of a less stiff femoral component in hemiarthroplasty of the hip without cement. *The Journal of Bone and Joint Surgery (Am)*, Vol. 79A, pp. 1381-1390.
- Turner, C.H., Rho, J., Takano, Y., Tsui, T.Y., Pharr, G.M. (1999). The elastic properties of trabecular and cortical bone tissues are similar: results from two microscopic measurement techniques. *Journal of Biomechanics*, Vol. 32, pp. 437-441.
- Van der Perre, G. (1984). Dynamic analysis of human bones. *Functional behaviour of Orthopaedic Biomaterials*. (Editors: P. Ducheyne and G.W. Hastings), pp. 99-159. CRC Press, Boca Raton, Florida.
- Van Lenthe, G.H., Van Den Bergh, J.P.W., Hermus, A.R.M.M., Huiskes, R. (2001). The Prospects of Estimating from the Combination of Ultrasound, Dual-Energy X-Ray Absorptiometry, Microcomputed Tomography and Microfinite Element Analysis. *Journal of Bone and Mineral Research*, Vol. 16(3), pp. 550-555.
- Viceconti, M., Casali, M., Massari, B., (1996). The "Standardized Femur Program" Proposal for a Reference Geometry to be used for the creation of Finite Element Models of the Femur. *Journal of Biomechanics*, Vol. 29 (9), pp. 1241.
- Voigt, W. (1889). Über die Bezielung zwischen den beiden Elastizitätskonstanten isotroper Körper. *Wied. Ann. (Annalen der Physik und chemie)*, Vol. 38, pp. 573-587.
- West, J.D., Mayor, M.B., Collier, J.P. (1987). Potential errors inherent in quantitative densitometric analysis of orthopaedic radiographs. A study after total hip arthroplasty. *The Journal of Bone and Joint Surgery (Am)*, Vol. 69A(1), pp. 58-64.

- White, L.M., Kim, J.K., Mehta, M., et al. (2000). Complications of total hip arthroplasty: MR imaging-initial experience. *Radiology*, Apr. 215(1), pp. 254-62.
- Whitehouse, W.J., and Dyson, E.D. (1974). Scanning electron microscope studies of trabecular bone in the proximal end of the human femur. *Journal of Anatomy*, Vol. 118, pp. 417-444.
- Wirtz, D.C., Schiffers, N., Pandorf, T., Radermacher, K., Weichert, D., Forst, R. (2000). Critical evaluation of known bone material properties to realize anisotropic FE-simulation of the proximal femur. *Journal of Biomechanics*, Vol. 33, pp. 1325-1330.
- Wixson, R.L., Stulberg, S.D., Van Flandern, G.J., et al. (1997). Maintenance of proximal bone mass with an uncemented femoral stem analysis with dual-energy x-ray absorptiometry. *Journal of Arthroplasty*, Vol. 12; pp. 365-372.
- Wolff, J. (1892). *Das Gesetz der Transformation der Knochen*. Berlin: Verlag von August Hirschwald.
- Yoon, H.S. and Katz, J.L. (1976). Ultrasonic wave propagation in human cortical bone – II. Measurements of elastic properties and microhardness. *Journal of Biomechanics*, Vol. 9(7), pp. 459-464.